METAL-ORGANIC FRAMEWORK BASED PHOTOCATALYSTS FOR WATER TREATMENT

SHA ZHOU

(M. Eng., South China University of Technology, China)

A THESIS SUBMITTED

FOR THE DEGREE OF DOCTOR OF PHILOSOPHY

DEPARTMENT OF CHEMISTRY

NATIONAL UNIVERSITY OF SINGAPORE

2015

Declaration

I hereby declare that this thesis is my original work and it has been written by me in its entirety, under the supervision of WU Jishan and CHAN Sze On Hardy, (in the laboratory S9-02-03), Chemistry Department, National University of Singapore, between January 2011 and December 2014.

I have duly acknowledged all the sources of information which have been used in the thesis.

This thesis has also not been submitted for any degree in any university previously.

The content of the thesis has been partly published in:

1) **Zhou Sha**, Jiulong Sun, Hardy Sze On Chan, Stephan Jaenicke and Jishan Wu, Bismuth tungstate incorporated zirconium metal-organic framework composite with enhanced visible-light photocatalytic performance, *RSC Advances*, 2014, 4, 64977–64984.
2) **Zhou Sha**, Jiulong Sun, Hardy Sze On Chan, Stephan Jaenicke, Jishan Wu, Enhanced photocatalytic activity of the AgI/UiO-66(Zr) composite for rhodamine B degradation under visible-light irradiation, *ChemPlusChem*, 2015, 80, 1321–1328.
3) **Zhou Sha**, Hardy Sze On Chan, Jishan Wu, Ag_2CO_3/UiO-66(Zr) composite with enhanced visible-light promoted photocatalytic activity for dye degradation, *Journal of Hazardous Materials*, 2015, 299, 132–140.
4) **Zhou Sha**, Jishan Wu, Enhanced visible-light photocatalytic performance of BiOBr/UiO-66(Zr) composite for dye degradation with the assistance of UiO-66, *RSC Advances*, 2015, 5, 39592–39600.

Sha Zhou	Sha Zhou	Sep 30, 2015
Name	Signature	Date

Acknowledgements

First and foremost, I would like to thank my supervisor Prof. Wu Jishan for his continuous support and guidance in my Ph.D. study and research. His patience, motivation, and immense knowledge in science have been inspiring me during my study. I could not have my thesis completed without his help and advice.

I am grateful to Prof. Chan Sze On Hardy for he was willing to be my co-supervisor, and his consideration and assist on my research and campus life. I am also deeply influenced by his energy and enthusiasm in science and research.

My most sincere gratitude also goes to Mr Sun Jiulong from Prof. Stephan Jaenicke's group and Mr Pan Yanlin from Prof. Xu Qinghua's group. They assisted me a lot on the photocatalysis experiment. Especially, Mr Sun Jiulong not only gave me advice on MOFs synthesis and helped me in material characterization, but also discussed with me for the result analysis. I am truly blessed to have such a generous collaborator during my Ph.D. study.

I also would like to thank Prof. Stephan Jaenicke for his insightful advice on my research and manuscript writing.

I would like to thank all my colleagues studying/working in Prof. Wu Jishan's group and Prof. Chi Chunyan's group for their help during my Ph.D. study.

Also, I owe sincere and earnest thankfulness to the friends I met in Singapore and NUS who have been generously providing me help whenever I needed them.

Last but not least, I am truly indebted to my wife Zheng Dan, my parents and my parents-in-law who have been ever supportive throughout the course of my Ph.D. To them I dedicate this thesis.

Table of Contents

Summary

Due to their outstanding properties, metal-organic frameworks (MOFs) are highly competent candidates for the application in water treatment. To date, the studies on MOF based active materials for visible-light photocatalytic water treatment are extremely limited. More research efforts are urgently required for the development of MOF based photocatalyst with high photocatalytic activity, good stability and reusability for the efficient degradation of organic contaminants in wastewater. Therefore, the aim of this study was to develop diverse MOF based visible-light prompted photocatalysts for the efficient degradation of organic dyes in water medium. Through incorporating MOFs with inorganic active materials, several MOF based photocatalysts were successfully prepared and demonstrated excellent activity for the degradation of organic dyes.

In the first study, UiO-66 (a zirconium based MOF) was integrated with Bi_2WO_6 by a simple hydrothermal method. The resulting Bi_2WO_6/UiO-66 composite not only possessed enhanced photocatalytic activity for the degradation of rhodamine B (RhB) under visible-light irradiation, but also demonstrated good catalyst stability. The highest photocatalytic activity was achieved at the optimum Bi_2WO_6 content. The mechanism of the photocatalytic RhB degradation by the Bi_2WO_6/UiO-66 composite was studied as well.

In the second study, UiO-66 was conjugated with AgI to prepare a AgI/UiO-66 photocatalyst by a simple solution method. The AgI/UiO-66 composite exhibited remarkable visible-light activity, and good structural stability and reusability for the degradation of RhB. The good stability of the composite can be attributed to the outstanding stability of UiO-66 as well as the good

interaction between AgI and the UiO-66 framework. The degradation mechanism of this composite was also investigated.

In the third study, a Ag_2CO_3/UiO-66 composite was developed by incorporating UiO-66 with Ag_2CO_3, and the resulting composite exhibited enhanced visible-light photocatalytic activity for RhB degradation compared to the mixture of pristine UiO-66 and Ag_2CO_3. The participation of UiO-66 during the synthesis of Ag_2CO_3 was supposed to be a crucial factor for such improvement. Although the photocorrosion of Ag_2CO_3 could not be completely prevented, the composite demonstrated good structural stability after the degradation experiment, and most of its photocatalytic activity was preserved after the recycle test.

In the last study, a series of BiOBr/UiO-66 composites with different BiOBr contents were prepared for the degradation of RhB. The resulting BiOBr/UiO-66 composite not only exhibited enhanced photocatalytic activity compared to the control experiments, but also demonstrated good stability and reusability which was verified by different characterization techniques. The good interaction between UiO-66 and BiOBr was expected to play a crucial role in achieving the excellent performance of the BiOBr/UiO-66 composite.

In conclusion, this study proposes several MOF based photocatalysts for organic dye degradation in water treatment. All of the MOF based composites are proved to be capable of efficiently degrading RhB under visible-light irradiation, and most of them also possess excellent stability and reusability. Moreover, the preparation of these photocatalysts is highly convenient and relatively cost-effective. Therefore it should be beneficial for mass-production for the application in water treatment. This study is also of considerable

significance because it opens up numerous opportunities to the development of various MOF based visible-light photocatalysts for water treatment and other related fields in the future.

List of Tables

List of Figures

List of Schemes

List of Symbols

α	absorption coefficient
E_g	band gap energy
h	Planck constant
k	reaction rate constant
P	equilibrium pressure of adsorbates at the temperature of adsorption
P_0	saturation pressure of adsorbates at the temperature of adsorption
v	light frequency

List of Abbreviations

AOP	advanced oxidation process
AOT	advanced oxidation technology
BDC	terephthalic acid (1,4-benzene-dicarboxylic acid)
BET	Brunauer-Emmett-Teller
BJH	Barrett-Joyner-Halenda
BPDC	4,4'-biphenyl-dicarboxylate
BQ	benzoquinone
CB	conduction band
DI	deionized
DMF	*N,N'*-dimethylformamide
EDS/EDX	Energy-dispersive X-ray spectroscopy
EDTA	Ethylenediaminetetraacetic acid
FESEM	Field Emission Scanning Electron Microscope
HKUST	Hong Kong University of Science and Technology
ICP	Inductively Coupled Plasma
IPA	isopropyl alcohol
IRMOF	Isoreticular Metal-Organic Framework
JCPDS	Joint Committee on Powder Diffraction Standards
MB	methylene blue
MIL	Materials of Institut Lavoisier
MO	methyl orange
MOF	Metal-Organic Framework
NHE	normal hydrogen electrode
NTU	Nanyang Technological University

NU	Northwestern University
PSM	post-synthetic modification
RhB	Rhodamine B
SEM	Scanning Electron Microscope
TEM	Transmission Electron Microscopy
TPDC	terphenyl-dicarboxylate
UiO	Universitetet I Oslo
UV	Ultraviolet
VB	valence band
Vis	Visible
XRD	X-ray diffraction
ZIF	Zeolitic imidazolate framework

List of Publications

1. **Zhou Sha**, Jiulong Sun, Hardy Sze On Chan, Stephan Jaenicke, **Jishan Wu**, Bismuth tungstate incorporated zirconium metal-organic framework composite with enhanced visible-light photocatalytic performance, *RSC Advances*, 2014, 4, 64977–64984.
2. **Zhou Sha**, Jiulong Sun, Hardy Sze On Chan, Stephan Jaenicke, **Jishan Wu**, Enhanced photocatalytic activity of the AgI/UiO-66(Zr) composite for rhodamine B degradation under visible-light irradiation, *ChemPlusChem*, 2015, 80, 1321–1328.
3. **Zhou Sha**, Hardy Sze On Chan, **Jishan Wu**, Ag_2CO_3/UiO-66(Zr) composite with enhanced visible-light promoted photocatalytic activity for dye degradation, *Journal of Hazardous Materials*, 2015, 299, 132–140.
4. **Zhou Sha**, **Jishan Wu**, Enhanced visible-light photocatalytic performance of BiOBr/UiO-66(Zr) composite for dye degradation with the assistance of UiO-66, *RSC Advances*, 2015, 5, 39592–39600.

Chapter 1 Introduction

Due to the development of various industries in modern society, water pollution has become one of the most serious environmental problems. Polluted water not only affects the ecological system, causing damages to the livings in water and those relying on the aquatic animals and plants, but also threatens human beings. One of the most common contaminants in wastewater is organic substances, most of which are very stable in natural environment.[1] Hence, they can aggregate in wastewater and are therefore harmful to the aquatic ecosystem. Unfortunately, many industries are producing organic pollutants containing wastewater, which aggravates the water pollution problems.[2] Therefore, how to treat wastewater, especially remove organic pollutants in wastewater is one of the most crucial problems for sustainable development.[3]

Currently, various water treatment methods have been proposed and some are even commercially employed for real wastewater treatment. However, most of these techniques have various limitations, such as low efficiency, high cost, failure to actually destroy pollutants, generation of secondary pollutants, etc. Consequently, to develop an ideal wastewater treatment method, through which the organic contaminants can be removed with high efficiency, relatively low cost and less side-effect is still a challenging task.

Recently, wastewater treatment by photocatalysis process has been drawing more and more attention.[4] In details, a certain kind of photocatalyst, which is usually a semiconductor material, is introduced to the wastewater system. Under light irradiation, active species are generated on the catalyst surface to react with the organic contaminants in the wastewater. During this process, the organic contaminants can be partially degraded to smaller molecules or even completely

mineralized to CO_2 and H_2O.[5] It is known that the photocatalysis process can proceed under UV-light or/and visible-light irradiation. Since visible-light occupies much higher spectral power within solar spectrum than UV-light, visible-light prompted photocatalysis is more advantageous for its efficient utilization of the solar irradiation.[6] Therefore, to develop a photocatalyst that can efficaciously degrade organic contaminants under visible-light irradiation is a highly promising direction in the application of wastewater treatment.

Metal-organic frameworks (MOFs) are a class of porous solid materials in which inorganic metal clusters are connected by organic linkers to form uniform framework structures. Because of their superior properties, such as high specific surface area, tunable pore size, great chemical variety, and relatively good thermostability, MOFs have been widely used in various applications. Furthermore, recent studies show that certain kinds of MOFs exhibit semiconductor behavior, meaning that MOFs could be a favorable candidate material for the development of photocatalysis.[7] Additionally, most studies are focusing on using MOFs as catalyst substrate to incorporate with other types of functional materials. The obtained composites possess the advantages of both MOFs and the functional materials.

The subsequent sections provide a brief overview of the possibilities and advantages of MOF based photocatalysts and more attention will be given to some pioneer studies to demonstrate the achievements and also limitations of MOF based photocatalyst applied in water treatment.

1.1 The urgency of water treatment

Besides air, water is the most important life-sustaining product on the earth. Water is called the universal solvent since it can dissolve much more types of

substances than any other liquid medium. As a result, water functions as a highly important carrier of valuable chemicals, minerals, and nutrients, either through the ground or human bodies. Even though water covers over 70% surface of the earth, only 3% is suitable for human consumption, of which two thirds is frozen and largely uninhabited ice caps and glaciers, leaving 1% accessible for consumption. Although fresh water is a renewable resource, with the unprecedentedly continuous increase of population all over the world, the steadily decreasing supply of clean water becomes a heavy burden for the society. Consequently, water is even considered as the new oil. Thus advanced technology must be developed to solve the challenges of fresh water supply in the future.[8]

On the other side, economic and social growth cannot be ensured without industrialization, which is reversely a culprit in spoiling the precious water resources due to the generation of significant amount of wastewater. Moreover, the urbanization with over concern of hygiene further intensifies the existing problem, leading to the production of additional wastewater from household kitchens, toilets, and restaurants, most of which is nontoxic but not suitable for human consumption. What is worse, up to 90% of untreated wastewater in developing countries directly flows into rivers, lakes and coastal zones, ultimately threatening human health and food safety.[9] Therefore, currently it is of exceptional urgency to treat wastewater to make it as clean as possible. The treated water may not be suitable for potable purpose, but can at least be used for industrial purposes, steam generation, gardening and agriculture.[10, 11]

1.2 Water treatment methods: overview

There are various kinds of water treatment methods, part of which have been commercially applied in water treatment plants. Generally, these methods can be classified into four categories: physical methods, chemical methods, combination of physical and chemical methods, and biological methods. However, most of the widely used water treatment technologies suffer from different limitations. For instance, the physical methods such as adsorption or coagulation can only transfer the pollutants to other phases rather than completely "eliminating" or "destroying" the pollutants.[12] Most chemical, or physical and chemical combined methods are very costly and may generate toxic secondary pollutants to the ecosystem, since intensive chemicals (such as those using ammonia, chlorine compounds, hydrochloric acid, sodium hydroxide, ozone, permanganate, ion exchange resins, etc.) are introduced during the treatment process so that residuals resulting from the treatments (sludge, brines, toxic waste, etc.) are remained in the treated water source.[13, 14] Regarding the biological methods, although they are proved to be effective to many kinds of contaminants, the disadvantages are also obvious, such as volatile emissions, waste sludge disposal, high energy costs, temperature sensitivity, relatively long period of treating time, etc.[15, 16] Hence, it is of both significant importance and considerable interest to develop more beneficial wastewater treatment methods.

1.2.1 Advanced oxidation processes

Recently, a kind of water treatment technology called advanced oxidation processes (AOPs) or advanced oxidation technologies (AOTs) is attracting great attention. It is defined as oxidation processes that generate highly active radicals (especially hydroxyl radicals (HO•)) in sufficient quantity to affect the water

treatment. Although oxidation processes involving HO• had been using for water treatment since the late 19th century (such as Fenton reaction), the concept of AOPs was originally established by Glaze et al. in 1987.[17] Relying on the formation of highly active chemical species (*i.e.*, H_2O_2, HO•, O_2^{-}•, O_3), it is possible for AOPs to degrade and mineralize almost all organic compounds, water pathogens and disinfection by-products when various active species are the main oxidizing reagents in the solution.[18, 19] This is one of the major advantages of AOPs, since other conventional oxidation processes, such as those using chlorine, peracetic acid, permanganate, hydrogen peroxide (H_2O_2), and ozone, can only partially oxidize the target compounds, leading to the generation of new hazardous compounds. The excellent performance of AOPs is due to the important characteristics of the active species, which are short-lived, easily produced, powerful in oxidation, electrophilic in behavior, ubiquitous in nature, highly active, nonselective, etc. Another advantage of AOPs is the production of negligible amount of residues and their applicability in the case of very low pollutant concentrations.[20] More than ten different AOPs techniques are available, which can be classified into four main categories, *i.e.*, (i) Fenton and photo-Fenton reaction, (ii) ozonolysis, (iii) photocatalysis, and (iv) sonolysis-based processes. To study the research interest regarding these four different directions in the last decade, the four categories were searched separately with "water treatment" in the Keyword function in Scopus (http://www.scopus.com/), and the number of relative publications is summarized in Fig. 1-1. It is obvious that photocatalysis is the hottest research field among the different categories of AOPs.

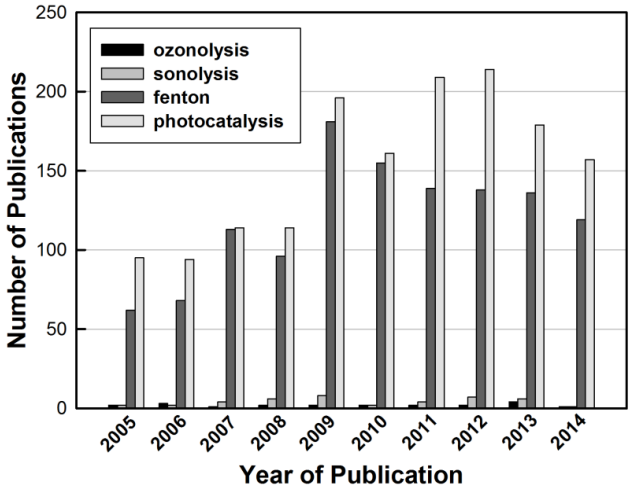

Fig. 1-1 Number of publications of AOPs in the field of water treatment in the past decade. Data was taken on Jan 7, 2015 from www.scopus.com using the four categories of AOPs and "water treatment" as keywords in the advanced search option.

1.2.2 Heterogeneous photocatalysis for water treatment

Heterogeneous photocatalysis has been extensively studied in the fields of alternative energy, organic synthesis and environmental treatment. Compared to homogeneous photocatalysis, heterogeneous photocatalysis is more advanced for water treatment application in terms of preventing the secondary contamination of treated water and facilitating the recycle of catalyst. Despite the differences in the character and proposed utilization of different materials exhibiting photocatalytic activity, most of the successfully exploited photoinduced processes have the same origin. For example, a semiconductor can be excited by light energy higher than its band gap, giving rise to the formation of energy-rich electron-hole pairs. Thus, heterogeneous photocatalysis process is referring to any chemical process catalyzed by a solid (commonly semiconductor material) under the excitation of external electromagnetic field (with wavelength in the UV-visible-infrared range).[21] Currently, it has been found that a great number of materials can initiate reaction

upon efficient light absorption, and most of them have been studied as photocatalysts for different applications. These photocatalysts include semiconductor based materials, composites, complex oxides, polyoxometallates and complex organic or organometallic compounds such as porphyrin, pthalocyanine, metalloporphyrins and metallophthalocyonines. In particular, because of their outstanding properties and performance, semiconductor based materials have thrived as the most suitable heterogeneous photocatalyst, especially in water treatment application. The benefits of applying semiconductor based photocatalyst for treating contaminated aqueous effluents include:[14]

- mild reaction conditions (process taking place at ambient temperature and without overpressure),
- complete oxidation of the substances into CO_2 and other inorganic species,
- convenient obtainment of oxygen necessary for the reaction from atmosphere,
- virtues of the catalyst (cheap, innocuous and reusable),
- possibility of attaching catalyst to different types of inert matrices,
- and efficient utilization of the sun energy for photo-exciting the catalyst.

The photocatalysis process of a semiconductor material under light irradiation, especially for the degradation of pollutants in water medium is illustrated in Fig. 1-2. After the absorption of a photon with an energy $h\nu$ greater than or equaling the band gap energy E_g, an electron-hole pair forms in the semiconductor. In this process, an electron is promoted from the valence band (VB) to the conduction band (CB), and the photoexcited electron leaves behind

a positive hole in the VB. Hence, the VB hole and the CB electron are referred to as an electron-hole pair and are responsible for the charge conduction in the semiconductor. After its formation, the charge carriers may either recombine in the bulk dissipating the input energy in the form of heat or light, or be trapped in metastable surface states, or move to the solid-liquid interface through diffusion or migration and then react with electron donors and acceptors adsorbed on the surface or bound within the electrical double layer. In the case of water treatment process, the CB electrons are good reductants (+0.5 to −1.5 V vs. NHE depending on the semiconductor and pH). The dissolved O_2 in water can be reduced by the CB electrons to form superoxide radicals (O_2^{-}•), which can cause the degradation of pollutants through an oxidation process. On the other hand, the holes in the VB are powerful oxidants (+1.0 to +3.5 V vs. NHE) and can decompose the organic substances through either direct or indirect path.[22] One important indirect path is that the holes in VB may react with water molecule to generate HO•, which can oxidize and mineralize almost any organic molecule, yielding CO_2 and inorganic ions.[20] For example, in the presence of the oxidative species (especially the HO•) formed in the photocatalysis process, the aromatic part of aromatic compounds can be hydroxylated and in successive oxidation/addition steps, ring opening happens. The resulting aldehydes and carboxylic acids are decarboxylated and finally CO_2 is produced.[14] Apparently, to improve the photocatalytic activity of the semiconductor material, it is essential to minimize the electron-hole recombination. The recombination can be suppressed through increasing the lifetime of the photogenerated electrons/holes and as such, separating them by transferring the electrons and holes to different acceptors. Different strategies

have been proposed to achieve this objective, such as semiconductor/semiconductor heterojunctions, metal/semiconductor coupled systems, non-metal/semiconductor composites, etc.

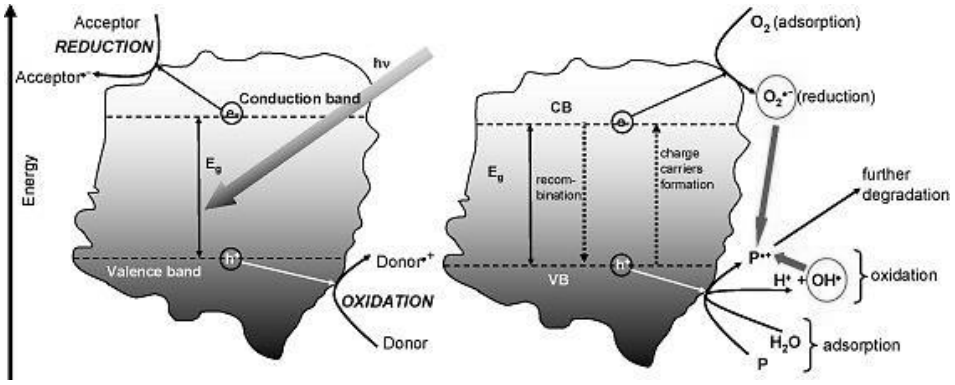

Fig. 1-2 Energy band diagram and fate of electrons and holes in a semiconductor particle in the presence of water containing a pollutant (P).[14]

Many semiconductor materials have been proved to be photoactive due to their electronic structures, such as TiO_2, ZnO, $SrTiO_3$, CeO_2, WO_3, Fe_2O_3, GaN, Bi_2S_3, CdS, ZnS, etc. Among these heterogeneous semiconductors, TiO_2 is the most widely used photocatalytic material because it has the advantages of semiconductor based photocatalyst, and it is also chemically and biologically inert, photostable and nontoxic. The study of the photocatalytic activity of TiO_2 can be traced back to approximately the early 20th century. In 1921, Renz found that in the presence of a suitable organic acceptor, TiO_2 and some other oxides could form dark reduction products under irradiation.[23] In 1938, Goodeeve and Kitchener utilized TiO_2 for the photo-decolorization of dye.[24] Thereafter, the oxidation of organic solvents was reported by Kato and Mashio in 1956.[25] Then it was in 1969 when Fujishima and Honda made a groundbreaking discovery on the utilization of n-type rutile TiO_2 anode for the photoelectrolysis of water. Afterwards, more and more studies were focusing on photon energy conversion through the 1970s to the early 1980s. To date, TiO_2 is still the most

popular study topic in the field of photocatalysis,[26-28] and TiO_2 based photocatalysts are even commercially available and used at pilot-plant scale.[29, 30]

1.2.3 Visible-light photocatalysis for water treatment

Despite the advantages of TiO_2, it is not a perfect material for photocatalysis. One of the main problems is the wide band gap of TiO_2 (3.2 eV for anatase TiO_2), which limits its absorption of light above the wavelength of 387 nm, thus TiO_2 can only utilize light energy in the UV-light range. However, it is known that the solar spectrum contains only a small proportion of UV-light (~5%) and this obviously restricts the practical applications of TiO_2 based photocatalyst in solar energy-driven water treatment.

In addition, the shortcoming of utilizing the UV-light energy is that the apparent quantum efficiency for the degradation of organic compounds in water is reported to be around 1% (under good conditions) under UV-light irradiation. Therefore, it can be reasonably anticipated an overall solar efficiency of merely about 0.05% for a UV-light excited semiconductor photocatalyst for water treatment. Hence, additional UV-light sources are required to enhance the efficiency of the semiconductor based photocatalysis water treatment system, which undoubtedly cause extra energy consumption. It is also worth mentioning that most of the water-related issues are found in developing countries, and most of these countries are also facing energy (*e.g.*, electricity supply) shortage problem, which further limit the utilization of UV-light excited photocatalysts. On the other side, visible-light possesses around 43% of the solar energy at the earth's surface, and this energy concentrates in a narrow range from 400 to 700 nm. Although infrared-light contributes almost all the rest of the solar energy

(around 52%), it distributes in a very broad wavelength (from 700 nm to 1 mm). As a result, it is a much more challenging and complicated task to design a photocatalyst with activity in the infrared-light range. Therefore, to develop a photocatalyst which can efficiently utilize the solar energy in the visible-light range is of more attractiveness and practical significance.

Therefore, great research efforts have been focused on modifying TiO_2 with other components in order to achieve visible-light activity. These attempts include surface modification with organic materials (sensitization by dye molecules), coupling with semiconductors, incorporating with metals (hence making use of surface plasmon resonances), doping with nonmetal elements such as N, C, F, S, and metal doping or bandgap modification by creating oxygen vacancies.[31, 32] However, the strategies of modifying TiO_2 are usually very complicated, and the preparation procedure may also be a thorny task. For instance, in some modification processes, several steps of post-processing and/or special morphology control procedure are involved, which increases the cost of preparing TiO_2 based photocatalysts with visible-light activity and thus is unfavorable for the practical water treatment application. This is also the same problem faced by other wide band gap semiconductor materials, such as ZnO, ZnS, SnO_2, NiO, etc. Therefore, it is wiser and more straightforward to develop visible-light photocatalyst by using narrow band gap semiconductor materials. Indeed, many semiconductor materials with visible-light activity such as Fe_2O_3, $ZnFe_2O_4$, WO_3, CdS, Bi_2O_3, etc. have been investigated for water treatment application.[33-37] Some of these materials are even considered as promising candidates for replacing TiO_2. However, besides the prerequisite visible-light activity of the alternative candidates, it is of

considerable interest to improve the photocatalystic activity of these materials. Some strategies focus on modifying these semiconductors with other materials to facilitate the separation of the electron-hole pairs. However, these strategies have the same drawback of complicating the preparation process and thus increasing the operation cost, which restrains their practical application. Alternatively, it is also meritorious to enhance the activity of photocatalyst by increasing its specific surface area through reducing the material particle size from bulk to nano-scale. The photocatalyst with increased specific surface area can thus contact with more target organic substances at the same time, which results in the improvement of the degradation efficiency. Nevertheless, photocatalyst with particle-size in nanometer may have the problems of low stability and poor reusability. As known, compared to bulk material, nanomaterial possesses higher catalytic activity but lower stability. Besides, due to its extremely small particle size, it is difficult to collect nanomaterial-based catalyst after using it for water treatment, leading to the loss of catalyst. To solve these problems, different strategies have been developed to prepare photocatalysts with large specific surface area and also relatively large particle size. An effective strategy is to modulate the microstructure of the photocatalysts and control their morphology. Nonetheless, surfactant or other mediator is needed in the synthesis process, hence increasing the preparation cost. Another strategy is to incorporate the photocatalyst with a supporting material, which should be stable enough to endure the water treatment process, and also possess large specific surface area for the attachment of the photocatalyst. In addition, the ideal supporting material should form good interaction with the photocatalyst. Thus, it is expected that this supported

photocatalyst should not only possess large specific surface area, but also has large bulk particle size and good stability for the purpose of water treatment.

1.3 Metal-Organic Frameworks

1.3.1 Introduction of MOFs

At the end of the 1990s, as a newly discovered porous compound with an inorganic-organic hybrid framework, metal-organic frameworks (MOFs) (also named porous coordination polymers (PCPs) or porous coordination networks (PCNs)) greatly influenced the area of porous materials and represented a new family for porous chemistry.[38] Due to their potential applications in a variety of fields, the studies on diverse kinds of MOFs and various MOF derived functional materials are extensively investigated. Briefly, MOFs are a type of porous solid materials, consisting of metal-based nodes (single ions or clusters) bridged by organic linkers in their structures to form a one-, two-, or three-dimensional coordination network.[39] Their extremely large surface area,[40] finely tunable pore surface properties,[41-44] and potential scalability to industrial scale[45] make MOFs a promising target for further investigation.

Conventionally, the synthesis of MOFs is achieved by a so-called modular synthesis, through which metal ions and organic ligands are combined to obtain a crystalline porous network. Various types of synthetic methods have been recently developed for the preparation of MOFs, and the experimental conditions resulting in the formation of desirable phases are widely variable. In fact, the reported synthesis procedures include a variety of reagent concentrations, reagent ratios, solvent compositions, temperatures, and reaction times, and the fine-tuning of all parameters is essential in optimizing the synthesis of MOFs to obtain desired microstructural parameters. Microwave

heating,[46] sonication-assisted synthesis,[47, 48] or mechanochemical procedures[49, 50] have also been used to effect the framework formation. More recently, the first study of electrosynthetic deposition of MOFs has also been reported.[51]

In most of the resulting MOFs, the solvent used during synthesis occupies the void space within the pores and can be removed by applying vacuum or heat, leading to the formation of large pore volume as well as large specific surface area accessible to guest molecules. Specific surface area is one of the most important parameters that affect the potential applications of MOFs. The first robust and highly porous MOF material called MOF-5 was synthesized in 1999.[52] It is comprised of $Zn_4O(CO_2)_6$ octahedra connected by 1,4-benzene-dicarboxylate (BDC) linkers, and has a Brunauer-Emmett-Teller (BET) surface area of 2320 $m^2\ g^{-1}$.[53] This value is substantially higher than that found in zeolites and activated carbon. Nevertheless, by careful structural design and judicious selection of organic linkers, the specific surface area of MOFs can be further enlarged. For instance, in 2004, MOF-177 with the highest BET surface area of 3780 $m^2\ g^{-1}$ was reported.[54] In 2010, this value was nearly doubled by MOF-200 and MOF-210 with the ultrahigh BET surface area of 4530 $m^2\ g^{-1}$ and 6240 $m^2\ g^{-1}$, respectively. Most recently, the record was renewed to 7140 $m^2\ g^{-1}$ by the NU-110 MOF.[55]

Besides specific surface area, thermal and chemical stability are another two important properties of MOFs. Although MOFs are composed entirely of strong bonds (*e.g.*, C-C, C-H, C-O, and M-O), they show variable thermal stability. In fact, the thermally stable range of most MOF materials is between 350 to 400 ℃. For instance, the IRMOF-6 has a stability range from 100 to 400 ℃.[56] Several

types of MOFs can even remain stable at higher temperature. MIL-53 was stated to decompose at 500 ℃,[57] and UiO-66 was showed to have a higher decomposition temperature of above 500 ℃.[58, 59] ZIF-8 and -11was reported to demonstrate thermal stability up to 550 ℃.[60] Due to their susceptibility to link-displacement reaction, it had been a challenge to synthesize MOFs with good chemical stability, especially when solvent treatment over extended reaction time was needed. Nevertheless, several kinds of MOFs have demonstrated their exceptional chemical stability. For example, ZIF-8 remained intact after immersed in boiling methanol, benzene, and water for up to 7 days, and in concentrated sodium hydroxide at 100 ℃ for 24 hours.[60] Besides, both MOF-525 and -545 revealed their chemical stability in methanol, water, and acidic conditions for 12 h.[61] There is also a pyrazolate-bridged MOF, which proved its chemical stability in a wide range of aqueous solutions (pH = 2 to 14) at 100 ℃ for 2 weeks.[62] Furthermore, UiO-66 and its NO_2- and Br-functionalized derivatives demonstrated their excellent capability to adapt to various aqueous environment because they could resist strong acid (HCl, pH = 1) and base (NaOH, pH = 14).[58, 59] The extraordinary chemical stability observed in these MOFs is expected to broaden the existing application areas of MOFs to water-containing processes, such as water splitting and water treatment.

1.3.2 Applications of MOFs

1.3.2.1 The application of MOFs in gas storage

Because of their ultra-high specific surface area and pore volume as described earlier, MOFs have important application in the area of gas storage. In 2002, Yaghi’s group studied the methane storage capacity of a series of isoreticular

MOF materials. Thereafter, the methane storage abilities of various MOFs were extensively investigated.[63] The H_2 storage data was also first reported by Yaghi's group in 2003. The H_2 adsorption by MOF-5 was up to 4.5 weight percent (17.2 H_2 molecules per formula unit) at 78 K and 1.0 weight percent at room temperature and pressure of 20 bar.[64] Since H_2 storage is considered as a key technology for the fuel cell industry, more and more studies pertaining the application of MOFs are focusing on H_2 storage.[65] So far, the highest excess H_2 storage capacity reported for MOFs was 99.5 mg g^{-1} at 56 bar and 77 K in NU-100, which had a total capacity of 164 mg g^{-1} at 77 K and 70 bar.[66] The highest total H_2 storage capacity reported was 176 mg g^{-1} (excess 86 mg g^{-1}) in MOF-210 at 77 K and 80 bar.[40] MOFs were also studied for CO_2 uptake to capture CO_2 from existing emission sources.[39] This is an important part of carbon capture and sequestration (CCS) technologies, which is expected to reduce the increasing level of atmospheric CO_2 resulting from anthropogenic emissions, especially from the combustion of fossil fuels. Very recently, MOFs was also applied in the area of O_2 storage.[67]

1.3.2.2 The application of MOFs in separation

Due to their porous structure, MOFs can work as a supporting medium for adsorption- and membrane-based separations. One of the most appealing areas of using MOFs for separation is selective adsorption and the separation of light gases in gas phase. For example, MOFs have been applied to separate CO_2 from N_2,[68] methane,[69] O_2,[70] H_2,[71] CO,[72] and Ar.[73] The selective separation of O_2 from other gases especially N_2 is an essential aspect in industrial application. Some MOFs have demonstrated higher selective adsorption of O_2 over N_2, Ar, CO, CO_2, acetylene, etc.[74-76] MOFs can also

be used to separate H_2 from other gases, including CO_2, CO, Ar, N_2 and O_2.[77] Since H_2 has the smallest molecular size compared to CO_2, CO, Ar, N_2 and O_2, molecular sieving effects should be the primary mechanism responsible for the observed selective adsorption of H_2 in MOFs with small pores, excluding in some special examples where structural transformations occur during gas adsorption. Other gases, such as gaseous olefin,[78] harmful gases (*e.g.*, SO_2, Cl_2, NH_3, CO, ethylene oxide, etc.),[79] and noble gases,[80] can also be selectively separated by different MOFs. MOFs are also competent candidates as adsorbents for liquid phase separations, which is also an important motivation for the application of MOFs in water treatment. It was reported that MOFs could separate different organic molecules from liquid phase based on the properties of these molecules, such as different functional groups,[81] different shape and size,[82] organosulfur compounds,[83] structural isomers,[84] and stereoisomers.[85] Additionally, selective exchange of cations or anions is also another major application of MOFs in liquid phase separation.[86, 87]

1.3.2.3 The application of MOFs in catalysis

In contrast to other crystalline porous solids, the high versatility of MOF design provides clear advantages for catalysis because of the possibility in rational and precise design of the active site as well as the environment of MOFs.[88] The catalytic function of MOFs can be implemented at the organic[89] or inorganic[90] component through direct synthesis of the envisaged scaffold or post-synthetic modification (PSM).[43] These advantages make MOFs a very suitable material for heterogeneous catalysis application. The first application of a Cd-based MOF framework in the catalytic cyanosilylation of aldehydes was reported in 1994.[91] Since then, MOFs were

intensively researched as catalyst for various reactions, such as alcohol oxidation, Suzuki C–C coupling, olefin hydrogenation,[92] peroxidative oxidation of alkanes,[93] cyclohexene oxidation,[94] oxidation of CO,[95] and many other reactions.[96] Besides, MOFs can also be used as catalyst support to couple with other functional materials possessing catalytic activity. For example, the Pd/MOF-5 catalyst was proved to be active for CO oxidation and cyclooctene hydrogenation.[97] Nanosized Au anchored on different types of MOFs exhibited activity to aerobic oxidation of alcohols.[98] And the Cu/ZnO/MOF-5 composite demonstrated catalytic activity for methanol synthesis.[99]

In the area of heterogeneous catalysis, MOFs have also been applied in photocatalysis. As illustrated in Fig. 1-3, there are at least three different strategies to develop photoactive materials based on MOFs.

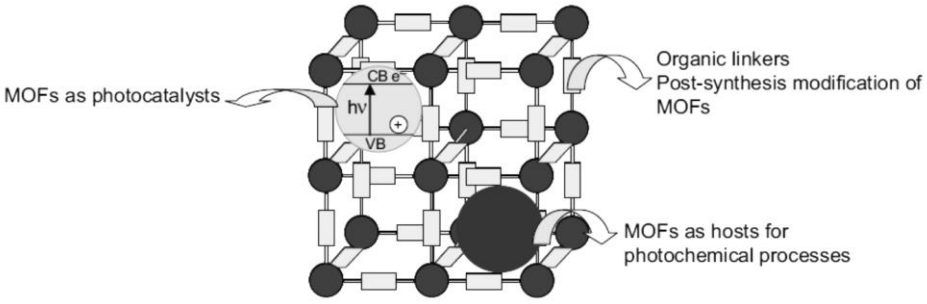

Fig. 1-3 Different strategies for developing photoactive materials based on MOFs.[100]

In the first strategy, the inherent photocatalytic activity of some MOF materials can be utilized. Theoretical calculations indicate that MOFs are semiconductors or insulators with band gaps between 1.0 and 5.5 eV (alterable by changing the degree of conjugation in the ligands).[101-103] Experimental results clearly reveal that MOFs exhibit semiconductor behavior,[7, 104] suggesting that such MOFs can facilitate charge transfer[105] or directly harvest

light irradiation.[106, 107] The light harvest ability of MOFs was also presented in other reports.[108-110] Thus, MOFs with photocatalytic activity have been studied for CO_2 reduction,[111] various organic reactions,[112-114] and water splitting.[115] In another strategy, MOF materials with photocatalytic activity can be prepared through PSM.[43] This is an effective method to functionalize MOFs with desired properties, when such functionalities cannot be achieved by direct synthesis. One example is shown in a recent study, in which the post-synthesized MOFs exhibited improved light absorption ability and enhanced photocatalytic oxidation activity in benzyl alcohol oxidation.[116] In another example, a platinum complex was immobilized in MOF-253 by post-synthesis modification strategy, and the resulting MOF-253-Pt composite exhibited enhanced photocatalytic activity for hydrogen evolution under visible-light irradiation.[117] In the third strategy, MOFs is used as a photocatalyst supporting material. This strategy further extends the potential photocatalytic applications of MOFs, since a great number of functional materials with photocatalytic activity can be immobilized on MOFs, which results in the enhancement of catalytic activity and the improvement of stability or other properties. For example, CdS was embedded on MIL-101 MOF for visible-light driven H_2 production.[118] HKUST-1 was decorated by amorphous TiO_2 for selective aerobic oxidation under sunlight irradiation.[119] $Cu_3(BTC)_2$ MOF could also form a core-shell structure with TiO_2, and the resulting composite was used as a platform to photocatalyze gaseous reactions.[105] Besides inorganic compounds, MOFs can also be coupled with organometallic complex for photocatalytic applications.[120-122] Another route to prepare MOF supported photocatalyst is to incorporate noble metal particles with MOFs.

Although most metal particles do not possess photocatalytic activity, charge transfer is anticipated between the MOF scaffold and the metal particles, giving rise to an enhanced photocatalytic activity in this metal/MOF composite.[123] There were a few studies applying Pt@MOF for hydrogen evolution,[124, 125] and Pd@MOF for water treatment.[126] However, noble metal is not a universal photocatalytic activity enhancer for MOF based composite. In one study, compared to pristine MOF, Pt/MOF composite showed an enhanced activity, whereas Au had a negative effect on the photocatalytic performance of Au/MOF.[127] Moreover, MOF based photocatalyst has also been used in the area of water treatment which will be discussed below.

1.3.2.4 Other applications of MOFs

Besides the applications described above, MOFs have also been widely investigated in many other areas, such as chemical sensor,[128, 129] drug delivery,[130, 131] biomedicine,[132] luminescence,[133] etc.[134, 135] Since these areas are not very relative to the potential utilization of MOFs in water treatment, the studies on these areas will not be discussed in details.

1.3.3 The utilization of MOFs in water treatment

Because of their many superior properties, MOFs have also been well studied in the area of water treatment where the most relevant abilities of MOFs on adsorption, separation and catalysis are perfectly utilized. For instance, it was proved that MOFs could effectively remove various pollutants from water medium through effect of adsorption and separation. Relative studies cover from selective removal of various organic molecules[136-138] to adsorption of different heavy metal ions,[139, 140] and even selective extraction of radionuclides from aqueous solution.[141] In details, water

treatment technologies based on most of these MOF based materials can be classified into two categories: physical adsorption and photocatalysis. Physical adsorption is a relatively straightforward strategy, which sufficiently utilizes various advantages of MOFs, such as great physicochemical variety, high specific surface area, tunable pore size, etc. For instance, MIL-101-Cr and MIL-53-Cr were studied for the adsorptive removal of methyl orange (MO) through electrostatic interactions.[142] In another work, the study on adsorption of phenol and p-nitrophenol over MIL-100-Fe and NH_2-MIL-101-Al showed that hydrogen bonding also occurred during adsorption of contaminants with MOFs.[143] MIL-101-Cr functionalized with acidic and basic groups was also reported for the use in adsorption of naproxen and clofibric acid.[144] Furthermore, it was suggested that MIL-53 adsorbed bisphenol-A through a π-π interaction mechanism.[145] The important hydrophobic interactions for adsorption of organics from aqueous media can also be utilized by MOFs. One study proved that Cu-BTC could efficiently remove oil droplets from water through hydrophobic interactions.[146] The physical adsorption of pollutants from water media by MOFs shows several advantages, such as ease of handling, relatively high adsorption capacity, possibility of selectively adsorbing specific sizes of contaminant molecules by MOFs with controlled pore size, building up of adsorption interactions through various mechanism, etc. However, the disadvantages of MOF based adsorbents for water treatment are also very significant, which should be considered before their further applications. Similar to other physical methods, MOF based adsorbents only concentrate or separate the pollutants from water, but does not completely “eliminate” or “destroy” them into biodegradable or

less toxic compounds. Also, removal efficiency based on physical adsorption may be very low if concentration of contaminant is not high enough. Moreover, MOFs are relatively more expensive than other commercial adsorbents such as activated carbon. In addition, most of them cannot endure the conventional high temperature process to recover the adsorbents. Hence, more and more research efforts are focusing on MOF based photocatalytic technique for water treatment, especially under visible-light irradiation. Pristine MOFs with photocatalytic activity was used directly for water treatment. In a pioneer work, MOF-5 was investigated for the photocatalytic degradation of phenol in aqueous solutions.[7] However, due to wide band gap of MOF-5, the degradation process could only proceed under UV-light irradiation. Afterwards, research focus was placed on MOFs with photocatalytic activity for organic pollutant degradation. For example, $Zn_3(BTC)_2$ films could degrade methylene blue (MB) under UV-Vis irradiation.[147] MIL-88A could also decompose MB under visible-light irradiation.[148] NTU-9 showed visible-light activity for the degradation of RhB.[149] A series of MIL-53 MOFs (MIL-53(Fe), MIL-53(Cr) and MIL-53(Al)) exhibited obvious activity for the decomposition of MB and RhB with visible-light promotion.[150, 151] Although there may exist some drawbacks such as relatively complicated design and synthesis process for obtaining MOFs with photocatalytic activity, MOF based photocatalysts are still attractive materials for water treatment. The most advantageous aspect of these photocatalysts is that they can degrade pollutants into easily biodegradable compounds or less toxic molecules, or even eventually mineralize them into innocuous CO_2 and H_2O. Their other advantages,

including ease of using and recycling, high efficiency for low contaminant concentration, and high flexibility for various modification, also make these photocatalysts very promising candidates for practical water treatment applications.

However, there are still a few problems to be solved before MOFs can become perfect photocatalyst for water treatment. The first issue is the photocatalytic activity of MOF based photocatalyst. Compared to the inorganic photocatalysts and some commercial standards, the photocatalytic activities of most MOF materials are unsatisfactory. Although the photocatalytic activity of MOFs could be improved through the inorganic cluster design, organic linker modification, MOF configuration control or PSM, complicated procedures may be involved in these strategies, which can hinder the practical application of the modified MOF materials. Another issue to be considered is the stability of MOFs. Specifically, for water treatment application, the leaching problem of the active metal (or organic components) and the poor reusability of catalyst should be solved in order to develop high performance MOF based photocatalysts.[152] Although some specific types of MOFs have been proved to possess good thermostability, and considerable stability in various organic solvents and water medium with diverse pH conditions, most of the other MOF materials that have been studied as photocatalyst may not be as stable as those models.

Therefore, it is more advisable and efficient to couple MOFs that possess excellent stability with inorganic compounds that have high photocatalytic activity to form hybrid composites for water treatment. This strategy not only combines the advantages of inorganic photocatalysts and MOFs, but also solves

the two important issues of MOF based photocatalyst used for water treatment described above. Additionally, due to their large specific surface area and excellent flexibility, MOFs have been proved to be a good support for various functional materials. Therefore, the integration of inorganic compounds and MOFs for the development of photocatalysts used in water treatment has been drawing more and more attention. Qiu et al. reported a composite with core-shell structure based on the coupling of MIL-100(Fe) and Fe_3O_4, and used it as photocatalyst for the decolorization of MB.[153] Wang et al. reported a Ag/AgCl/ZIF-8 composite exhibiting enhanced visible-light photocatalytic activity for the RhB degradation.[154] Nevertheless, the studies on MOF based hybrid photocatalyst for water treatment are still very limited. Much more research efforts are urgently needed in this promising area.

1.3.4 UiO-66 MOF

1.3.4.1 Introduction of UiO-66

As a zirconium based MOF, UiO-66 was first reported by Lillerud's group in 2008.[58] In the framework structure of UiO-66, the $Zr_6O_4(OH)_4$ octahedral clusters are connected by BDC linkers to form a 3D framework (Fig. 1-4b). If the Zr based clusters are connected by 4,4'-biphenyl-dicarboxylate (BPDC) linkers, the resulting framework is UiO-67 (Fig. 1-4c). If the linkers are replaced by terphenyl-dicarboxylate (TPDC), then UiO-68 will be obtained (Fig. 1-4d). These Zr based MOFs not only possess the common outstanding properties of MOFs, but also exhibit higher thermostability and chemical stability compared to other types of MOFs.[58] Besides, their band gaps can be changed by replacing different functional groups of the linkers.[155] Among these zirconium based MOFs, UiO-66 has been attracting more and more concerns

(Fig. 1-5). Great research exertions have been made in the applications of UIO-66 for catalysis, hydrogen generation, gas storage, drug delivery, etc.[125, 156-159] More importantly, it was reported that UiO-66 demonstrates high structural stability in water medium,[160, 161] and such stability can even be preserved after incorporating UiO-66 with active functional groups,[59] or introducing missing-linker defects to it.[162] Thus, it should be a propitious strategy to incorporate UiO-66 with other functional materials for the applications in aqueous medium, such as water splitting and water treatment.

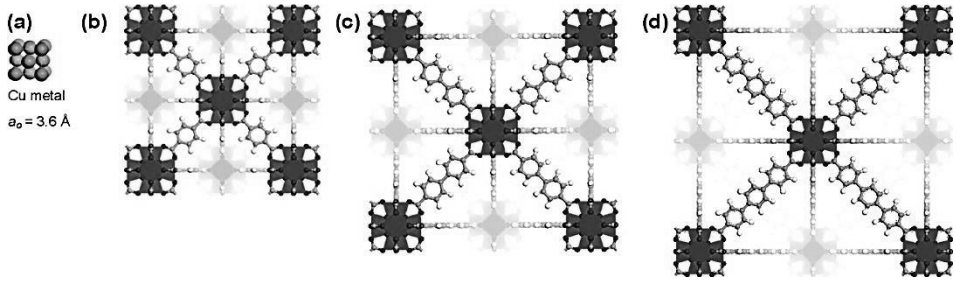

Fig. 1-4 (a) One unit cell of copper drawn to scale with: (b) UiO-66 Zr-MOF with BDC as linker, (c) UiO-67 Zr-MOF with BPDC as linker, (d) UiO-68 Zr-MOF with TPDC as linker.[58]

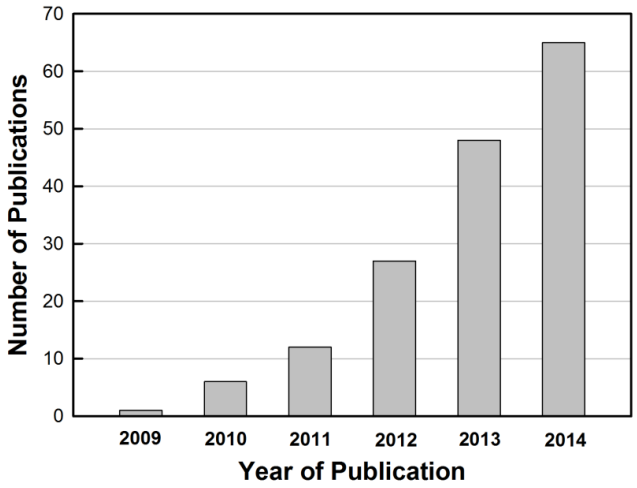

Fig. 1-5 Number of articles published in the past six years pertaining to UiO-66. Data was taken on Jan 7, 2015 from www.scopus.com using "UiO-66" in the fields of Article Title, Abstract and Keywords.

1.3.4.2 The utilization of UiO-66 in water treatment

Due to the superior properties of UiO-66, it is a very promising candidate material for water treatment application. Indeed, some pioneer studies have been reported in this attractive direction. For example, UiO-66 or derived materials have been used for Hg sorption,[163] defluoridation,[164] dye adsorption,[165] selective discrimination of some toxic metal ions,[166] and removal of pyridine.[167] Nevertheless, these water treatment methods cannot degrade the pollutants and make them harmless to the environment. Consequently, more and more studies are focusing on UiO-66 based photocatalytic water treatment, especially on the development of photocatalyst with visible-light activity. Although the relatively wide band gap of UiO-66 may limit its optical absorption in the visible-light range, certain strategies can solve this problem and prepare UiO-66 based visible-light photocatalysts. These strategies include modifying the organic linker with functional groups,[168] or incorporating UiO-66 with narrow band gap semiconductors.[169] Wu's group reported that NH_2-mediated UiO-66 (UiO-66-NH_2) could reduce Cr (VI) in aqueous solution under visible-light irradiation.[170] Although the photocatalyst showed relatively high activity and good reusability, there may not be much practical value of reducing Cr (VI) in the area of water treatment. Thereafter, the same group published a very similar work, in which UiO-66-NH_2 was coupled with graphene, and the composite was also used for Cr (VI) reduction under visible-light irradiation.[171] However, this study also has the same drawback as that of the first work. Then, Wu and co-workers modified UiO-66 with different functional groups to prepare UiO-66-X (X = H, NH_2, NO_2, Br), whose visible-light photocatalytic activities were tested for As (III) oxidation and Cr (VI) reduction in aqueous solution.[172] The results showed

that UiO-66-NH_2 exhibited the highest activity in both tests. It is a systematic work, but indeed there is not breakthrough of photocatalytic activity in this study. Then, Wu's group described a UiO-66-NH_2 anchored with Pd nanoparticles as photocatalyst to degrade MO and MB.[126] However, Cr (VI) had to be introduced into the system in order to promote the degradation process, which is obviously unpractical in water treatment. Very recently, another group reported a UiO-66 derived MOF and used it for the degradation of MO.[173] In this study, the original linker of UiO-66 was replaced by an analog, in which functional groups were introduced. Although this UiO-66 based photocatalyst show an intense adsorption in the visible-light range, UV-light irradiation is required for the photocatalytic experiment. Besides, no data regarding the stability and reusability of the photocatalyst for the MO degradation is reported. Additionally, the photocatalytic mechanism has not been studied. Furthermore, the photocatalytic activity of this catalyst is not very high, implying that it may not be an effective strategy to significantly enhance the photocatalytic activity through direct modification of UiO-66.

1.4 Overview of the thesis

1.4.1 Research gaps of current research

Based on the discussion of existing studies, the research gaps in this rapidly growing area of MOF based photocatalyts in water treatment are summarized as below:

- Compared to physical methods, photocatalysis is more advantageous for water treatment, especially for the degradation of organic pollutants. Additionally, due to its efficient utilization of the solar energy, visible-

light promoted photocatalysis is preferred than those techniques which require UV-light irradiation.

- In some strategy where MOFs are directly modified to obtain enhanced photocatalytic activity, special reagents and/or complicated synthetic procedure are involved. Thus, the target MOFs may need to meet certain special requirements, which can limit their flexibility and even sacrifice part of their excellent properties. At the same time, the cost of producing these special MOFs may also increase, hindering the practical application of the resulting MOFs. Moreover, when being used as photocatalyst for water treatment, most of these directly modified MOFs face certain crucial problems, such as unremarkable photocatalytic activity and dubious stability/reusability.
- The studies on the application of UiO-66 based photocatalyst in water treatment are extremely limited so far. Furthermore, the photocatalytic results of the existing UiO-66 based photocatalysts for water treatment are not very significant. In addition, the function of UiO-66 in different catalytic systems needs to be further investigated.

1.4.2 Objectives

This study aimed to develop novel MOF based photocatalysts for highly efficient visible-light promoted organic dye degradation in water treatment. The specific objectives of this research were to:

- Develop different types of MOF based photocatalysts for high performance dye degradation under visible-light irradiation, and use relatively conventional procedure to facilitate the mass-production of photocatalysts.

- Characterize various parameters of the developed MOF based photocatalysts, evaluate the photocatalytic activity and optimize the composition of the components in the MOF based photocatalysts to achieve the highest photocatalytic activity.
- Evaluate the stability and reusability of these MOF based photocatalysts, and analyze the factors influencing the stability/instability of the photocatalysts.
- Investigate the dye degradation mechanism of the MOF based photocatalysts through introducing different scavengers to compete with the potential active species involved in the degradation process.

1.4.3 Significance and scope

As expounded earlier, visible-light prompted photocatalysis is a highly efficient method for the removal of organic contaminants in wastewater. It is expected that after the photocatalytic process, the organic contaminants in wastewater can be nearly completely degraded, or partially degraded to facilitate the following treatment by other conventional wastewater treatment methods. Besides, compared to other inorganic materials, MOFs are relatively inexpensive and easy to be mass-produced. Therefore, the development of MOF based photocatalyst in this thesis may contribute to the practical applications and also the economic aspect in wastewater treatment. Last but not least, this study is of considerable significance because it opens up numerous opportunities to the development of various MOF based visible-light photocatalysts for water treatment and other related fields in the future.

To develop photocatalyst with remarkable activity for water treatment based on current technologies, this study will not focus on the direct modification of

the MOF materials, and research emphasis will be placed on inorganic active material/MOF composites. Moreover, in the case of a composite consisting of more than one active material and/or more than one MOF substrate, the interactions between these materials will be very complex and thus may be difficult to clarify. Therefore, only a single type of active material will be integrated with one MOF substrate in each of the photocatalyst systems that will be discussed in the following chapters. Moreover, the composition of dyes in real wastewater is very complicated and variable, making the evaluation results unreliable and very challenging to reproduce. Hence, in this thesis, only one commercial organic dye will be chosen as model contaminant to evaluate the activity of the MOF based photocatalysts. In addition, using commercial organic dyes as model contaminants is also a popular method in water treatment studies. Besides, although total degradation is desired, partial degradation of the organic contaminants is still practically beneficial; therefore, this study will not only focus on the total degradation of organic contaminants. Finally, the investigation of the photocatalysis mechanism will be based on qualitative analysis, for quantitative analysis could be very complicated and thus difficult to manage according to the current experimental conditions. Comprehensive investigation on the degradation mechanism will be also beyond the topic of this study.

1.4.4 Arrangement of the thesis

The experimental details of this thesis will be provided in Chapter 2. The development of various UiO-66 based photocatalysts (*i.e.*, Bi_2WO_6/UiO-66 composite, AgI/UiO-66 composite, Ag_2CO_3/UiO-66 composite, and BiOBr/UiO-66 composite) and their applications in water treatment will be

discussed in Chapter 3 to 6. Finally, conclusions and recommendations will be given in Chapter 7.

Chapter 2 Experimental

2.1 Synthesis of UiO-66

In this study, the synthesis of UiO-66 followed two slightly different procedures. The main difference was that acetic acid was added as a modulator in the second synthetic procedure.

2.1.1 Synthesis of UiO-66 with procedure A

The UiO-66 synthesized by procedure A was used in the studies of Bi_2WO_6/UiO-66, AgI/UiO-66, and Ag_2CO_3/UiO-66 composites. In this procedure, UiO-66 was synthesized in *N,N'*-dimethylformamide (DMF) by hydrothermal method following the previous report.[58] Briefly, $ZrCl_4$ (0.053 g, 0.227 mmol) and BDC (0.034 g, 0.227 mmol) were dissolved in DMF (24.9 g, 340 mmol) at room temperature. The obtained mixture was then sealed in a Teflon-lined autoclave and heated in an oven at 120 ℃ for 24 h. The resulting white solid was collected by filtration and thoroughly washed by ethanol.

2.1.2 Synthesis of UiO-66 with procedure B

The UiO-66 synthesized by procedure B was used for the study of BiOBr/UiO-66 composite. In this procedure, UiO-66 was synthesized according to a modified procedure reported previously.[174] Typically, 80.4 mg $ZrCl_4$ (0.345 mmol) and 57.3 mg BDC (0.345 mmol) were dissolved in 40 mL DMF. At the same time, 30 equivalents (with respect to $ZrCl_4$) acetic acid was added as a modulator, and the obtained mixture was stirred at room temperature for 30 min. Thereafter, the mixture was transferred in a 50 mL Teflon-lined autoclave, sealed and heated in an oven at 120 ℃ for 24 h. The resulting white solid was collected by filtration, thoroughly washed by ethanol, and dried in vacuum oven at 80 ℃.

2.2 Characterization techniques

2.2.1 X-ray diffraction

Powder X-ray diffraction (XRD) technique was used to characterize the composition of different samples. The data were collected from a Bruker-AXS D8 DISCOVER with GADDS Powder X-ray diffractometer. The Cu Kα line (λ = 1.5406 Å) was used as the radiation source.

2.2.2 Scanning electron microscopy

Scanning electron microscopy (SEM) was used to examine the morphology of the sample surface. In this study, the sample morphology was characterized by a JEOL FESEM (JSM-6701F) at 5 kV.

2.2.3 Transmission electron microscopy

Transmission electron microscopy (TEM) was used to examine the internal structure of the samples in a more detailed manner. In this study, the sample was characterized by a JEOL TEM (JSM-3010) at 300 kV.

2.2.4 Energy-dispersive X-ray spectroscopy

Energy-dispersive X-ray spectroscopy (EDS/EDX) technique was used to examine the elements distribution in different samples. In this study, EDS data were measured by an Oxford EDS system integrated with the JEOL JSM-6701F FESEM, while EDX data were obtained on an Oxford INCA EDX system integrated with the JEOL JSM-3010 TEM.

2.2.5 Ultraviolet-visible diffuse reflectance

Ultraviolet-visible (UV-Vis) diffuse reflectance technique was used to measure the optical absorption ability of the solid sample at different wavelengths. In this study, the UV-Vis diffuse reflectance spectra were recorded by a Shimadzu UV-2450 UV/VIS spectrometer with an ISR-240A

Integrating Sphere Attachment, with $BaSO_4$ as reference. The band gap energy of the samples was calculated by the following equation:[175]

$$\alpha h\nu = A(h\nu - E_g)^{n/2}$$

where α, ν, E_g, and A are absorption coefficient, light frequency, band gap, and a constant, respectively. n is determined by the optical transition type of the semiconductor (*i.e.*, n equals 1 for direct allowed transition and 4 for indirect forbidden transition). According to the previous reports, UiO-66 and AgI exhibit the character of direct band transition,[176, 177] thus the E_g of pristine UiO-66 and AgI were determined by the plot of $(\alpha h\nu)^2$ versus energy ($h\nu$). At the same time, BiOBr shows the feature of indirect transition.[178] Hence, the E_g of pristine BiOBr and BiOBr/UiO-66 composites were estimated from the plots of $(\alpha h\nu)^{1/2}$ versus energy ($h\nu$).

2.2.6 Specific surface area

The specific surface area of the samples was measured by N_2 adsorption using BET method, and the pore size distributions were calculated by the Barrett-Joyner-Halenda (BJH) equation. N_2 adsorption-desorption isotherms were collected with a Micromeritics Tristar 3000 at liquid nitrogen temperature. The total pore volumes were obtained at $P/P_0 = 0.99$.

2.2.7 Ultraviolet-visible spectroscopy

Ultraviolet-visible (UV-Vis) spectroscopy technique was used to measure the optical absorption ability of the liquid samples at different wavelengths. In this study, the dye concentration during the degradation experiment was measured by a Shimadzu UV-1700 UV/VIS spectrometer.

2.2.8 Fluorescence spectroscopy

Fluorescence spectroscopy technique was used to measure the emission fluorescence intensity at different wavelengths when the samples were excited with light of certain wavelength. In this study, the fluorescence spectra data were measured by a Shimadzu RF-5301PC spectrofluorophotometer.

2.3 Evaluation of the photocatalytic activity

The photocatalytic activity of the catalyst was evaluated by measuring the absorbance of the RhB (Fig. 2-1) solution at 554 nm during the degradation process. For the degradation experiment with different UiO-66 based composites, 15 mg sample was mixed with 30 mL RhB aqueous solution (0.03 mM) in a 50 mL round bottom flask. To reach complete adsorption equilibrium, the mixture was first stirred thoroughly with a magnetic stirrer in dark for 1 h. Afterwards, the suspension was irradiated by a 500 W halogen lamp. A 420 nm cutoff filter (Newport, 65CGA-420) and a water filter were placed between the suspension and the light source to eliminate the UV and infrared irradiation. The irradiation intensity in the center of the flask was measured to be about 82 mW cm^{-2} (for the experiments with AgI/UiO-66, Ag_2CO_3/UiO-66, or BiOBr/UiO-66) or 38 mW cm^{-2} (for the experiment with Bi_2WO_6/UiO-66) by an Ophir Nova II power/energy meter. During the entire process of dye degradation, the solid suspension was under magnetic stirring, and to maintain constant dissolved oxygen content, air was continuously bubbled to the reaction mixture at a rate of 10 mL min^{-1}. At certain time intervals, 0.8 mL aliquots were sampled and centrifuged. The dye concentration of the clear supernatant was then measured by UV-Vis spectroscopy technique. The blank experiment was also handled under the same conditions, but no catalyst was added.

The usage of catalyst in control experiments in different studies is described as below:

- For the degradation experiment of Bi_2WO_6/UiO-66 composite, the control experiment was conducted with the mechanical mixture of pristine UiO-66 and Bi_2WO_6, and the amount of pristine UiO-66 or Bi_2WO_6 was equal to the actual amount of UiO-66 or Bi_2WO_6 contained in BWO/UiO-66-1. All conditions were the same as those in the experiments with other Bi_2WO_6/UiO-66 composites.
- For the degradation experiment of AgI/UiO-66 composite, the control experiment was conducted with the mechanical mixture of pristine UiO-66 and AgI, and the amount of pristine UiO-66 or AgI was equal to the actual amount of UiO-66 or AgI contained in AgI/UiO-66-1. All conditions were the same as those in the experiments with other AgI/UiO-66 composites.
- For the degradation experiment of Ag_2CO_3/UiO-66 composite, the control experiment was conducted with the mechanical mixture of pristine UiO-66 and Ag_2CO_3, and the amount of pristine UiO-66 or Ag_2CO_3 was equal to the actual amount of UiO-66 or Ag_2CO_3 contained in AgCO/UiO-66-0.5. All conditions were the same as those in the experiments with other Ag_2CO_3/UiO-66 composites.
- For the degradation experiment of BiOBr/UiO-66 composite, three control experiments were conducted separately with different catalysts added to the RhB solution, which were the mechanical mixture of pristine UiO-66 and BiOBr, pristine UiO-66, and pristine BiOBr; the amount of pristine UiO-66 or BiOBr was equal to the actual amount of

that in BiOBr/UiO-66-3. All conditions were the same as those in the experiments with other BiOBr/UiO-66 composites.

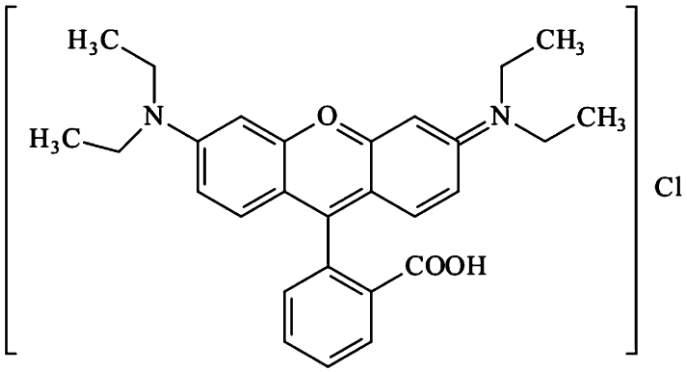

Fig. 2-1 The molecular formula of RhB.

2.4 Investigation of the photocatalytic mechanism

To study the photocatalytic mechanism of the catalyst, isopropyl alcohol (IPA), benzoquinone (BQ), and EDTA were introduced as scavengers for HO•, O_2^-•, and holes (h^+), respectively.[179-181] IPA, BQ, or EDTA was added to the RhB solution to obtain concentrations of 500 mM, 1 mM, or 1 mM before the addition of the catalyst, and all other conditions were remained the same as those used in the photodegradation experiment. For the experiment with N_2 purging, air was replaced by N_2 to bubble in the suspension at the same rate with other conditions unchanged. The potential HO• formed on the surface of the catalyst composite was detected by the photoluminescence technique, in which terephthalic acid was used as a probe molecule.[182] The detection process was similar to the evaluation of photocatalytic activity, except that RhB solution was replaced by 30 mL aqueous solution of 5×10^{-4} M terephthalic acid and 2×10^{-3} M NaOH. During light irradiation, 0.8 mL reaction solution was sampled at selected timing to measure the fluorescence intensity at 425 nm by Fluorescence spectroscopy technique with the excitation wavelength of 315 nm. The catalysts used for photocatalytic mechanism investigations were

BWO/UiO-66-1 for the study on Bi_2WO_6/UiO-66 composite, AgI/UiO-66-1 for the study on AgI/UiO-66 composite, AgCO/UiO-66-0.5 for the study on Ag_2CO_3/UiO-66 composite, and BiOBr/UiO-66-3 for the study on BiOBr/UiO-66 composite.

Chapter 3 Bi_2WO_6 incorporated zirconium metal-organic framework composite with enhanced visible-light photocatalytic performance

3.1 Introduction

As a narrow band gap semiconductor material, bismuth tungstate (Bi_2WO_6) has been intensively used for the degradation of organic contaminants under visible-light irradiation.[183, 184] Currently, the major strategies to improve the photocatalytic activity of Bi_2WO_6 are synthesizing Bi_2WO_6 with specially designed morphology,[185, 186] and incorporating it with another semiconductor.[187, 188] Nevertheless, photocatalysts based on Bi_2WO_6/MOF composites have not been reported yet. Due to the superior properties of Bi_2WO_6 and UiO-66, the composite is expected to exhibit enhanced visible-light photocatalytic activity and good stability.

In this study, a Bi_2WO_6 incorporated UiO-66 composite is prepared as photocatalyst for the application of highly efficient dye degradation in water treatment. This Bi_2WO_6/UiO-66 composite is prepared by a simple hydrothermal method, and good interfacial interaction is formed between the two semiconductor materials based on the ingeniously designed procedure. The activity of the Bi_2WO_6/UiO-66 composite is evaluated for the degradation of RhB under visible-light irradiation as test reaction, and the mechanism of the photocatalysis is also investigated.

3.2 Preparation of Bi_2WO_6/UiO-66 composites

A series of Bi_2WO_6/UiO-66 composites with varying Bi_2WO_6 contents were prepared based on the molar ratio of Bi : Zr. The formula of UiO-66

is reported as $Zr_{24}O_{120}C_{192}H_{96}$.[58] To prepare a Bi_2WO_6/UiO-66 composite with a Bi : Zr molar ratio of 1 : 1 (denoted as BWO/UiO-66-1), 30.4 mg (0.092 mmol) $Na_2WO_4 \cdot 2H_2O$ was dissolved in 10 mL deionized water (DI water) by vigorous stirring. 50 mg (7.7×10^{-3} mmol) UiO-66 was then added, and the resulting mixture was kept stirring for 1 h. Thereafter, 89.3 mg (0.184 mmol) $Bi(NO_3)_3 \cdot 5H_2O$ was dissolved in 10 mL DMF, and this $Bi(NO_3)_3$ DMF solution was added to the UiO-66 prepared as described in step 1. The reaction precursor was then stirred for another 30 min, and transferred to a 25 mL autoclave. Subsequently, the autoclave was sealed and heated in an oven at 120 ℃ for 12h. Finally, the solid product was collected by filtration, and washed several times with DI water. Other composites with Bi : Zr molar ratios of 0.1 : 1 (denoted as BWO/UiO-66-0.1), 0.5 : 1 (denoted as BWO/UiO-66-0.5), 2 : 1 (denoted as BWO/UiO-66-2) were also prepared through a similar procedure by adjusting the amount of the precursors for Bi_2WO_6. Pristine Bi_2WO_6 was also synthesized by the same procedure, excluding the addition of UiO-66.

3.3 Results and discussion

3.3.1 Material characterization

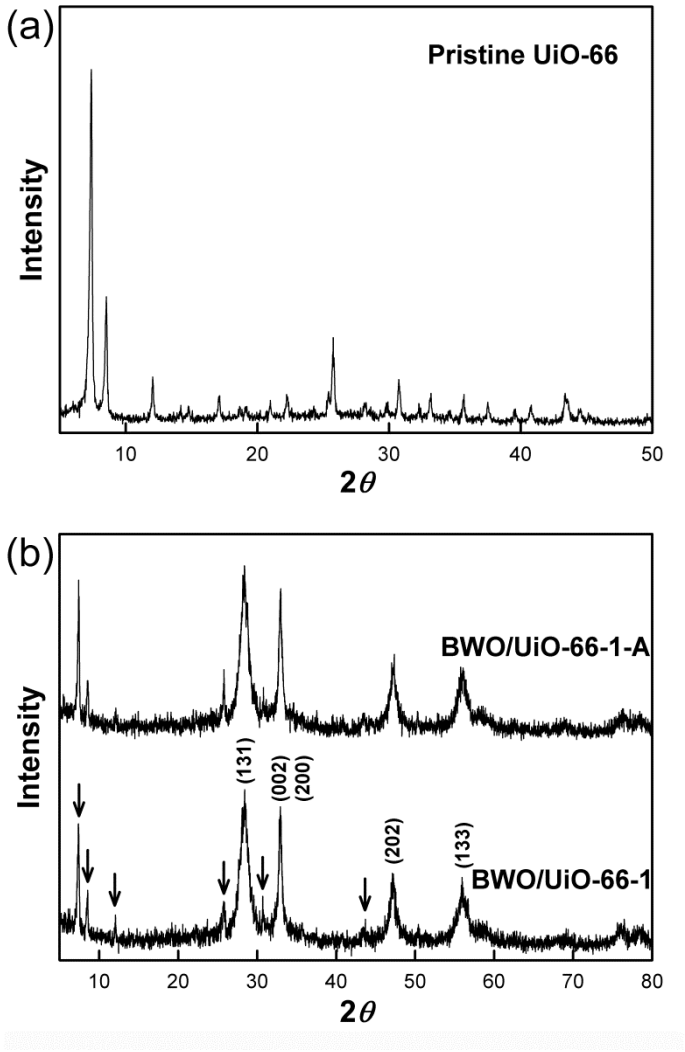

Fig. 3-1 XRD patterns of (a) UiO-66, (b) BWO/UiO-66-1, and BWO/UiO-66-1 after RhB degradation experiment (denoted as BWO/UiO-66-1-A). In the pattern of BWO/UiO-66-1, the peaks belonging to UiO-66 were indicated by arrows.

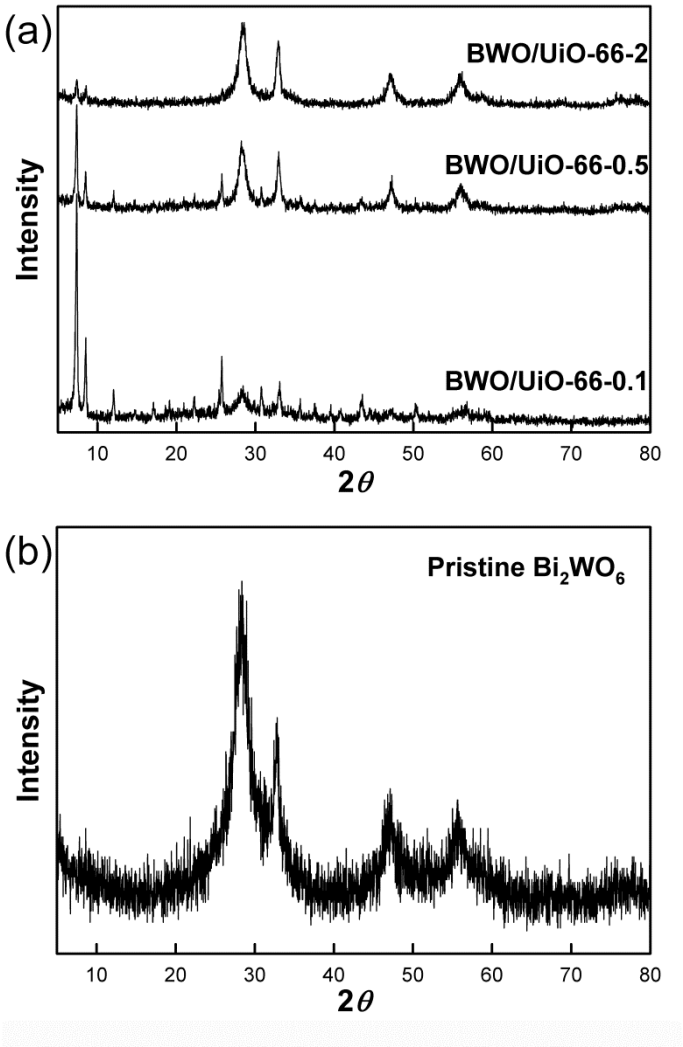

Fig. 3-2 XRD patterns of (a) BWO/UiO-66-0.1, BWO/UiO-66-0.5, BWO/UiO-66-2, and (b) pristine Bi_2WO_6.

To confirm the composition of Bi_2WO_6/UiO-66, samples with different Bi_2WO_6 contents were characterized by XRD. Fig. 3-1a shows the XRD pattern of the pristine UiO-66 sample. The pattern is consistent with that reported in the literature,[58] indicating the successful synthesis of UiO-66. After incorporation of Bi_2WO_6, most of the peaks characteristic for UiO-66 can still be clearly identified in all composites, suggesting that the UiO-66 remained intact after the incorporation of Bi_2WO_6 during the hydrothermal synthesis process (Fig. 3-1b, Fig. 3-2a). This should be due

to the superior stability of UiO-66 as mentioned before, which further confirms that UiO-66 is one of the most suitable porous materials to incorporate with Bi_2WO_6. In addition, all of the Bi_2WO_6/UiO-66 composites display good crystallinity and show sharp diffraction peaks corresponding to Bi_2WO_6 (JCPDS: 73-1126). The result implies that crystallized Bi_2WO_6 was successfully obtained in the current synthetic conditions. Also, with the increase in Bi_2WO_6 content in the composite, the diffraction peaks of UiO-66 weakened, while the peaks belonging to Bi_2WO_6 became correspondingly more intense. This could be due to the suppression of the diffraction peaks of UiO-66 by those of Bi_2WO_6, which become dominant in the composites with the increase in Bi : Zr ratio. Pristine Bi_2WO_6 was also synthesized under the same experimental conditions as that of BWO/UiO-66-1, excluding the addition of UiO-66. As shown in Fig. 3-2b, pristine Bi_2WO_6 was also successfully synthesized. Besides, the width of the diffraction peaks of pristine Bi_2WO_6 was slightly broader than that of BWO/UiO-66-1, indicating a smaller crystallite size of Bi_2WO_6 in the pristine sample.

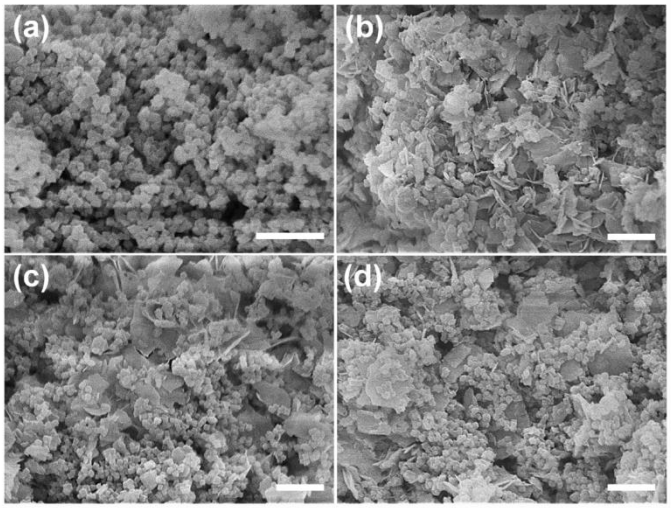

Fig. 3-3 SEM images of (a) pristine UiO-66, (b, c) BWO/UiO-66-1, and (d) BWO/UiO-66-1 after RhB degradation experiment (scale bars are 500 nm).

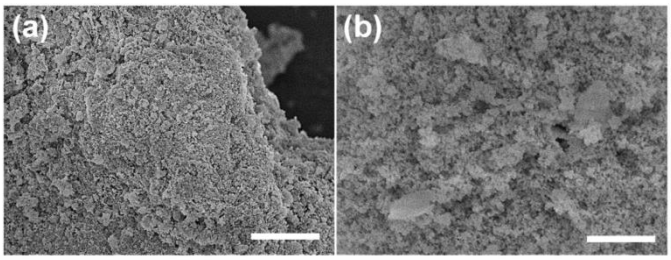

Fig. 3-4 SEM images of pristine Bi_2WO_6 (scale bars are 5 μm in (a), and 500 nm in (b)).

Fig. 3-3a shows the SEM image of pristine UiO-66. The UiO-66 nanoparticles exhibit nanocube morphology, and the size of the nanoparticles is less than 100 nm. However, the exact dimension of these nanocubes cannot be identified from the SEM image. Fig. 3-3b and 3-3c show the SEM images of BWO/UiO-66-1, from which the UiO-66 nanoparticles can be clearly distinguished. This result is also in line with that of XRD characterization, suggesting that the structure of UiO-66 was conserved in the obtained Bi_2WO_6/UiO-66 composites. It can be easily observed that there are many nanoplates inserted among the UiO-66 nanoparticles, and the dimension of these nanoplates is larger than a few

hundred nanometers. It is believed that these nanoplates are Bi_2WO_6, which was further confirmed by EDX. These Bi_2WO_6 nanoplates are uniformly dispersed in the UiO-66 nanoparticles, and it is expected that such a pattern might facilitate the interaction between Bi_2WO_6 and UiO-66. A Bi_2WO_6 crystalline structure with nanoplate morphology was also reported by other researchers.[189-191] However, the SEM images of pristine Bi_2WO_6 (Fig. 3-4) showed that instead of nanoplates, only nanoparticles were obtained.

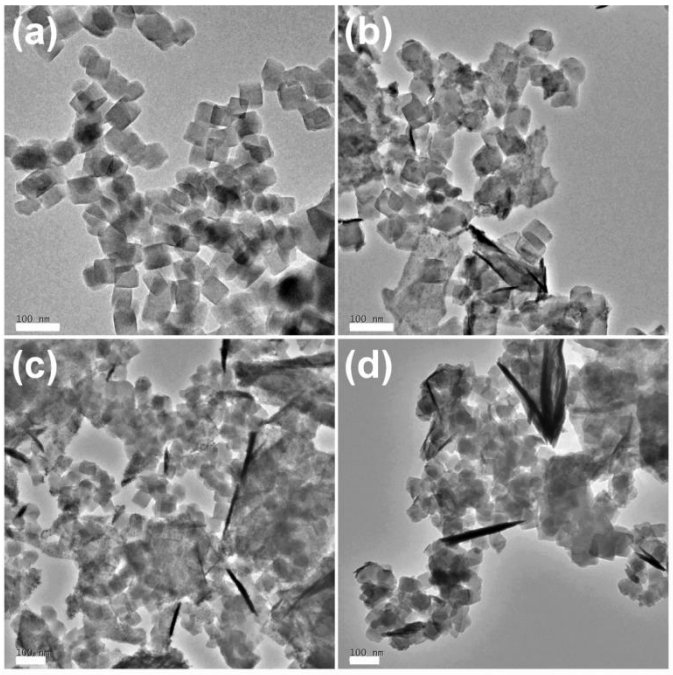

Fig. 3-5 TEM images of (a) pristine UiO-66, (b, c) BWO/UiO-66-1, and (d) BWO/UiO-66-1 after RhB degradation experiment (scale bars are 100 nm).

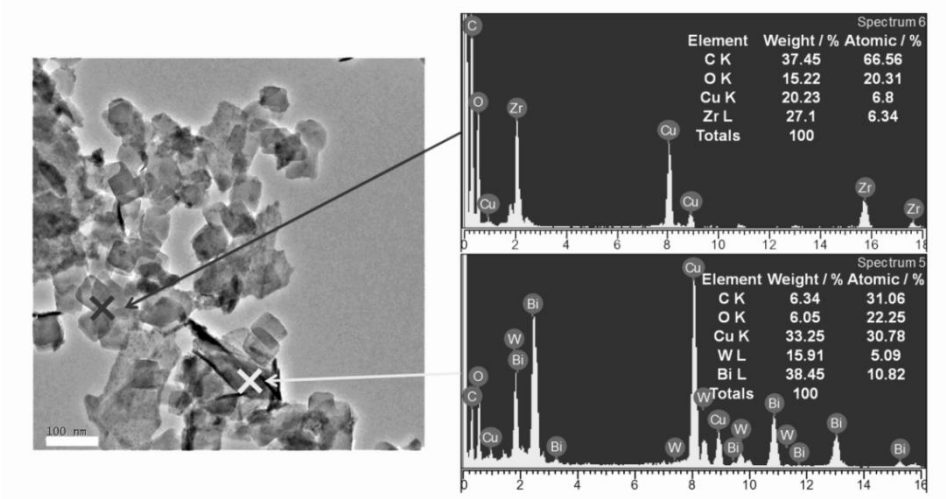

Fig. 3-6 EDX spectra of the corresponding measure spots in the TEM image of BWO/UiO-66-1 (scale bar is 100 nm). Inserts in the spectra show the contents of corresponding elements (copper element is due to the TEM grid).

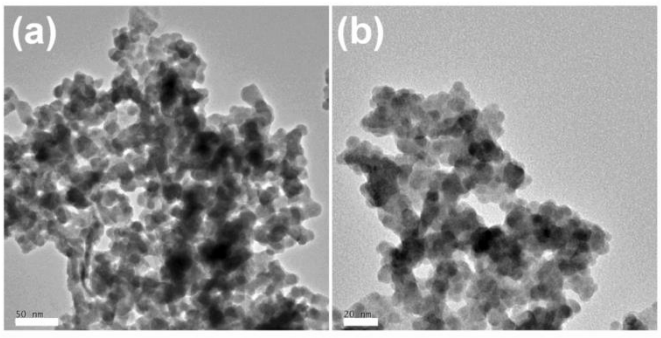

Fig. 3-7 TEM images of pristine Bi_2WO_6 (scale bars are 50 nm in (a), and 20 nm in (b)).

The morphology of pristine UiO-66, Bi_2WO_6 and BWO/UiO-66-1 was also characterized by TEM. As shown in Fig. 3-5a, the UiO-66 nanoparticles display uniform nanocube morphology, which is in agreement with the result of SEM characterization. The size of these UiO-66 nanocubes is around 50 nm. After the incorporation of Bi_2WO_6 (Fig. 3-5b, 3-5c), the UiO-66 nanocubes can still be clearly identified, in agreement with the results of XRD and SEM. Noticeably, the nanoplate structure of Bi_2WO_6 is also observed in the TEM images of the BWO/UiO-66-1 sample. Additionally, small spot EDX was used to

analyse the composition of the nanocubes and nanoplates (Fig. 3-6). Only the metal element Zr was found in the EDX result of the nanocubes, demonstrating that these nanocubes should be UiO-66. In addition, the nanoplates should be consisted of Bi_2WO_6, proved by the dominant metal elements Bi and W observed in the EDX result of the nanoplates. Moreover, the atomic ratio of Bi : W roughly equals 2 : 1, consistent with the formula of Bi_2WO_6. Interestingly, the morphology of the pristine Bi_2WO_6 is small nanoparticles (Fig. 3-7), which is quite different from that of the Bi_2WO_6 component in the BWO/UiO-66-1. These nanoparticles are relatively uniform, and the size is less than 20 nm. It is proposed that the existence of UiO-66 affects the growth process of the Bi_2WO_6 crystals, meaning that the Bi_2WO_6 crystals may selectively grow in certain directions in the presence of UiO-66, leading to the formation of the nanoplate morphology. In contrast, in the absence of UiO-66, it is much more likely for Bi_2WO_6 to grow unrestricted and form the nanoparticle morphology.

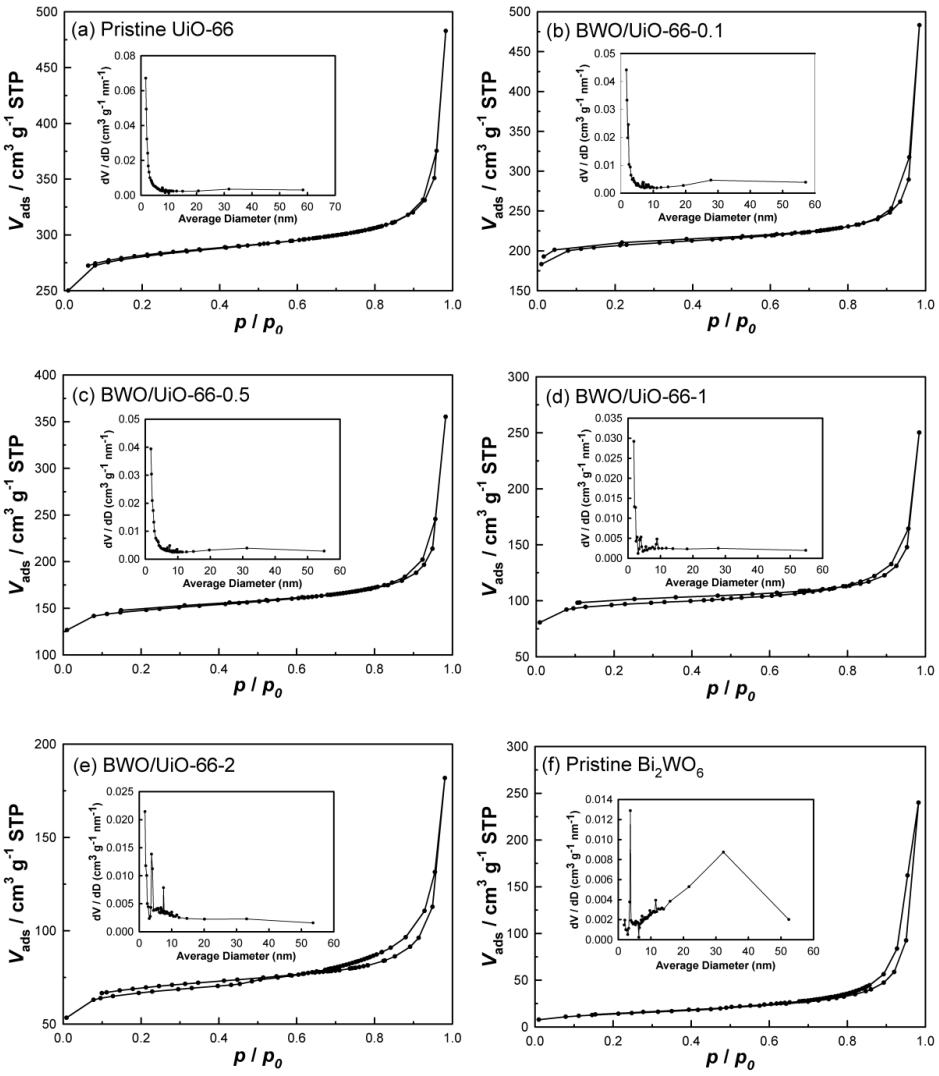

Fig. 3-8 Nitrogen adsorption-desorption isotherms and pore size distributions (inset) of (a) pristine UiO-66, (b) BWO/UiO-66-0.1, (c) BWO/UiO-66-0.5, (d) BWO/UiO-66-1, I BWO/UiO-66-2, and (f) pristine Bi_2WO_6.

The specific surface areas of the Bi_2WO_6/UiO-66 composites, and pristine UiO-66 and Bi_2WO_6 were evaluated by N_2 adsorption. The pore size distributions of these samples were calculated by the BJH equation. The results are listed in Table 3-1, and the figures of adsorption-desorption isotherms and pore size distributions are shown in Fig. 3-8. The specific surface area of the pristine UiO-66 obtained in this study is 808 m^2 g^{-1}. Although this value is slightly lower than some model

examples, such as 1069 m^2 g^{-1} [176] and 1110 m^2 g^{-1},[192] it is comparable the values cited by other studies, *e.g.*, 700 m^2 g^{-1} [174] or 850 m^2 g^{-1}.[193] Note that no moderator, such as acetic acid,[162, 174] was added during the synthesis of UiO-66 in this study, and the synthesis conditions were not optimized, either. Increasing Bi_2WO_6 content leads to a decrease of the specific surface areas of the composites. The specific surface area of the pristine Bi_2WO_6 is relatively low, less than 50 m^2 g^{-1}. The total pore volumes of the composites were also lower after introduction of Bi_2WO_6.

Table 3-1 Comparison of the properties (*i.e.*, Bi : Zr ratio, specific surface area and total pore volume) and photocatalytic activity (reaction rate constant) of different catalyst samples and blank experiment.

Sample	Bi : Zr Ratio[a]	Specific surface area[b] / m^2 g^{-1}	Total pore volume[c] / cm^3 g^{-1}	Reaction rate constant (k)[d] / min^{-1}
BWO/UiO-66-0.1	0.1 : 1	583.9	0.75	0.0090
BWO/UiO-66-0.5	0.5 : 1	363.6	0.55	0.0159
BWO/UiO-66-1	1 : 1	275.1	0.39	0.0226
BWO/UiO-66-2	2 : 1	198.3	0.28	0.0104
Pristine UiO-66	–	807.7	0.75	0.0062[e]
Pristine Bi_2WO_6	–	48.3	0.37	
Blank[f]	–	–	–	0.0001

[a] The Bi : Zr ratios were molar ratios, and were determined based on the reaction precursor. [b] The specific surface areas were evaluated by the BET method. [c] The total pore volumes were obtained at P/P_0 = 0.99. [d] The reaction rate constants (k) were calculated based on a pseudo-first-order kinetic model. [e] The reaction rate constant of the control experiment was obtained from the mixture of pristine UiO-66 and Bi_2WO_6, and the amount of UiO-66 or Bi_2WO_6 was equal to the actual amount of that contained in BWO/UiO-66-1. [f] In the blank degradation experiment, no catalyst was added.

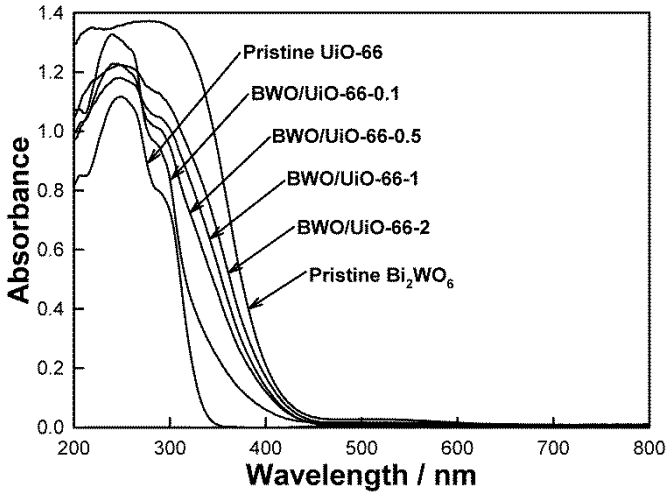

Fig. 3-9 UV-Vis diffuse reflectance spectra of pristine UiO-66, pristine Bi_2WO_6, and Bi_2WO_6/UiO-66 composites with different Bi_2WO_6 contents.

The optical absorption of different Bi_2WO_6/UiO-66 composites, and pristine UiO-66 and Bi_2WO_6 samples was measured by UV-Vis. As illustrated in Fig. 3-9, UiO-66 is transparent in the wavelength range from 350 to 800 nm, which is in line with the result that UiO-66 only absorbed UV-light.[176] Similar to the pristine Bi_2WO_6, all of the Bi_2WO_6/UiO-66 composites have an absorption edge at about 450 nm, demonstrating that these composites all possess some visible-light absorption ability. Therefore, these Bi_2WO_6/UiO-66 composites should be capable of utilizing visible-light energy.

3.3.2 Photocatalytic activity

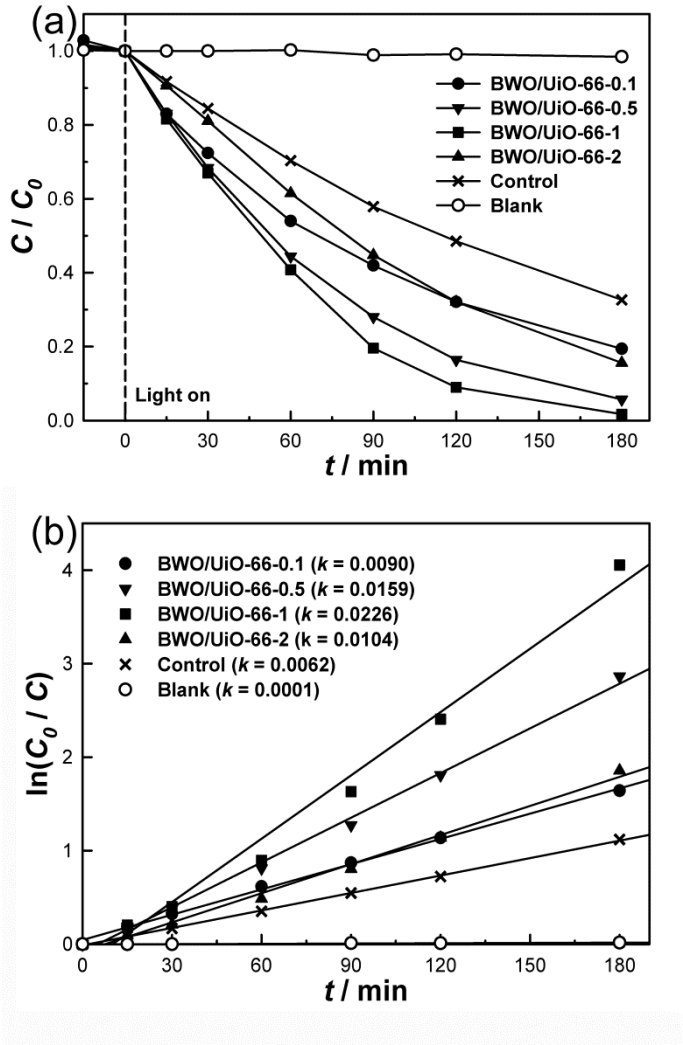

Fig. 3-10 (a) Photocatalytic degradation of RhB in the presence and absence (blank) of different catalysts (BWO/UiO-66-0.1, BWO/UiO-66-0.5, BWO/UiO-66-1, and BWO/UiO-66-2) under visible-light irradiation. For the control experiment (mechanical mixture of pristine UiO-66 and pristine Bi_2WO_6), the amount of pristine UiO-66 or Bi_2WO_6 was equal to the actual amount of that in BWO/UiO-66-1. (b) Comparison of the reaction rate constant (*k*) in the presence of different catalysts (assuming that the reactions follow the pseudo-first-order kinetic model).

The photocatalytic activities of the Bi_2WO_6/UiO-66 composites were evaluated by using them for the degradation of RhB in aqueous solution under visible-light irradiation. In the control experiment, RhB was degraded in the presence of a mechanical mixture of pristine UiO-66 and Bi_2WO_6 (where the amount of UiO-66 and Bi_2WO_6 was equal to the

amount used in the BWO/UiO-66-1 composite). The blank experiment (*i.e.*, without catalyst) was performed under the same conditions as in the other RhB degradation experiments. As illustrated in Fig. 3-10a, the BWO/UiO-66-1 sample exhibits the fastest degradation rate, and RhB was almost completely degraded in 180 min. In the control experiment, although the pristine UiO-66 and Bi_2WO_6 mixture show some activity, the degradation rate is the lower compared to those of the composites. To quantify the photocatalytic activities of these samples, the reaction rate constants (k) for RhB degradation were calculated, assuming that the reactions follow a pseudo-first-order kinetic model (Table 3-1 and Fig. 3-10b).[194] By comparing the reaction rate constants, it is clearly seen that the photocatalytic activity of the Bi_2WO_6/UiO-66 composite increases when the Bi : Zr ratio is enhanced from 0.1 : 1 to 1 : 1. The BWO/UiO-66-1 sample with Bi : Zr ratio equaling 1 : 1 shows the highest photocatalytic activity. However, when the Bi : Zr ratio is increased further to 2 : 1, the photocatalytic activity of the composite drops drastically, and is almost the same as that of the composite with Bi : Zr ratio of 0.1 : 1. The pristine UiO-66 and Bi_2WO_6 mixture in the control experiment exhibits the lowest photocatalytic activity of all the photocatalyst samples prepared for this study. This suggests that there is a cooperative synergism between the Bi_2WO_6 and UiO-66 in the composites. This good interaction may be attributed to the ingeniously designed preparation strategy, which will be discussed below. In the control experiment with mechanical mixing, it is expected that no such good interaction could form. Therefore, compared to those of the specially

prepared composites, the photocatalytic activity of the sample in the control experiment is much lower. Also note that the photolysis of RhB in the absence of any catalyst is negligible (Fig. 3-10a, blank).

3.3.3 Photocatalyst stability

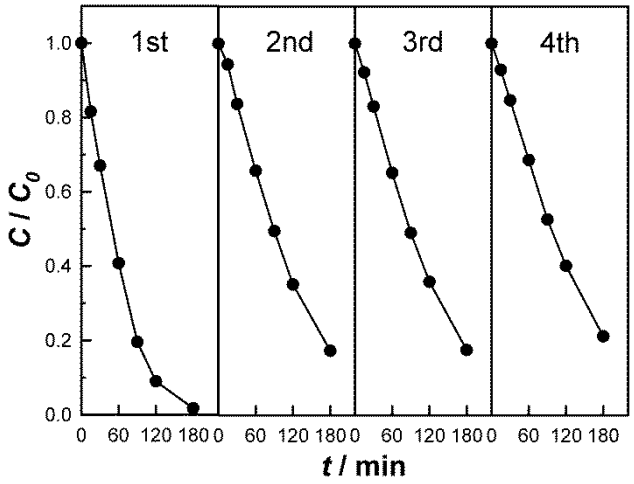

Fig. 3-11 Four cycles of the RhB degradation in the presence of BWO/UiO-66-1 under visible-light irradiation.

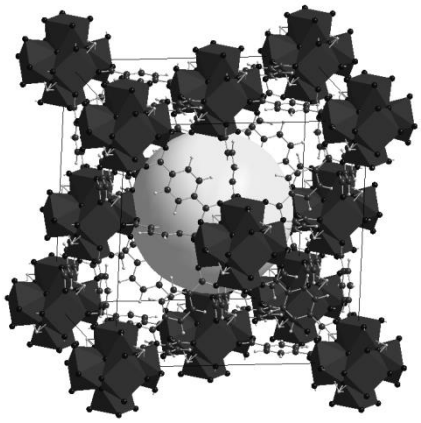

Fig. 3-12 Crystal structural illustration of UiO-66. The large sphere represents the enclosed cavity.

The structure of BWO/UiO-66-1 was characterized before and after 180 min of RhB degradation to assess its stability under the current experimental conditions. As shown in Fig. 3-1b, no apparent variation in the XRD patterns of BWO/UiO-66-1 is observed before and after RhB degradation. The comparison

of the SEM images of BWO/UiO-66-1 before (Fig. 3-3b, 3-3c) and after (Fig. 3-3d) RhB degradation also indicates that there is no observable morphology change. Furthermore, the same conclusion can also be obtained based on comparison of the TEM figures of the same sample before (Fig. 3-5b, 3-5c) and after (Fig. 3-5d) the degradation experiment. The stability and reusability of BWO/UiO-66-1 were further studied by reusing the composite for four cycles of dye degradation experiments. As illustrated in Fig. 3-11, the activity of the catalyst decreased in the second cycle. A possible explanation is that part of the degradation products might be adsorbed or trapped in the pores of the composite. These stuck molecules would reduce the accessible surface area of the catalyst, leading to the decline of its activity.[195] Fortunately, most surface area of the composite was still accessible after the first degradation experiment, since more than 80% of the dye was degraded in the second degradation cycle. Furthermore, no obvious loss of photocatalytic stability can be observed in the third and fourth cycles, which implies the excellent stability of the Bi_2WO_6/UiO-66 photocatalyst. The superior stability of UiO-66 and the excellent stability of Bi_2WO_6 both contribute to the stability of this Bi_2WO_6/UiO-66 composite. The stability of Bi_2WO_6 under various degradation conditions was also reported by other researchers.[184, 185] However, it is worth to mention that the good interaction between Bi_2WO_6 and UiO-66 in this composite might be another important factor contributing to the stability of the photocatalyst. To achieve this effect, highly crystalline UiO-66 was first obtained, and the order of addition of the reagents is important. During the preparation process of the Bi_2WO_6/UiO-66 composites, UiO-66 was first dispersed in the aqueous solution of Na_2WO_4. Since the $Zr_6O_4(OH)_4$ octahedra (dark grey clusters shown in Fig.

3-12) are positively charged, it is foreseen that an electrostatic interaction will occur between these octahedral and the negatively charged WO_4^{2-} anions.[176] Therefore, the WO_4^{2-} anions accumulate around the UiO-66 framework structure, and then react with the next reagent (*i.e.*, $Bi_2O_2^{2+}$ cations),[185, 189] resulting in the incorporation of Bi_2WO_6 to the UiO-66 framework structure during the synthesis process.

3.3.4 Photocatalytic mechanism

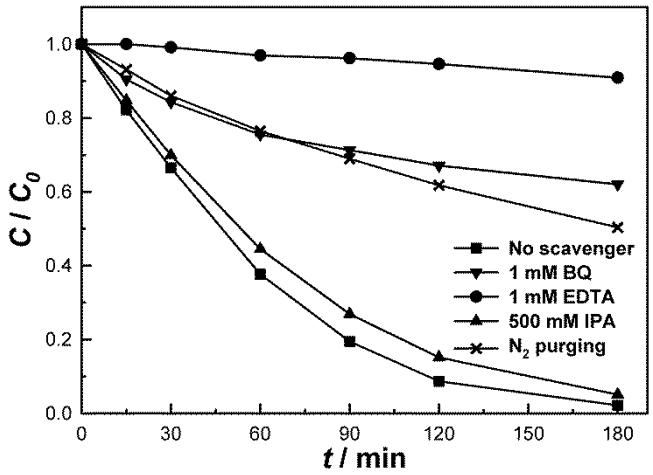

Fig. 3-13 Effects of different scavengers and N_2 purging on the degradation of RhB in the presence of BWO/UiO-66-1 under visible-light irradiation.

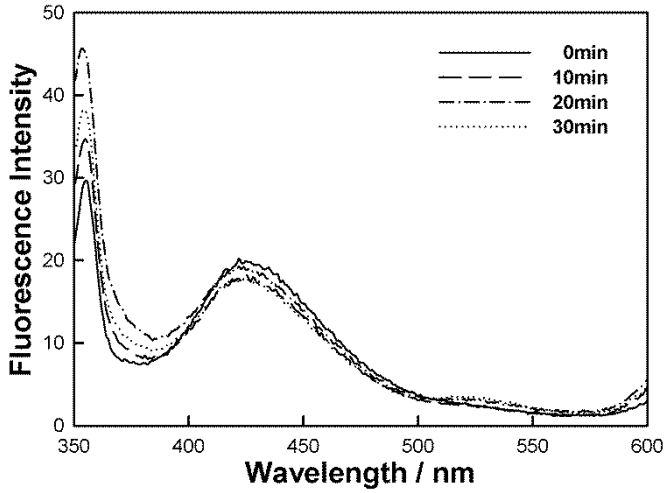

Fig. 3-14 Photoluminescence spectral changes with visible-light irradiation time in the presence of BWO/UiO-66-1 in a 5×10^{-4} M basic solution of terephthalic acid.

To understand the photocatalytic mechanism of this Bi_2WO_6/UiO-66 photocatalyst system for the degradation of RhB, the potential roles of HO•, O_2^-•, and h^+ during the degradation process were investigated. These are the three species mostly responsible for initiating the photocatalytic oxidation.[5, 19, 196, 197] To identify the contributions of these different species, IPA, BQ, and EDTA were introduced in the degradation process separately to attempt to trap HO•, O_2^-•, and h^+, respectively.[179-181] As shown in Fig. 3-13, the introduction of IPA, a scavenger of HO•, does not cause any significant change in the RhB degradation rate. This implies that HO• is not an important active species for the photocatalytic process. To further confirm this result, the HO• generated on the surface of the photocatalyst was detected by a photoluminescence technique, in which terephthalic acid was used as a probe molecule.[182] As illustrated in Fig. 3-14, during the 30 min monitoring process, no obvious change in photoluminescence intensity is observed, demonstrating that almost no HO• was formed by the Bi_2WO_6/UiO-66 photocatalyst under visible-light irradiation. This further supports the conclusion that HO• radicals do not dominate the photodegradation of RhB by the Bi_2WO_6/UiO-66 photocatalyst. However, the introduction of BQ obviously decreases the degradation rate of RhB (Fig. 3-13). Since BQ is able to quench O_2^-•, this result suggests that O_2^-• should be one of the major contributors to the decomposition of RhB. Considering that the dissolved O_2 is the crucial reagent to form O_2^-•, N_2 was purged instead of air in a control experiment to study its effect on the change in degradation rate. As shown in Fig. 3-13, N_2 purging also has a negative effect on the degradation rate, and the

result is very similar to that of the experiment in the presence of BQ. Thus, it is established that O_2^{-}• is an important active species for RhB degradation in the current Bi_2WO_6/UiO-66 system. Nevertheless, BQ addition and N_2 purging could only partially suppress the degradation reaction, implying that RhB was also decomposed by other routes. To understand the mechanism further, EDTA was added to the reaction system to trap h^+. Only very limited degradation of RhB was observed in the presence of EDTA. Since the addition of EDTA accelerates the surface recombination of e^- and h^+, this effect also decreases e^- generation in the conduction band, resulting in the suppression of the generation of O_2^{-}•. Hence, by cutting off the formation of O_2^{-}• and h^+ at the same time, the degradation of RhB was almost totally restrained. Therefore, in the Bi_2WO_6/UiO-66 photocatalyst system, RhB can also be oxidized by the photogenerated h^+. The result that O_2^{-}• and h^+ are the two main active species for the Bi_2WO_6 based photocatalyst system was also confirmed by other research groups.[184, 198]

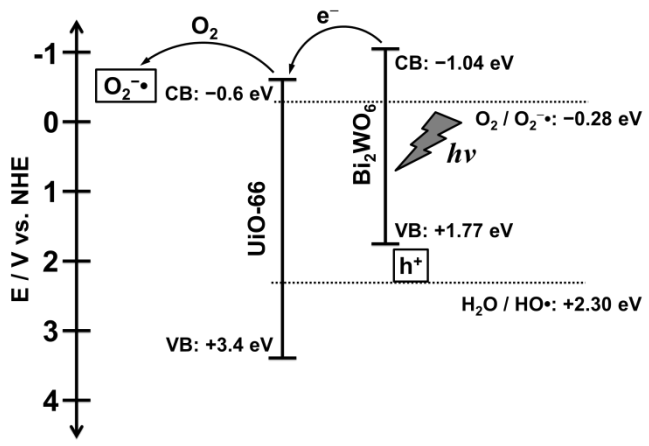

Scheme 3-1 Proposed mechanism of photocatalytic degradation of RhB by the Bi_2WO_6/UiO-66 composite under visible-light irradiation.

According to the reported properties of UiO-66 and Bi_2WO_6, a possible photocatalytic mechanism of the Bi_2WO_6/UiO-66 photocatalyst is proposed and shown in Scheme 3-1.[125, 176, 199] Based on this mechanism, Bi_2WO_6/UiO-66 may promote the separation of the photogenerated electron-hole pairs, which explains the enhanced photocatalytic activity. Note that the photogenerated e^- in the conduction band of UiO-66 is negative enough to react with dissolved O_2 to form O_2^{-}•. Meanwhile, although the h^+ generated on the valence band of Bi_2WO_6 is not positive enough to react with H_2O to form HO•, they can still directly oxidize RhB. This proposed photocatalytic mechanism also supports the conclusion of the investigation of active species.

3.4 Conclusion

In summary, UiO-66 was incorporated with Bi_2WO_6 by a simple hydrothermal method. The developed Bi_2WO_6/UiO-66 composite exhibited enhanced photocatalytic activity for the degradation of RhB under visible-light irradiation, compared to the mechanical mixture of the individual UiO-66 and Bi_2WO_6. It is proposed that the enhancement of the activity is due to the good interaction between Bi_2WO_6 and UiO-66, by which the photogenerated electron-hole pairs can be efficiently separated. Furthermore, the ingenious preparation strategy is the critical step to achieve the intimate combination of Bi_2WO_6 and UiO-66. In addition, by adjusting the Bi_2WO_6 content in the Bi_2WO_6/UiO-66 composite, a molar ratio of Bi : Zr equaling 1 : 1 was found to be optimum for the composite to achieve the highest photocatalytic activity. This Bi_2WO_6/UiO-66 photocatalyst also exhibited good stability, since no obvious changes in the structure and morphology were observed after a

complete degradation experiment and most of the activity was reserved in the long-term degradation. The mechanism of photocatalytic degradation of RhB by the Bi_2WO_6/UiO-66 composite was also investigated, and the results implied that O_2^{-}• and h^+ were two main active species involving in the degradation process of RhB.

Chapter 4 Enhanced photocatalytic activity of AgI/UiO-66(Zr) composite for rhodamine B degradation under visible-light irradiation

4.1 Introduction

Recently, silver halides (AgX, X = Cl, Br, I) modified on different substrates have been used as photocatalysts for the degradation of various organic dyes due to their high photocatalytic activity.[200-203] In these studies, the substrate supported photocatalysts all demonstrated high efficiency and good stability. In particular, AgI is the subject of many studies into visible-light induced degradation of organic dyes.[204-207] Typically, AgI is coupled with another semiconductor material to obtain a composite with higher photocatalytic activity, and the resulting composites also exhibited satisfactory stability during the photocatalytic degradation process. Despite the good photocatalytic activity of pristine AgI under visible-light irradiation, the specific surface area of the material is normally quite low unless the surface morphology is specifically controlled. However, the morphology control strategies to obtain AgI with large specific surface area are relatively complex, and surfactant is usually needed in the synthetic process.[208, 209] Hence, to maximize the inherent potential of AgI as an catalyst for water treatment, it is critically important to develop a suitable substrate capable of supporting AgI and simplifying the synthesis of AgI. The desired properties for the substrate are high specific surface area, high water stability and good structural stability. In addition, its synthesis should be straightforward, and it should be able to form strong interactions with AgI. UiO-66 has many of the required properties, and could be an ideal substrate for AgI in the photocatalyst preparation.

In this study, a AgI conjugated UiO-66 photocatalyst is prepared. UiO-66 is used as the substrate because of its high specific surface area and outstanding stability in aqueous medium. AgI crystals are in-situ synthesized on the UiO-66 framework by a simple solution method. The activity of the AgI/UiO-66 photocatalyst is evaluated by the degradation of RhB under visible-light irradiation, and the stability of the photocatalyst is investigated through various characterization methods. Moreover, the photocatalytic mechanism is also studied.

4.2 Preparation of AgI/UiO-66 composites

Four AgI/UiO-66 composites with different AgI contents were prepared. AgI content was controlled by adjusting the precursor of AgI based on the molar ratio of Ag : Zr in the final composite. The structural formula of UiO-66 is reported as $Zr_{24}O_{120}C_{192}H_{96}$.[58] For the preparation of a AgI/UiO-66 composite with Ag : Zr molar ratio equal (1 : 1) (denoted as AgI/UiO-66-1), 30.6 mg (0.184 mmol) KI was dissolved in 9.1 mL DI water. Then, with vigorous stirring, 50 mg (7.7×10^{-3} mmol) UiO-66 was added to the KI solution. After stirring for 1 h, 0.922 mL 0.2 M $AgNO_3$ aqueous solution (containing 0.184 mmol $AgNO_3$) was added to the above UiO-66 mixture dropwise. The total reaction mixture was about 10 mL, and was kept stirring at room temperature for 12 h. Afterward, the product was collected by filtration, washed thoroughly several times with DI water, and finally dried in vacuum at 80 ℃. AgI/UiO-66 composites with Ag : Zr molar ratios of (0.1 : 1) (denoted as AgI/UiO-66-0.1), (0.5 : 1) (denoted as AgI/UiO-66-0.5), and (2 : 1) (denoted as AgI/UiO-66-2) were also prepared following a similar procedure by changing the amount of the precursor for AgI.

Pristine AgI was also synthesized following the same procedure, except the addition of UiO-66.

4.3 Results and Discussion

4.3.1 Material characterization

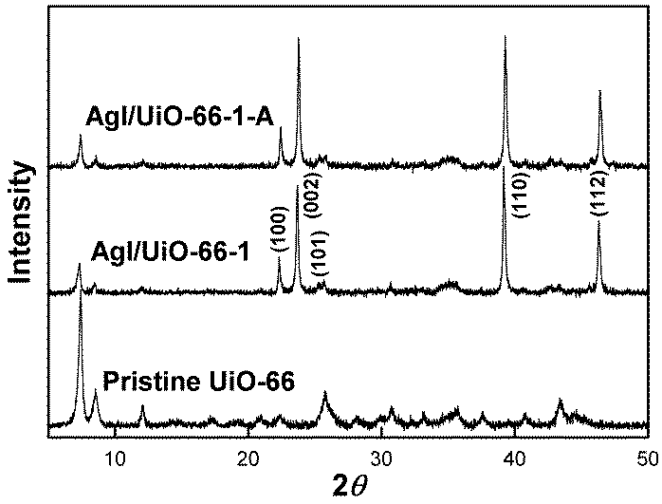

Fig. 4-1 XRD patterns of pristine UiO-66, AgI/UiO-66-1, and AgI/UiO-66-1 after RhB degradation experiment (denoted as AgI/UiO-66-1-A).

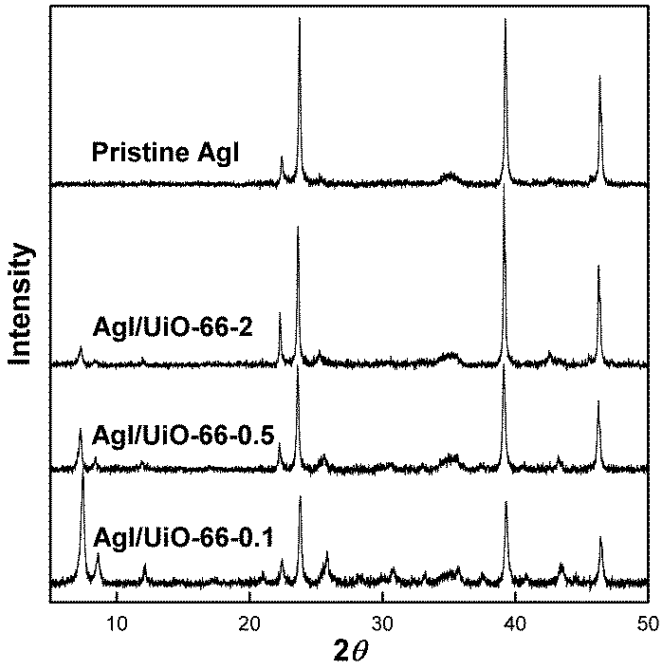

Fig. 4-2 XRD patterns of AgI/UiO-66-0.1, AgI/UiO-66-0.5, AgI/UiO-66-2, and pristine AgI.

The composition of different samples was characterized by XRD. As illustrated in Fig. 4-1, the diffraction pattern of pristine UiO-66 is consistent with that reported in the literature,[58] confirming the successful synthesis of UiO-66. Besides, compared to pristine UiO-66, all the AgI/UiO-66 composites show a few new diffraction peaks (Fig. 4-1 and Fig. 4-2 in Supporting Information). These peaks are not only consistent with those of pristine AgI, but also those of β-AgI crystals (JCPDS: 09-0374). It is reported that high reaction temperature can lead to a gradual transformation from β-AgI to α-AgI, and the latter possesses much lower photocatalytic activity.[208] Thus, in the current study, AgI was synthesized at room temperature in order to prevent the generation of α-AgI. Note that the main peaks characteristic for UiO-66 can still be clearly identified in the reflection patterns of all the AgI/UiO-66 composites, indicating that UiO-66 remained intact after the conjugation of AgI. As the contents of AgI increase in the AgI/UiO-66 composites, the reflection peaks of AgI heighten since AgI becomes the dominant component. On the contrary, the reflection peaks belonging to UiO-66 weaken correspondingly, but several strong peaks are still distinguishable even in the XRD pattern of AgI/UiO-66-2 sample.

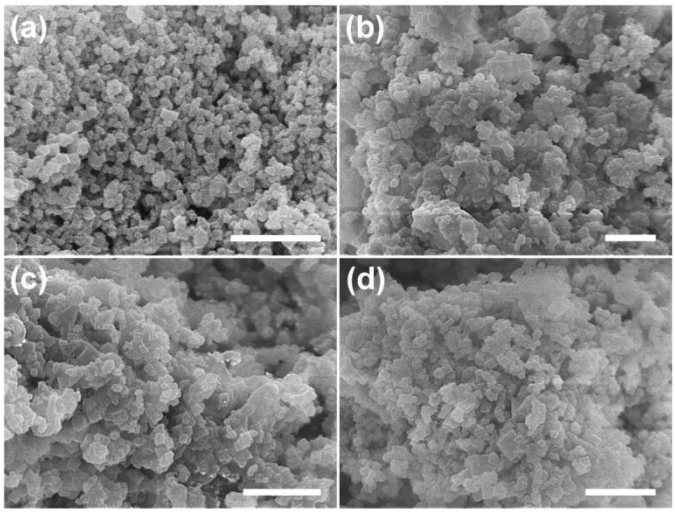

Fig. 4-3 SEM images of (a) pristine UiO-66, (b, c) AgI/UiO-66-1, and (d) AgI/UiO-66-1 after RhB degradation experiment (scale bars are 500 nm).

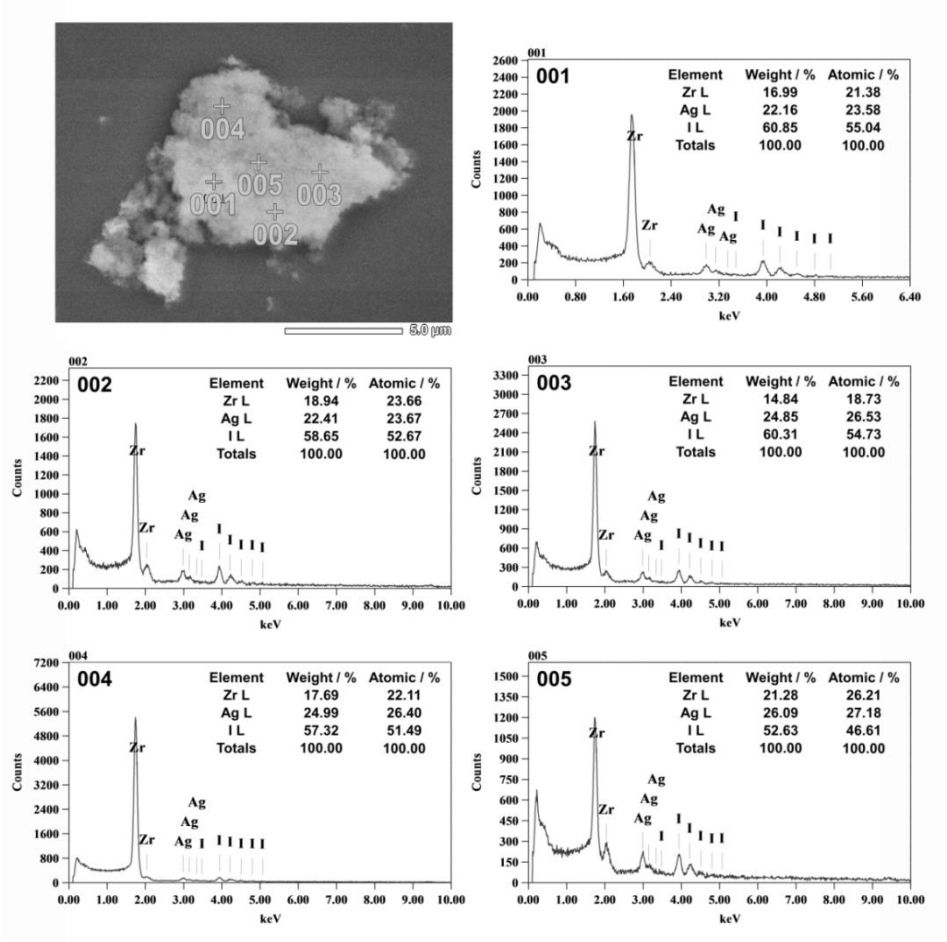

Fig. 4-4 EDS spectra of the corresponding measuring spots in the SEM image of AgI/UiO-66-1 (scale bar is 5.0 μm). Inserts in the spectra (001-005) show the contents of corresponding elements.

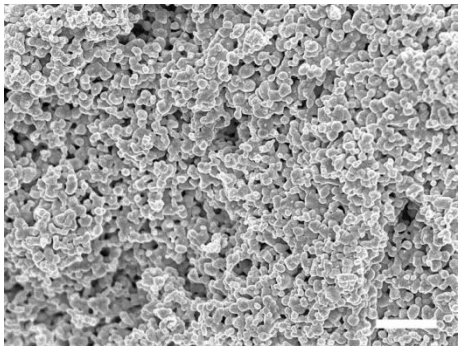

Fig. 4-5 SEM images of pristine AgI (scale bar is 2 μm).

Fig. 4-3a and Fig. 4-3b, 4-3c show the SEM images of pristine UiO-66 and freshly prepared AgI/UiO-66-1. The pristine UiO-66 appears as separate and uniform particles, and the size of these particles is less than 100 nm. After the conjugation of AgI, most of the interspace among the UiO-66 nanoparticles is filled by an inserting material and as such, the UiO-66 nanoparticles are glued together by the filling material. This filling material is believed to be AgI, confirmed by the result of small spot EDS. The composition of the selected five spots at different positions of a chunk of AgI/UiO-66-1 sample was analyzed. As illustrated in Fig. 4-4, element Zr, Ag and I are found at all of these positions, indicating that the sample uniformly consist of UiO-66 and AgI. Thus, the filling material, by which UiO-66 nanoparticles are bonded together, should be AgI. Moreover, at most of these positions, the atomic ratios of Ag : Zr roughly equal (1 : 1), further confirming the uniformity of the AgI/UiO-66-1 sample. Note that the morphology of pristine AgI is particles with size between 200 nm to 500 nm (Fig. 4-5). Most of these AgI particles are bonded together to form a porous structure.

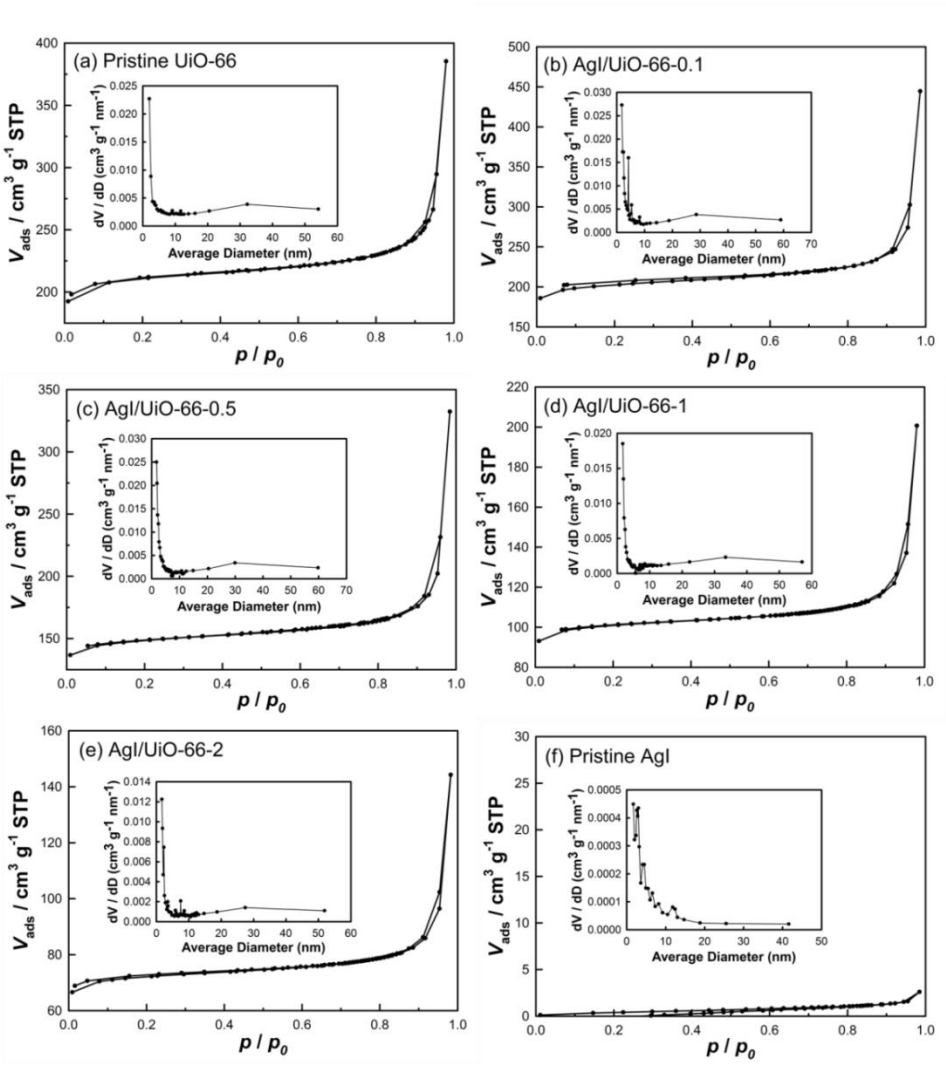

Fig. 4-6 Nitrogen adsorption-desorption isotherms and pore size distributions (inset) of (a) pristine UiO-66, (b) AgI/UiO-66-0.1, (c) AgI/UiO-66-0.5, (d) AgI/UiO-66-1, (e) AgI/UiO-66-2, and (f) pristine AgI.

N_2 adsorption was used to evaluate the specific surface areas of pristine UiO-66 and AgI, and the AgI/UiO-66 composites. The pore size distributions of these samples were calculated by the BJH equation. The adsorption-desorption isotherms and pore size distributions are shown in Fig. 4-6, and the results are listed in Table 4-1. Although the specific surface area of UiO-66 obtained in this study (808 m^2 g^{-1}) is slightly lower than that reported by others, such as 1069 m^2 g^{-1} and 1110 m^2 g^{-1},[176, 192] it is comparable to the value cited in recent studies, *e.g.*, 700 m^2 g^{-1} or 850 m^2 g^{-1}.[174, 193] It has to be noted that

no moderator, such as acetic acid,[162, 174] was added during the synthesis of UiO-66 in this study, and that the synthesis conditions were not optimized. The specific surface areas of the composites decrease with the increase of AgI content in the UiO-66/AgI composite. This is caused by the low specific surface area of AgI of only 2.5 $m^2 g^{-1}$, compared to that of UiO-66. The same trend is reflected in the total pore volume, which rapidly decreases with increasing AgI content.

Table 4-1 Comparison of the properties (i. e., Ag : Zr ratio, specific surface area and total pore volume) and photocatalytic activity (reaction rate constant) of different catalyst samples and blank experiment.

Sample	Ag : Zr ratio[a]	Specific surface area[b] / $m^2 g^{-1}$	Total pore volume[c] / $cm^3 g^{-1}$	Reaction rate constant (k)[d] / min^{-1}
AgI/UiO-66-0.1	0.1 : 1	558.1	0.69	0.0545
AgI/UiO-66-0.5	0.5 : 1	427.6	0.51	0.0645
AgI/UiO-66-1	1 : 1	288.6	0.31	0.0706
AgI/UiO-66-2	2 : 1	214.6	0.22	0.0664
Pristine UiO-66	–	807.7	0.75	0.0294[e]
Pristine AgI	–	2.5	0.004	
Blank[f]	–	–	–	0.0001

[a] The Ag : Zr ratios were molar ratios, and were determined based on the reaction precursor. [b] The specific surface areas were evaluated by the BET method. [c] The total pore volumes were obtained at P/P_0 = 0.99. [d] The rate constants (k) were calculated based on a pseudo-first-order kinetic model. [e] The reaction rate constant of the control experiment was obtained from the mechanical mixture of pure UiO-66 and AgI, where the amount of UiO-66 or AgI was kept equal to the actual amount of contained in the AgI/UiO-66-1 composite. [f] For the blank degradation experiment, no catalyst was added.

Based on the results of morphology characterization and specific surface area measurement, the relationship between AgI and UiO-66 in the composite can be illustrated in Scheme 4-1. At first, the initially generated AgI attaches on the surface of UiO-66, forming an outer AgI layer (Scheme 4-1a, 4-1b). With the increase in the AgI content, more AgI is generated and deposited on top of the earlier AgI layer, which not only increases the thickness of the AgI layer, but also glues the UiO-66 particles together (Scheme 4-1c). If the AgI content is further enhanced, it is possible that the excess AgI aggregates on the composite surface, and blocks the pore structure in the composite (Scheme 4-1d). Hence, the specific surface area and the total pore volume of the composite are expected to decrease with increasing AgI content.

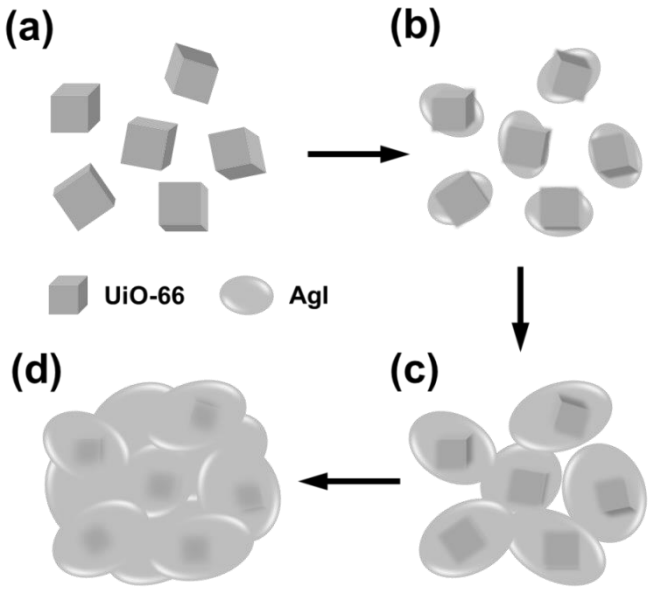

Scheme 4-1 Illustration of AgI conjugated UiO-66 composite with increasing AgI content from (a) to (d).

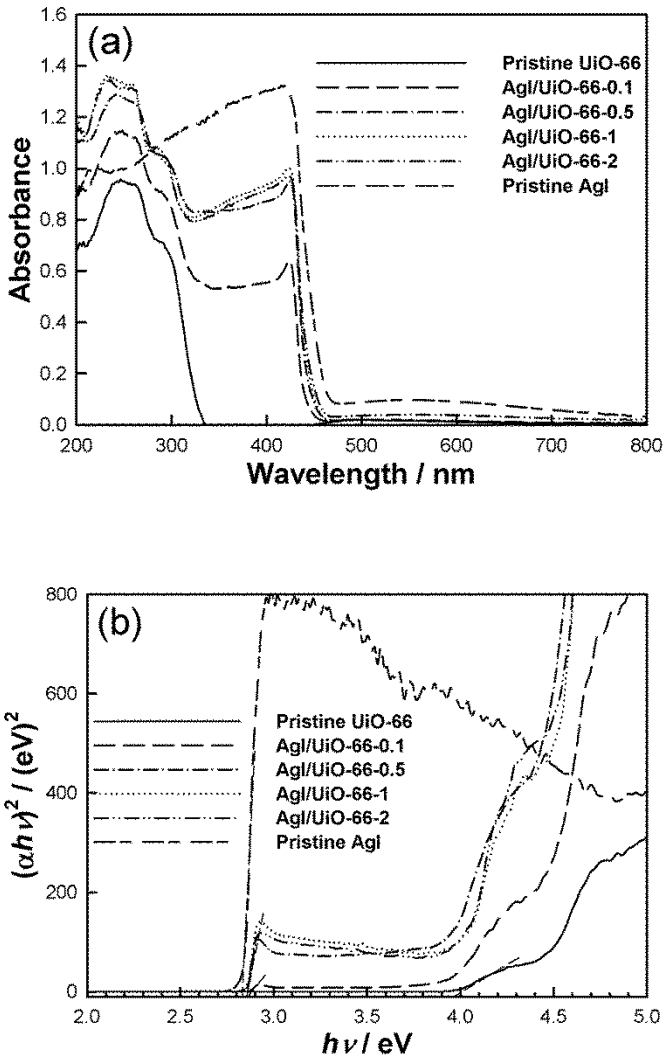

Fig. 4-7 (a) UV-vis diffuse reflectance spectra, and (b) plots of $(\alpha h\nu)^2$ versus energy ($h\nu$) to obtain the band gap energy of the samples.

The UV-vis diffuse reflectance spectra of different samples were obtained to investigate the change of the absorption spectrum with composition. As shown in Fig. 4-7a, pristine AgI has an absorption edge at about 470 nm, so that the absorption extends well into the visible spectral range. However, pristine UiO-66 is transparent between 340 nm and 800 nm, so that it can only be excited with photon energies in the UV range. However, all the AgI/UiO-66 composites in which varying contents of AgI were conjugated with UiO-66, have an absorption edge at about 460 nm, demonstrating that these samples all possess

good visible-light absorption ability. The band gap energies (E_g) of these samples were extrapolated from the spectra. According to Fig. 4-7b, the E_g of pristine AgI and UiO-66 are about 2.83 eV and 4.0 eV, very similar to the reported values.[155, 176, 200] The band gaps E_g of all the AgI/UiO-66 composites are around 2.86 eV, implying their ability to utilize the visible-light energy.

4.3.2 Photocatalytic activity

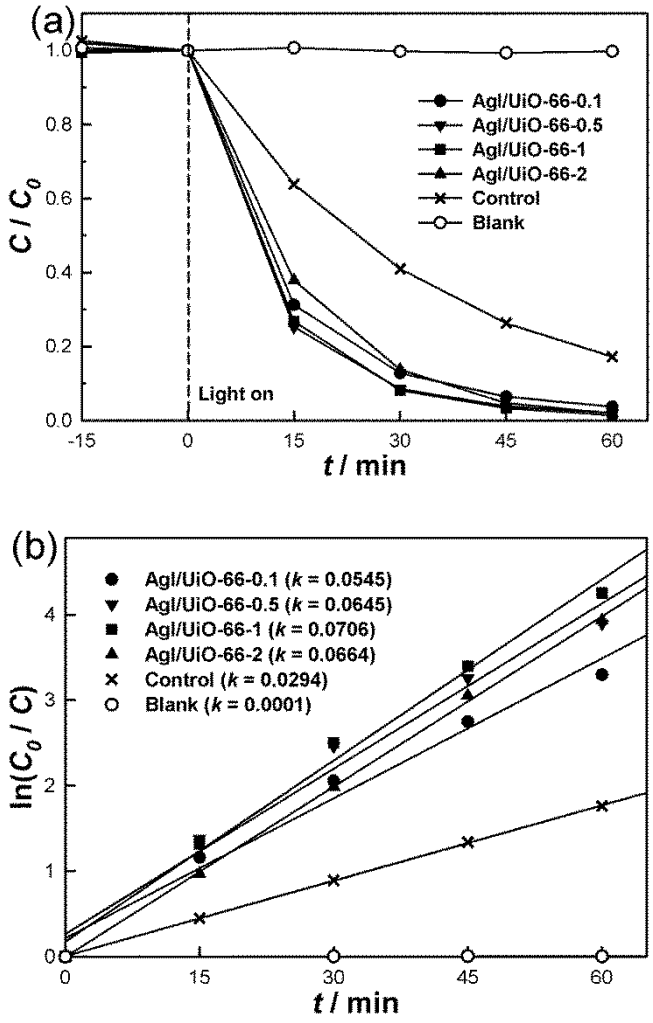

Fig. 4-8 (a) Photocatalytic degradation of RhB in the presence and absence (blank) of different catalysts (AgI/UiO-66-0.1, AgI/UiO-66-0.5, AgI/UiO-66-1, and AgI/UiO-66-2) under visible-light irradiation. For the control experiment (mechanical mixture of UiO-66 and AgI), the amount of pristine UiO-66 or AgI was equal to the actual amount of that in AgI/UiO-66-1. (b) Comparison of the reaction rate constant (k) in the presence of different catalysts (assuming that the reactions follow the pseudo-first-order kinetic model).

The photocatalytic activities of the AgI/UiO-66 composites were evaluated from their degradation efficiency of RhB in aqueous solution under visible-light irradiation. In a control experiment, the RhB solution was irradiated in the presence of a mechanical mixture of pristine UiO-66 and AgI, where the amounts were equal to those contained in the composite AgI/UiO-66-1. A blank experiment without any catalyst was also performed under the same conditions as in the other RhB degradation experiments. As illustrated in Fig. 4-8a, all the AgI/UiO-66 composites show high activity, and RhB was almost completely degraded in 60 min. However, it is difficult to decide which composite possesses the highest photocatalytic activity, especially in the case of AgI/UiO-66-0.5 and AgI/UiO-66-1. Hence, the RhB degradation rates of the AgI/UiO-66 composites were compared in terms of the reaction rate constants (k), which were calculated assuming that all the reactions follow a pseudo-first-order kinetic model (Fig. 4-8b).[194] The results are listed in Table 4-1, together with the results of the control and blank experiments. By comparing the reaction rate constants, it is clearly seen that the photocatalytic activity of the AgI/UiO-66 composites increases when the Ag : Zr ratio increases from (0.1 : 1) to (1 : 1). However, the activity begins to decline when the Ag : Zr ratio is further increased to (2 : 1). Thus, the AgI/UiO-66-1 sample with Ag : Zr ratio equaling (1 : 1) possesses the highest photocatalytic activity. The degradation rate in the control experiment was lower than that of any AgI/UiO-66 composite, although the amounts of UiO-66 and AgI added to the reaction system were equal to those in the degradation experiment with AgI/UiO-66-1. The blank experiment shows that the photolysis of RhB in the absence of any catalyst is negligible (Fig. 4-8a, blank).

The photocatalytic activity of the AgI/UiO-66 composite is primarily affected by two factors, the AgI content in the composite and the specific surface area. Although the increase of AgI content contributes to the enhancement of photocatalytic activity, the specific surface area of the composite declines when more and more AgI is incorporated, as demonstrated previously by the BET data. The decrease in specific area hinders the effective contact between the composite and the RhB solution. When the Ag : Zr ratio increases from (0.1 : 1) to (1 : 1), although the specific surface area of the composite decreases due to the increase in AgI content, the photocatalytic activity of the AgI/UiO-66 composite shows 29.5% increase, from 0.0545 min^{-1} to 0.0706 min^{-1} (Table 4-1). The reason may be that before Ag : Zr ratio reaching (1 : 1), most of the AgI surface is still accessible, resulting in the formation of more active sites on the surface of the AgI/UiO-66 composite. Hence, the photocatalytic activity of the composite is enhanced due to the increase of the AgI active sites involved in the degradation process. However, as the Ag : Zr ratio is further increased to (2 : 1), the excess AgI aggregates on the surface of the composite, and blocks the accessible pore structure of the composite, causing the decrease in the amount of AgI active sites. In the control experiment, the same amounts of AgI and UiO-66 are introduced, but the degradation rate is much lower. This can be attributed to the low specific surface area of the pristine AgI. Without the mediation of UiO-66, the synthesized AgI will aggregate together, so that the obtained pristine AgI has low specific surface area and thus few active sites. Indeed, the specific surface area of pristine AgI is only 2.5 $m^2 g^{-1}$, compared to 288.6 $m^2 g^{-1}$ for the AgI/UiO-66-1 composite (Table 4-1). Therefore, in this AgI/UiO-66 composite, UiO-66 acts as a support that leads to high dispersion

of the AgI, increase the amount of AgI active sites, and thus enhance the photocatalytic activity of AgI. The important role of UiO-66 is based on the good interaction between the AgI and UiO-66, which will be discussed below. In summary, to achieve the highest photocatalytic activity for the RhB degradation, the molar ratio of Ag : Zr in the AgI/UiO-66 composite is optimized to be (1 : 1).

4.3.3 Photocatalyst stability

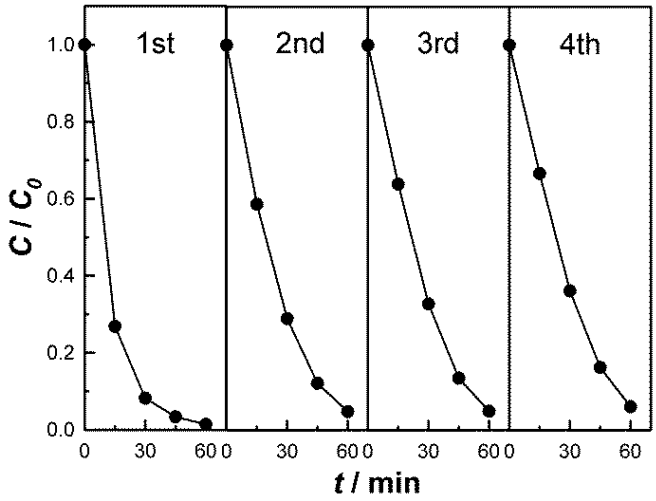

Fig. 4-9 Four cycles of the RhB degradation in the presence of AgI/UiO-66-1 under visible-light irradiation.

The structural stability of the AgI/UiO-66 photocatalyst was evaluated by XRD and SEM. As shown in Fig. 4-1, after the RhB degradation experiment, the reflection peaks of the AgI/UiO-66-1 composite are almost the same as those of the freshly prepared material, indicating that the crystalline structure of AgI/UiO-66-1 did not change during the RhB degradation. Moreover, the SEM images do not show any obvious change in the morphology before (Fig. 4-3b, 4-3c) and after (Fig. 4-3d) the RhB degradation. The cubic morphology of the UiO-66 particles conjugated with AgI is completely retained. Thus, the structure of the AgI/UiO-66 composite can effectively endure the degradation process in

the current study. The stability of AgI/UiO-66-1 was further studied by collecting the composite after dye degradation and then reusing it for another cycle (Fig. 4-9). In the second cycle, the degradation rate decreased slightly, but the catalyst still exhibits high activity, and more than 95% RhB can be degraded during the 1 h degradation experiment. With regard to the decrease of degradation rate, a possible explanation is that part of the degradation products generated in the first degradation cycle might be adsorbed or trapped in the porous structure of the composite, leading to the reduction of active sites accessible by other dye molecules.[195] Apparently, the decrease of active sites limits the number of dye molecules the catalyst could simultaneously interact with, so the degradation rate declines. However, the activity of the catalyst deteriorated only slightly, which may be ascribed to the high activity of the unblocked AgI active sites. It is worth noting that no further decrease in the degradation rate was observed for the third and fourth degradation cycles, which provides clear evidence that the AgI/UiO-66 composite has good stability on long term degradation. Moreover, the degraded solution was filtrated and analyzed by inductively coupled plasma (ICP), and no Zr or Ag was detected, which further suggests the stability of the composite. It is not difficult to attribute the good structural stability of the AgI/UiO-66 composite to the outstanding stability of UiO-66. However, the good interaction between AgI and UiO-66 is another important factor that may contribute to the stability of the final composite. To achieve this effect, during the preparation of the AgI/UiO-66 composites, iodide salt was first added in the UiO-66 aqueous suspension. Because of the positively charged $Zr_6O_4(OH)_4$ octahedra (dark grey clusters shown in Fig. 3-12), electrostatic interactions could occur between

these octahedral and the negatively charged iodide ions.[176] Thus, the iodide ions accumulated in the UiO-66 framework structure, and then reacted with the next reagent (*i.e.* silver ions), leading to the generation of AgI around the UiO-66 framework structure. It is anticipated that this in-situ synthesized AgI should adhere very well to the UiO-66 framework. In addition, UiO-66 has been reported as a semiconductor material, which might accept photogenerated electrons from AgI.[115, 176] Therefore, it is expected that the good interaction between AgI and UiO-66 might facilitate the electron transfer from AgI to UiO-66 to some extent. This effect could prevent the corrosion of AgI by the photogenerated electrons and further contribute to the stability of the AgI/UiO-66 photocatalyst.

4.3.4 Photocatalytic mechanism

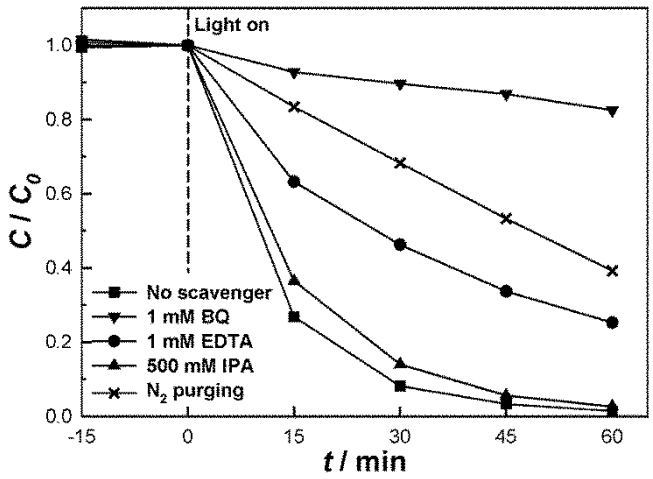

Fig. 4-10 Effects of different scavengers and N_2 purging on the degradation of RhB in the presence of AgI/UiO-66-1 under visible-light irradiation.

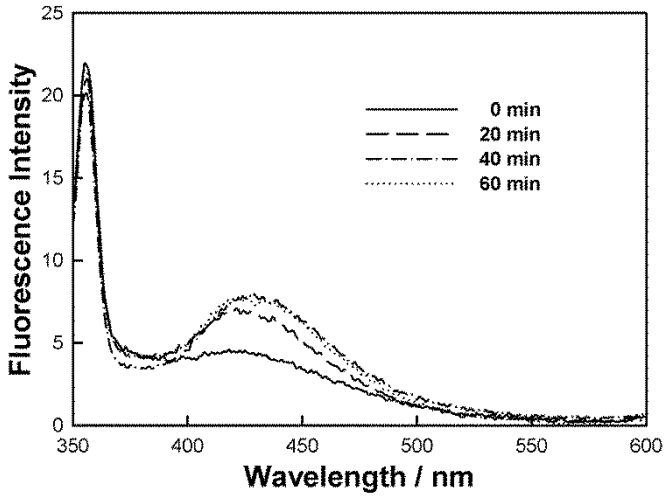

Fig. 4-11 Photoluminescence spectral changes with visible-light irradiation time in the presence of AgI/UiO-66-1 in a 5×10^{-4} M basic solution of terephthalic acid.

It is known that HO•, O_2^-• and h^+ are the three main active species involved in the photocatalytic oxidation process.[5, 19, 196, 197] To further investigate the photocatalytic mechanism of RhB degradation through the AgI/UiO-66 composite, IPA, BQ, and EDTA were introduced in the degradation process to attempt to trap HO•, O_2^-• and h^+, respectively.[179-181] Fig. 4-10 shows the effect of these scavengers as well as of N_2 purging on the photocatalytic activity of AgI/UiO-66-1. There was no significant effect on the degradation rate when IPA was added, suggesting that HO• is not a dominant active species in the degradation process. This was further confirmed by the photoluminescence technique, where terephthalic acid is used as a probe molecule to monitor the generating of HO• on the surface of the catalyst.[182] As shown in Fig. 4-11, although there is very slight increase in the fluorescence signal during the first 20 min, no more signal change is observed after 40 min and 60 min irradiation. This further verifies that HO• is not an important contributor for the RhB degradation. However, the degradation rate decreases significantly after the

introduction of BQ, which is able to quench O_2^{-}•. Thus, O_2^{-}• is identified as the major active species for the decomposition of RhB. Since dissolved O_2 is required for generation of O_2^{-}•, the role of O_2^{-}• in the degradation process was validated by purging the dye solution with N_2 to decrease the amount of dissolved O_2. The result clearly demonstrates the negative effect of N_2 purging on the degradation rate. Hence, this result further indicates that O_2^{-}• is an important species involved in the RhB degradation. EDTA was added to the system to suppress h^+. As shown in Fig. 4-10, the introduction of EDTA (filled circles) significantly lowers the degradation rate, implying that RhB can also be oxidized by the photogenerated h^+ in the AgI/UiO-66 photocatalyst system. Therefore, O_2^{-}• and h^+ are the two main active species in the degradation process of RhB by the AgI/UiO-66 photocatalyst. This is in agreement with other studies on the AgI based photocatalyst system.[206, 207, 210, 211]

4.4 Conclusion

A novel AgI/UiO-66 photocatalyst was developed by conjugating AgI to the UiO-66 framework through a simple solution method. The photocatalyst exhibited remarkable activity toward the degradation of RhB under visible-light irradiation. At a molar ratio Ag : Zr of (1 : 1) in the composite, the highest photocatalytic activity was achieved. In this AgI/UiO-66 photocatalyst, UiO-66 not only works as a highly stable framework material, but also ensured a strong interaction with AgI. The resulting AgI/UiO-66 material exhibited good structural stability, and preserved most of its photocatalytic activity during long term degradation tests. The mechanism of the photocatalytic activity of the AgI/UiO-66 composite was also investigated, and the results imply that O_2^{-}• and h^+ are the major contributors to the degradation process of RhB. The

synthesis of this AgI/UiO-66 photocatalyst is convenient and easy to scale up. Field trials with this catalyst for water treatment are under way.

Chapter 5 Ag_2CO_3/UiO-66(Zr) composite with enhanced visible-light promoted photocatalytic activity for dye degradation

5.1 Introduction

As a narrow band gap semiconductor material with remarkable photocatalytic activity in the visible-light range, silver carbonate (Ag_2CO_3) has been studied as an efficient photocatalyst for the degradation of various organic dyes. In spite of the good photocatalytic activity of pristine Ag_2CO_3,[212-214] most of the studies was focusing on diverse substrates supported Ag_2CO_3 as photocatalyst for water treatment.[215-218] Almost all of these studies aimed to enhance the photocatalytic activity of pristine Ag_2CO_3, and a few of them declared that the substrates could also assist in inhibiting the photocorrosion of Ag_2CO_3.[219, 220] Even so, in most of the Ag_2CO_3 based photocatalyst studies, photocorrosion is still a highly common phenomenon,[214, 215, 218, 221] which also happens in the case of other silver-containing photocatalysts, such as Ag_3PO_4.[222, 223] Thus, the improvement in photocatalytic activity and stability of pristine Ag_2CO_3 are the two main objectives for the current Ag_2CO_3 based photocatalyst studies. Therefore, based on the excellent properties of UiO-66 described earlier, it is worthy to study the Ag_2CO_3/UiO-66 composite as a photocatalyst for water treatment. Nevertheless, UiO-66 incorporated with Ag_2CO_3 for photocatalytic application has not been reported yet.

In this study, a Ag_2CO_3/UiO-66 composite is prepared through a simple solution method, in which UiO-66 is used as the substrate and also a mediator for the synthesis of Ag_2CO_3. The photocatalytic activity of the Ag_2CO_3/UiO-66 composite is evaluated through the degradation of RhB under visible-light irradiation. In addition, the stability of the Ag_2CO_3/UiO-66 composite and the

photocorrosion of Ag_2CO_3 in the composite are analyzed and discussed. Moreover, the photocatalytic mechanism is also investigated.

5.2 Preparation of Ag_2CO_3/UiO-66 composites

Ag_2CO_3/UiO-66 composites were prepared by a simple solution method. Three Ag_2CO_3/UiO-66 composites with different Ag_2CO_3 contents were prepared based on the molar ratio of Ag : Zr. Typically, for the preparation of Ag_2CO_3/UiO-66 composite with Ag : Zr molar ratio of (0.5 : 1) (denoted as AgCO/UiO-66-0.5), 3.9 mg (0.046 mmol) $NaHCO_3$ was dissolved in 9.5 mL DI water. Thereafter, 50 mg (7.7×10^{-3} mmol, formula reported as $Zr_{24}O_{120}C_{192}H_{96}$ [58]) UiO-66 was added to the $NaHCO_3$ solution. After stirring for 1 h, 0.46 mL 0.2 M $AgNO_3$ aqueous solution (containing 0.092 mmol $AgNO_3$) was added to the UiO-66 mixture dropwise. The total reaction mixture was about 10 mL in volume, and was kept vigorous stirring at room temperature for 12 h. Finally, the product was collected by filtration, thoroughly washed with DI water for several times, and dried in vacuum oven at 80 ℃. Other Ag_2CO_3/UiO-66 composites with Ag : Zr molar ratio of (0.1 : 1) (denoted as AgCO/UiO-66-0.1) and (1 : 1) (denoted as AgCO/UiO-66-1) were also prepared following the similar procedure through varying the precursor amount of Ag_2CO_3. Pristine Ag_2CO_3 was also synthesized from the same procedure without the addition of UiO-66.

5.3 Results and discussion

5.3.1 Material characterization

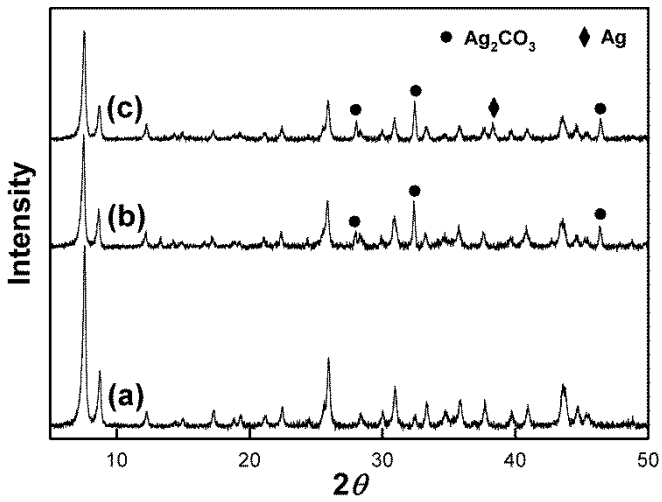

Fig. 5-1 XRD patterns of (a) pristine UiO-66, (b) AgCO/UiO-66-0.5, and (c) AgCO/UiO-66-0.5 after RhB degradation experiment.

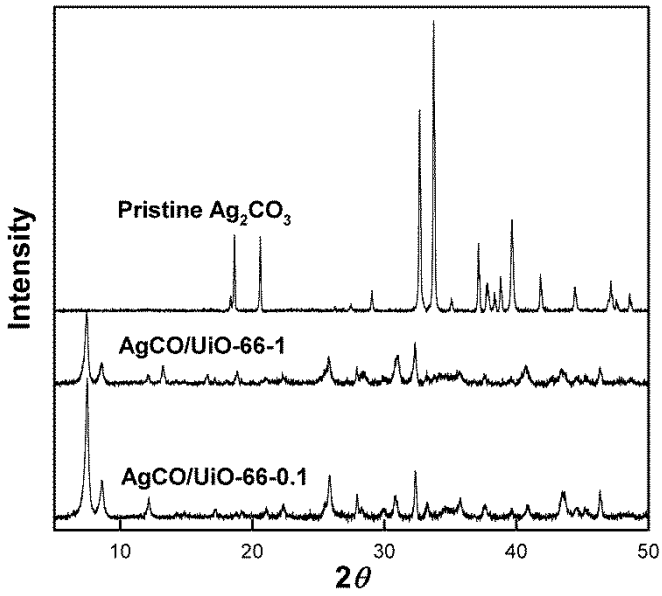

Fig. 5-2 XRD patterns of AgCO/UiO-66-0.1, AgCO/UiO-66-1, and pristine Ag_2CO_3.

XRD was used to characterize the composition of different samples. As shown in Fig. 5-1, the diffraction pattern of pristine UiO-66 fits well with that given in the previous report, providing clear evidence of the successful synthesis of UiO-66.[58] After the incorporation of Ag_2CO_3, the peaks belonging to UiO-66 can still be clearly identified, even in the case of AgCO/UiO-66-1, the sample with the highest Ag_2CO_3 content in this study (Fig. 5-2), indicating that the

structure of UiO-66 is intact during the synthesis of Ag_2CO_3. However, from the XRD pattern of AgCO/UiO-66-0.5, only a few new peaks that may be attributed to Ag_2CO_3 are observed. One possible reason is that in the presence of UiO-66, the crystallinity of the resulting Ag_2CO_3 is not good enough so that the intensity of the diffraction peaks from Ag_2CO_3 can be very weak. Additionally, the small particle size of the Ag_2CO_3 nanoparticles, which can be confirmed from the SEM and TEM images, may further weaken the diffraction peaks. It is also notable that, the content of Ag_2CO_3 in the composite is relatively low, and even the AgCO/UiO-66-1 sample contains only 33.7 wt% of Ag_2CO_3. In fact, it was reported that when the content of Ag_2CO_3 in the final product decreased to 50 wt%, the XRD diffraction peaks belonging to Ag_2CO_3 became very weak.[224] Therefore, in the presence of the strong peaks of the well crystallized UiO-66, it is likely that the peaks of Ag_2CO_3 cannot be easily identified. For the pristine Ag_2CO_3 synthesized under the same condition in the absence of UiO-66, all the diffraction peaks can be attributed to a monoclinic phase (JCPDS: 70-2184).

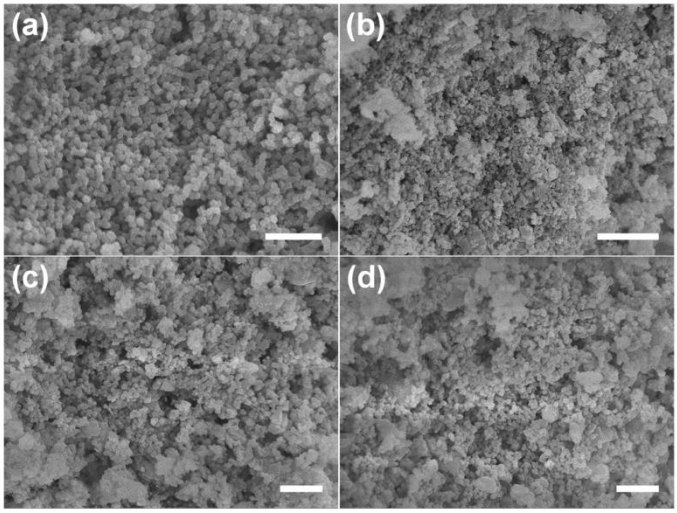

Fig. 5-3 SEM images of (a) pristine UiO-66, (b, c) AgCO/UiO-66-0.5, and (d) AgCO/UiO-66-0.5 after RhB degradation experiment (scale bars are 500 nm for (a, c, d), 1 μm for (b)).

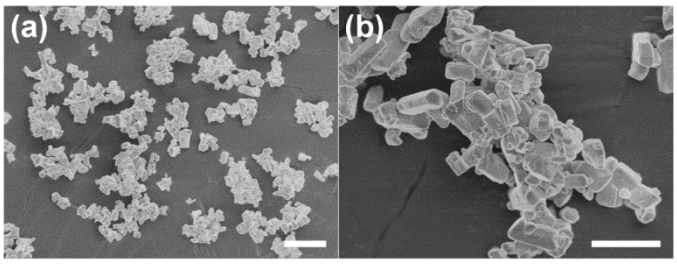

Fig. 5-4 SEM images of pristine Ag_2CO_3 (scale bars are 10 μm in (a), and 5 μm in (b)).

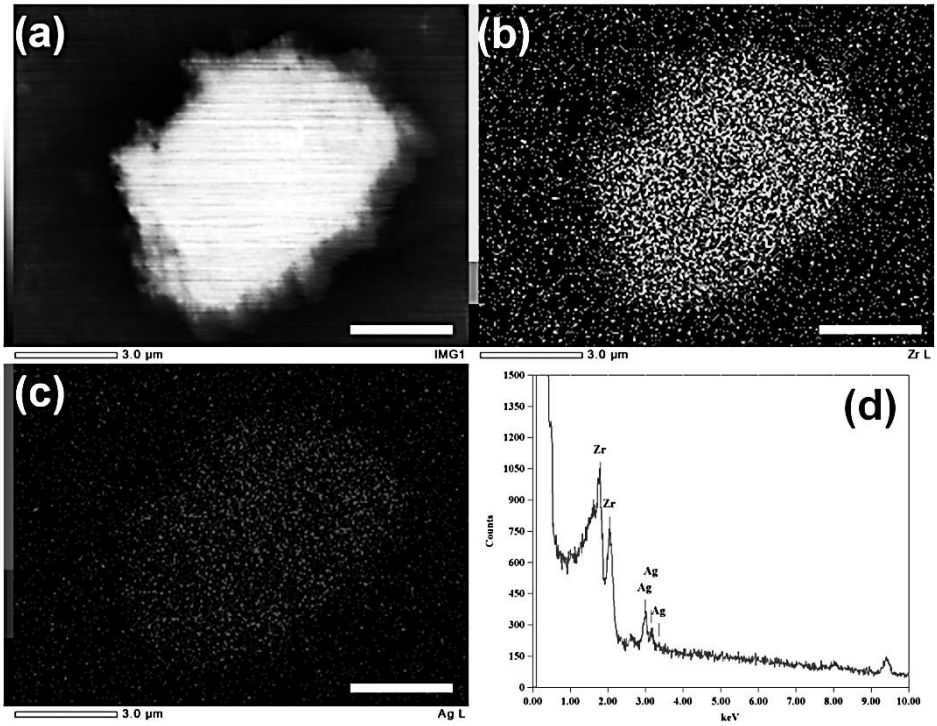

Fig. 5-5 (a) SEM image of AgCO/UiO-66-0.5, and corresponding EDS elemental mapping images of (b) Zr and (c) Ag, and (d) corresponding EDS spectrum (scale bars are 3 μm).

The morphology of AgCO/UiO-66-0.5, pristine UiO-66 and Ag_2CO_3 was characterized by SEM and TEM. From the SEM image in Fig. 5-3a, pristine UiO-66 shows very uniform particle morphology, and the particle size is less than 100 nm. After the incorporation of Ag_2CO_3, the AgCO/UiO-66-0.5 sample still consists of small particles (Fig. 5-3b, 5-3c). Part of these particles is believed to be UiO-66, indicating that the structure of UiO-66 is preserved, which is in line with the result of XRD. Besides UiO-66, there are some other particles forming uniform mixture with UiO-66, and such particles are

anticipated to be Ag_2CO_3. They are found to attach on the UiO-66 particles or even glue the UiO-66 particles together to form larger aggregation. Hence, there might be some interaction between UiO-66 and Ag_2CO_3 in the Ag_2CO_3/UiO-66 composite. In contrast, in the absence of UiO-66, the obtained pristine Ag_2CO_3 presents in a form of large chunks (Fig. 5-4). The dimension of these Ag_2CO_3 chunks is not very uniform, and most of them are several micrometers in size. It is obvious that under the influence of UiO-66, the Ag_2CO_3 particle size considerably decreases and becomes more uniform. Although the XRD data show that the crystallinity of Ag_2CO_3 in the Ag_2CO_3/UiO-66 composite is not as good as that of pristine Ag_2CO_3, the specific surface area is expected to be significantly increased due to the decreased particle size. EDS mapping was used to study the distribution of Zr and Ag elements in AgCO/UiO-66-0.5. As shown in Fig. 5-5, Zr and Ag elements are found uniformly distributing in this sample.

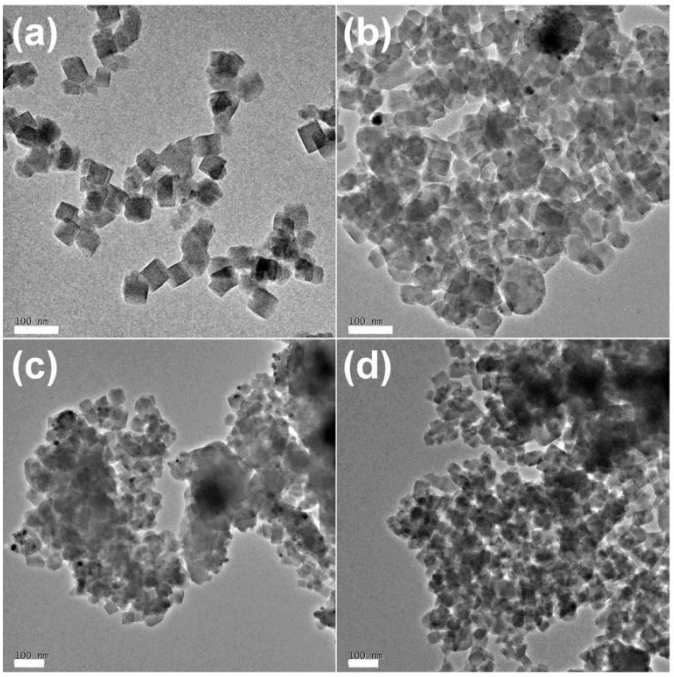

Fig. 5-6 TEM images of (a) pristine UiO-66, (b, c) AgCO/UiO-66-0.5, and (d) AgCO/UiO-66-0.5 after RhB degradation experiment (scale bars are 100 nm).

In addition, the results from TEM data are also consistent with the observation from SEM images. As shown in Fig. 5-6a, most of the UiO-66 particles are between 50–100 nm in size. For the AgCO/UiO-66-0.5 sample, the UiO-66 particles can still be clearly observed in the composite (Fig. 5-6b, 5-6c). Moreover, the UiO-66 particles aggregate together uniformly with another material which is believed to be Ag_2CO_3. Although it is difficult to estimate the size of these Ag_2CO_3 particles from the TEM images, they are found to have comparable size as that of UiO-66.

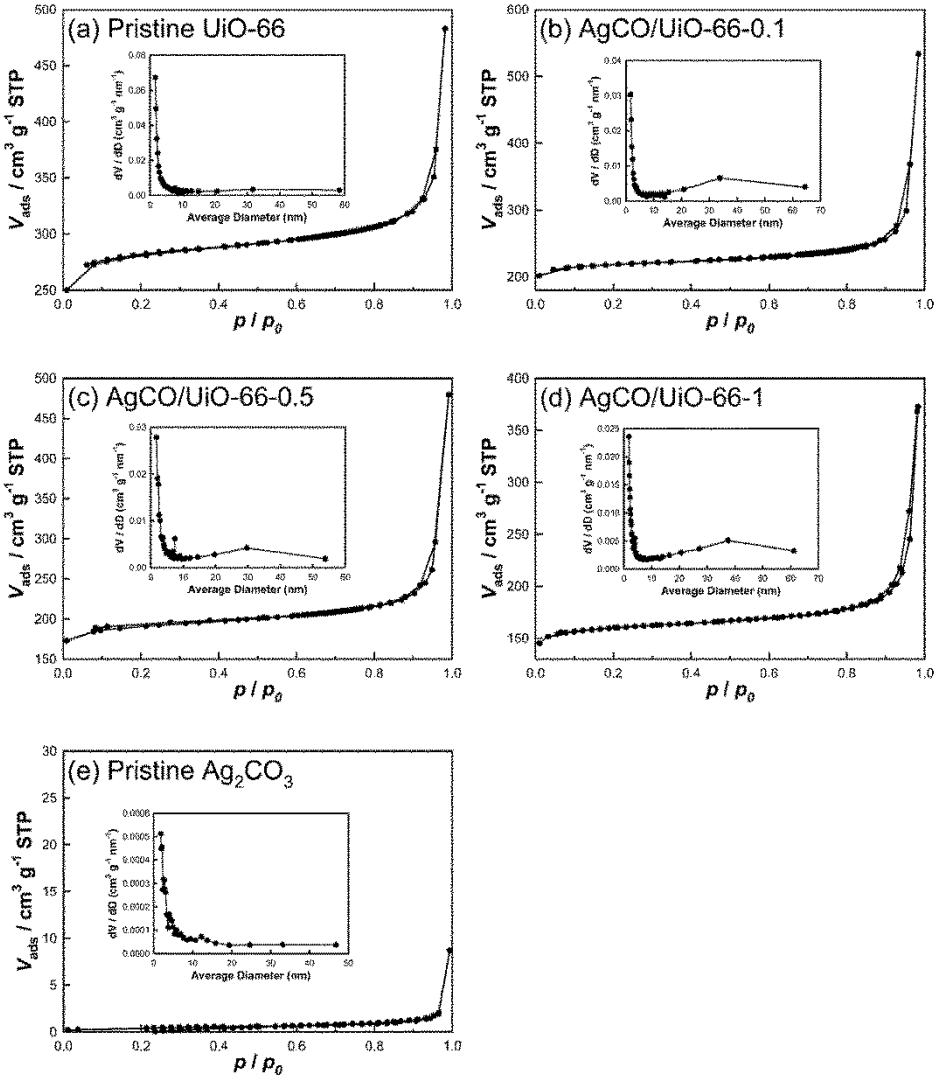

Fig. 5-7 Nitrogen adsorption-desorption isotherms and pore size distributions (inset) of (a) pristine UiO-66, (b) AgCO/UiO-66-0.1, (c) AgCO/UiO-66-0.5, (d) AgCO/UiO-66-1, and (e) pristine Ag_2CO_3.

The specific surface areas of the Ag_2CO_3/UiO-66 composites, pristine UiO-66 and Ag_2CO_3 were evaluated by the N_2 adsorption method. Fig. 5-7 shows the adsorption-desorption isotherms and pore size distributions of different samples, and the results are summarized in Table 5-1. As shown in Table 5-1, the specific surface area of pristine UiO-66 is 808 $m^2 g^{-1}$. This value is slightly lower than that of some model examples, such as 1069 $m^2 g^{-1}$ [176] and 1110 $m^2 g^{-1}$,[192] and it is comparable to the value reported by other studies, *e.g.*, 700 $m^2 g^{-1}$ [174] or 850 $m^2 g^{-1}$.[193] It is notable that no moderator, such as acetic acid,[162, 174] was added during the synthesis of UiO-66 in this study, and the synthesis conditions were not optimized, either. For the Ag_2CO_3/UiO-66 composites, the specific surface areas decrease with the increase in Ag_2CO_3 contents. This should be due to the much lower specific surface area of Ag_2CO_3 than that of UiO-66. As a reference, the specific surface area of pristine Ag_2CO_3 is only 1.5 $m^2 g^{-1}$. With regard to the total pore volume of the Ag_2CO_3/UiO-66 composites, it first increases from 0.75 $cm^3 g^{-1}$ of pristine UiO-66 to 0.83 $cm^3 g^{-1}$ of AgCO/UiO-66-0.1, then drops to 0.74 $cm^3 g^{-1}$ of AgCO/UiO-66-0.5, and finally to 0.58 $cm^3 g^{-1}$ of AgCO/UiO-66-1. Considering the total pore volume of pristine Ag_2CO_3 is much smaller (only 0.013 $cm^3 g^{-1}$), Ag_2CO_3 in the composite should have a notable pore volume. A possible explanation of such change is that the Ag_2CO_3 in the Ag_2CO_3/UiO-66 composites is different from the pristine Ag_2CO_3, not only in terms of morphology, but also structure. This may also be the reason of the poor crystallization of Ag_2CO_3 in the Ag_2CO_3/UiO-66 composites.

Table 5-1 Comparison of the properties (*i.e.*, Ag : Zr ratio, specific surface area and total pore volume) and photocatalytic activity (reaction rate constant) of different catalyst samples and blank experiment.

Sample	Ag : Zr ratio[a]	Specific surface area[b] / $m^2\ g^{-1}$	Total pore volume[c] / $cm^3\ g^{-1}$	Reaction rate constant (k)[d] / min^{-1}
AgCO/UiO-66-0.1	0.1 : 1	627	0.83	0.0177
AgCO/UiO-66-0.5	0.5 : 1	522	0.74	0.0240
AgCO/UiO-66-1	1 : 1	424	0.58	0.0221
Pristine UiO-66	–	808	0.75	0.0138[e]
Pristine Ag_2CO_3	–	1.5	0.013	
Blank[f]	–	–	–	0.0002

[a] The Ag : Zr ratios were molar ratios, and were determined based on the reaction precursor. [b] The specific surface areas were evaluated by the BET method. [c] The total pore volumes were obtained at $P/P_0 = 0.99$. [d] The reaction rate constants (k) were calculated based on a pseudo-first-order kinetic model. [e] The reaction rate constant of the control experiment was obtained from the mixture of pristine UiO-66 and Ag_2CO_3, and the amount of UiO-66 or Ag_2CO_3 was equal to the actual amount of that contained in AgCO/UiO-66-0.5. [f] In the blank degradation experiment, no catalyst was added.

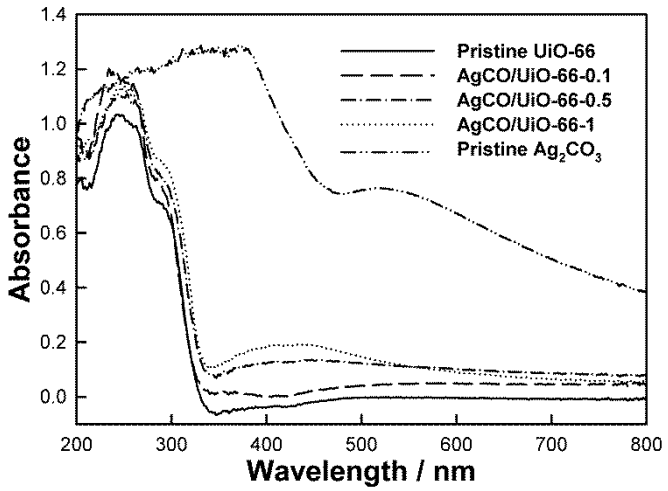

Fig. 5-8 UV-Vis diffuse reflectance spectra of pristine UiO-66, Ag_2CO_3/UiO-66 composites with different Ag_2CO_3 contents, and pristine Ag_2CO_3.

The absorption abilities of different samples at different wavelength were investigated through the UV-Vis diffuse reflectance measurement. As shown in Fig. 5-8, there is no obvious absorption observed in pristine UiO-66 between

340 and 800 nm, indicating that UiO-66 does not possess the ability to utilize photo-energy in the visible-light range. On the other hand, pristine Ag_2CO_3 shows a strong absorption in the visible-light range, suggesting its potential capability of effectively utilizing visible-light energy. For the Ag_2CO_3/UiO-66 composites with different Ag_2CO_3 contents, although their absorption in the visible-light range is weaker than that of pristine Ag_2CO_3, it is obvious that their absorption increases with the enhancement in Ag_2CO_3 contents. The weaker absorption of Ag_2CO_3/UiO-66 composites may be owing to the poor crystallization of Ag_2CO_3 in the presence of UiO-66 and the relatively low Ag_2CO_3 contents in the composites.

5.3.2 Photocatalytic activity

In this study, RhB was chosen as a model dye to simulate the contaminant in wastewater. As illustrated in Fig. 5-9a, for all Ag_2CO_3/UiO-66 composites, most of the RhB molecules can be degraded in 120 min. In addition, compared to the other two composites, the AgCO/UiO-66-0.5 sample shows the fastest degradation rate. In contrast, in the control experiment, RhB is degraded at a much lower rate than the three composites and almost no degradation can be observed in the blank experiment. To compare the photocatalytic activity in a more systematic manner, the degradation rates of different experiments were quantified based on reaction rate constants (k), which were calculated assuming that all the reactions follow a pseudo-first-order kinetic model (Fig. 5-9b and Table 5-1).[194] The same tendency of the highest photocatalytic activity observed in AgCO/UiO-66-0.5 and the lowest in the control experiment is clearly shown. Notably, the extremely small reaction rate constant of the blank experiment indicates that the self-photolysis of RhB is negligible in this study.

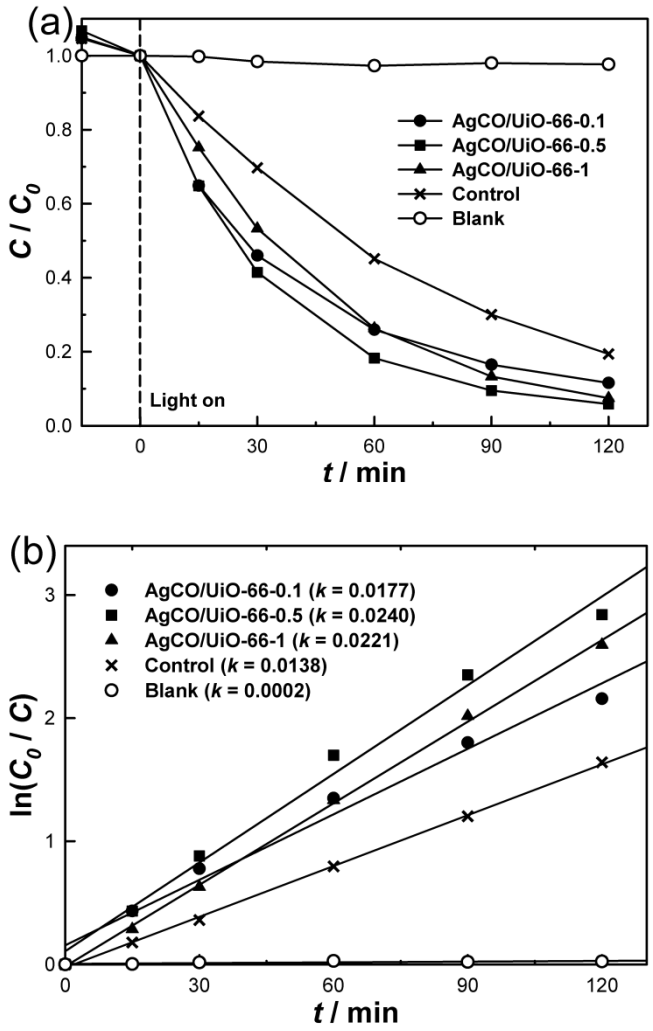

Fig. 5-9 (a) Photocatalytic degradation of RhB in the presence and absence (blank) of different catalysts (AgCO/UiO-66-0.1, AgCO/UiO-66-0.5, AgCO/UiO-66-1) under visible-light irradiation. For the control experiment (mechanical mixture of pristine UiO-66 and pristine Ag_2CO_3), the amount of pristine UiO-66 or Ag_2CO_3 was equal to the actual amount of that in AgCO/UiO-66-0.5. (b) Comparison of the reaction rate constant (k) in the presence of different catalysts (assuming that the reactions follow the pseudo-first-order kinetic model).

To have a better understanding of the difference in the performance of these samples, the factors that may affect the photocatalytic activity were studied. For the three Ag_2CO_3/UiO-66 composites, the key influential factors should be the content of Ag_2CO_3 and the specific surface area of the composites. When the Ag : Zr ratio is enhanced from (0.1 : 1) to (0.5 : 1), the Ag_2CO_3 content increases from 4.8 to 20.3 wt%, and the specific surface area decreases from 627 to 522

m^2 g^{-1}. The result of the degradation experiment implies that regardless of the reduce in specific surface area, there are more Ag_2CO_3 active sites on the surface of AgCO/UiO-66-0.5 due to the enhanced Ag_2CO_3 content. When the Ag : Zr ratio is further enhanced to (1 : 1), the Ag_2CO_3 content reaches 33.7 wt%, and the specific surface area of the composite drops to 424 m^2 g^{-1}. The lowered photocatalytic activity suggests the decrease of the Ag_2CO_3 active sites. A possible reason is that the aggregation of excessive Ag_2CO_3 particles not only decreases the specific surface area, but also reduces the Ag_2CO_3 active sites on the surface of the final composite. Therefore, it is reasonable that there should be a balance between the Ag_2CO_3 content and the specific surface area of the Ag_2CO_3/UiO-66 composite, which is obtained when the Ag : Zr ratio is optimized to (0.5 : 1) in this study. In the control experiment, the content of Ag_2CO_3 is the same as that of AgCO/UiO-66-0.5. Hence, the main factors influencing the photocatalytic activity should be the crystallization and the specific surface area of Ag_2CO_3. Although pristine Ag_2CO_3 has better crystallization, its specific surface area is extremely small, so the number of Ag_2CO_3 active sites are much less than that on the surface of AgCO/UiO-66-0.5, leading to a lower photocatalytic activity.

5.3.3 Photocatalyst stability

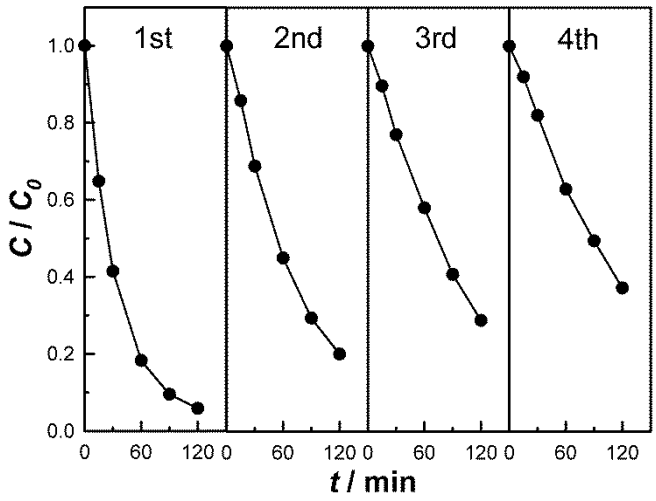

Fig. 5-10 Four cycles of the RhB degradation in the presence of AgCO/UiO-66-0.5 under visible-light irradiation.

Although Ag_2CO_3 possesses remarkable visible-light photocatalytic activity, the photocorrosion of Ag_2CO_3 during the dye degradation process is still a thorny problem. Briefly, the photocorrosion is caused through the irreversible reaction between the photogenerated electrons and the Ag^+ provided by Ag_2CO_3, in which the Ag^+ is reduced to form metallic Ag.[212, 213] Different strategies have been proposed and studied to solve the photocorrosion problem of Ag_2CO_3, such as adding different inhibitors in the degradation solution,[212, 213] or coupling Ag_2CO_3 with other materials that can act as electron acceptors.[219, 220] To study the stability of the Ag_2CO_3/UiO-66 composite, AgCO/UiO-66-0.5 after dye degradation was examined by different techniques. The morphology change was characterized by SEM and TEM. As shown in Fig. 5-3d and Fig. 5-6d, no obvious morphological change is observed in AgCO/UiO-66-0.5 before and after the dye degradation experiment. However, the XRD pattern of AgCO/UiO-66-0.5 used for dye degradation shows a small new peak between 38 ° and 39 ° that should belong to metallic Ag (JCPDS: 65-2871), implying that Ag_2CO_3 in the Ag_2CO_3/UiO-66 composite was photocorroded

under the visible-light irradiation (Fig. 5-1d). This phenomenon was also reported in other Ag_2CO_3 based photocatalyst studies.[213, 218, 225] The stability of AgCO/UiO-66-0.5 was further studied by reusing the composite for three more cycles of dye degradation. As shown in Fig. 5-10, although there is a decrease in the degradation rate for each degradation cycle, more than 60% of RhB can still be degraded in the fourth cycle, indicating that most activity of the Ag_2CO_3/UiO-66 composite was preserved. The stability of the Ag_2CO_3/UiO-66 composite was further examined by analyzing the amount of Zr and Ag elements in the degradation liquid of AgCO/UiO-66-0.5 after the degradation experiment through ICP. The potential residual Zr and Ag elements in the degradation liquid should be generated from the photocorrosion process of the composite. The degradation liquid from the control experiment was also analyzed. The ICP result shows that no Zr element was detected in the degradation liquid of both samples, which is another evidence supporting the outstanding stability of UiO-66. Nevertheless, 0.47 ppm Ag element was found residual in the degradation liquid of AgCO/UiO-66-0.5, further confirming the decomposition of Ag_2CO_3 in the Ag_2CO_3/UiO-66 composite. However, the residual Ag element found in the degradation liquid of the control experiment was 30.08 ppm, and it was 63 folds higher than that detected in the AgCO/UiO-66-0.5 system. Such result suggests that the stability of Ag_2CO_3 in the Ag_2CO_3/UiO-66 composite is enhanced compared to that of the pristine Ag_2CO_3, which may be attributed to the good interaction between Ag_2CO_3 and UiO-66 in the composite, and the semiconductor property of UiO-66. The good interaction between Ag_2CO_3 and UiO-66 should be formed in the preparation process of the composite. Specifically, bicarbonate salt was first introduced in

the UiO-66 aqueous suspension. Since the $Zr_6O_4(OH)_4$ octahedra (dark grey clusters shown in Fig. 3-12) are positively charged, electrostatic interactions could occur between these octahedral and the negatively charged bicarbonate ions/carbonate ions.[176] Then, these bicarbonate ions/carbonate ions accumulated around the UiO-66 frameworks and reacted with the subsequently added silver ions. Finally, the generated Ag_2CO_3 particles could attach around the UiO-66 particles, and might have good interaction with the UiO-66 frameworks. Additionally, UiO-66 was reported as a semiconductor material.[115, 176] Due to its good interaction with Ag_2CO_3, it is possible that UiO-66 may accept the photogenerated electrons and thus separate them from Ag_2CO_3, which slows down the reduction of Ag^+ to metallic Ag, so that the photocorrosion rate of Ag_2CO_3 is declined and the stability of the Ag_2CO_3/UiO-66 composite is enhanced. This mechanism was also proposed in other studies.[219, 220]

5.3.4 Photocatalytic mechanism

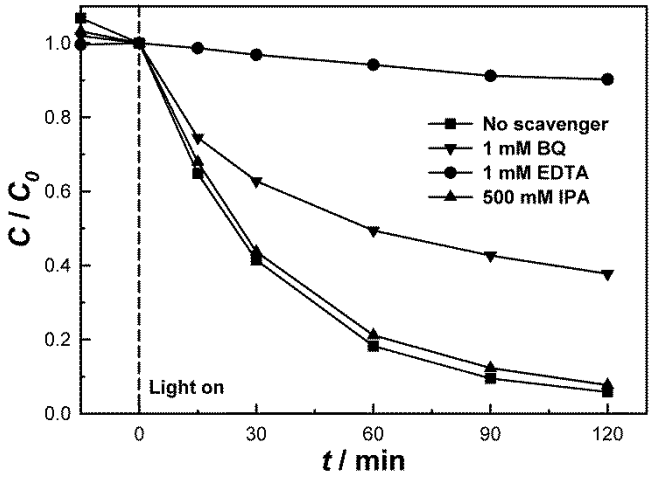

Fig. 5-11 Effects of different scavengers on the degradation of RhB in the presence of AgCO/UiO-66-0.5 under visible-light irradiation.

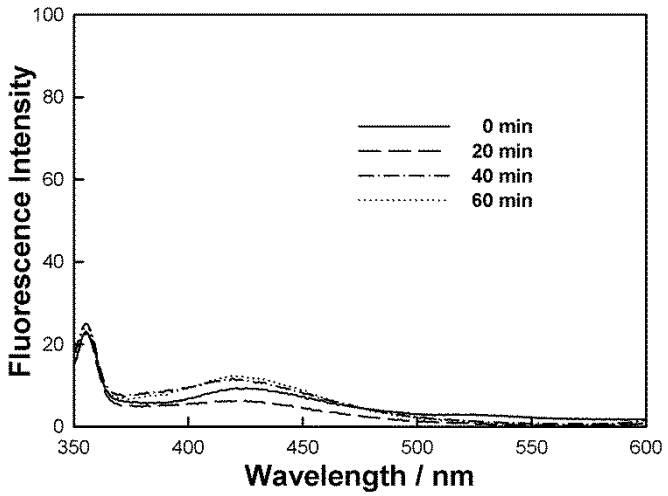

Fig. 5-12 Photoluminescence spectral changes with visible-light irradiation time in the presence of AgCO/UiO-66-0.5 in a 5×10^{-4} M basic solution of terephthalic acid.

The photocatalytic mechanism of the Ag_2CO_3/UiO-66 composite was investigated through determining the potential roles of HO•, O_2^-•, and h^+ during the degradation, since they are known as the three main active species involved in the photocatalytic oxidation process.[5, 19, 196, 197] To identify the contribution of these active species, three different scavengers, IPA, BQ, and EDTA were separately introduced in the degradation process to attempt to trap HO•, O_2^-•, and h^+.[179-181] As shown in Fig. 5-11, the presence of BQ significantly decreases the degradation rate. Since BQ is a O_2^-• quencher, O_2^-• should be one of the main active species participating in the decomposition process of RhB. Because the addition of BQ only partially suppressed the degradation rate, one or more other species may also be involved in the degradation process. However, the addition of IPA does not cause obvious change in the RhB degradation rate, indicating that HO• should not be an important contributor to the photocatalytic process. The potential role of HO• was further confirmed by a photoluminescence technique, in which terephthalic

acid was used as a probe molecule to detect the HO• generated on the photocatalyst surface.[182] As illustrated in Fig. 5-12, no obvious fluorescence intensity change can be observed during the 60 min test period, suggesting that almost no HO• was generated on the AgCO/UiO-66-0.5 surface. In addition, after the introduction of EDTA, only slight degradation of RhB can be observed (filled circles). EDTA is able to suppress the generation of h^+ in the valence band, which may not only suppress the activity of h^+, but also accelerate the recombination of e^- and h^+. Thus, the formation of O_2^{-}• was also suppressed in the presence of EDTA. As a result, the degradation of RhB was almost restrained by EDTA due to the limited generation of h^+ and O_2^{-}•. The conclusion that O_2^{-}• and h^+ are the main active species in the Ag_2CO_3 based photocatalyst system was also described by other groups.[220, 226]

5.4 Conclusion

In summary, the Ag_2CO_3/UiO-66 composite was developed by incorporating UiO-66 with Ag_2CO_3 through a convenient solution method. Due to the participation of UiO-66, the resulting Ag_2CO_3 particles were more uniform and much smaller in size, and possessed modified structure compared to the pristine Ag_2CO_3 synthesized in the absence of UiO-66. To be used as a photocatalyst for RhB degradation under visible-light irradiation, the Ag_2CO_3/UiO-66 composite exhibited enhanced photocatalytic activity than the mixture of pristine UiO-66 and Ag_2CO_3. The enhancement of the photocatalytic activity could be attributed to more Ag_2CO_3 active sites on the composite surface, because of the increase in specific surface area of Ag_2CO_3 in the composite. By adjusting the content of Ag_2CO_3, it was found that the Ag_2CO_3/UiO-66 composite with Ag : Zr molar ratio equaling (0.5 : 1) showed the highest

photocatalytic activity for the degradation of RhB. Although the photocorrosion issue of Ag_2CO_3 could not be completely prevented, the Ag_2CO_3/UiO-66 composite was still able to preserve most of its initial photocatalytic activity after four cycles of degradation experiments. In addition, compared to the simple mixture of pristine UiO-66 and Ag_2CO_3, the Ag_2CO_3/UiO-66 composite also revealed noticeable enhancement of Ag_2CO_3 stability, which may be due to the good interaction between Ag_2CO_3 and UiO-66 in the composite. The study on the photocatalytic mechanism of the Ag_2CO_3/UiO-66 composite implies that O_2^{-}• and h^+ should be the major contributors to the degradation process of RhB.

Chapter 6 Enhanced Visible-Light Photocatalytic Performance of BiOBr/UiO-66(Zr) Composite for Dye Degradation with the Assistance of UiO-66

6.1 Introduction

Recently, there was a significant increase in the number of reports focusing on bismuth oxyhalides (BiOX, X = Cl, Br, I) based photocatalysts, owing to their high photocatalytic activity and relatively convenient synthesis procedure.[227-230] Among these bismuth oxyhalides, BiOBr is the subject of many studies for visible-light induced photodegradation of organic dyes.[231-233] Although pristine BiOBr possesses excellent visible-light photocatalytic activity, there is very limited interspace between the BiOBr particles synthesized without microstructure modulations, leading to the fairly low accessible surface area of this material. Hence, to maximize the potential of BiOBr for photocatalytic application, it is a straightforward method to increase its accessible surface area for more contact of target molecules. To achieve this goal, a common strategy is to modulate the microstructure of BiOBr. However, it is relatively complex to prepare BiOBr with large accessible surface area by controlling its morphology, and surfactant or other mediator is required in the synthetic process.[234-236] Alternatively, it is also feasible to enhance the accessible surface area of BiOBr by integrating BiOBr and a supporting material that is sufficiently robust for the photocatalytic process in water medium.

In this study, a BiOBr incorporated UiO-66 composite with enhanced visible-light photocatalytic activity is prepared through a convenient solution method, in which the accessible surface area of BiOBr is enlarged and a good interaction is formed between the two components. The photocatalytic activity of the

BiOBr/UiO-66 composite was determined by the degradation of RhB under visible-light irradiation, and its stability and reusability for dye degradation is evaluated by means of various characterization methods. Furthermore, the photocatalytic mechanism is also studied.

6.2 Preparation of BiOBr/UiO-66 composites.

BiOBr/UiO-66 composites were prepared through a simple solution method. Five BiOBr/UiO-66 composites with different BiOBr contents were prepared based on the adjustment of the molar ratio of Bi : Zr. In details, for the preparation of BiOBr/UiO-66 composite with Bi : Zr molar ratio of (3 : 1) (denoted as BiOBr/UiO-66-3), 113.2 mg NaBr (1.10 mmol) was dissolved in 8 mL HBr aqueous solution (pH was around 2.5). Then, 50 mg UiO-66 (7.7×10^{-3} mmol, formula reported as $Zr_{24}O_{120}C_{192}H_{96}$ [58]) was added, and the mixture was kept stirring vigorously for 1 h. Afterwards, 266.8 mg $Bi(NO_3)_3 \cdot 5H_2O$ (0.55 mmol) was dissolved in 2 mL DMF, and this $Bi(NO_3)_3$ DMF solution was added to the UiO-66 mixture dropwise to reach the total reaction mixture of 10 mL in volume. After stirred for another 30 min, the mixture was kept undisturbed for 3 h at room temperature. Finally, the product was collected by filtration, thoroughly washed with DI water for several times, and dried in vacuum oven at 80 ℃. Other BiOBr/UiO-66 composites with Bi : Zr molar ratios of (0.5 : 1) (denoted as BiOBr/UiO-66-0.5), (1 : 1) (denoted as BiOBr/UiO-66-1), (2 : 1) (denoted as BiOBr/UiO-66-2), and (4 : 1) (denoted as BiOBr/UiO-66-4) were also prepared following the similar procedure by adjusting the amount of precursors for BiOBr. Pristine BiOBr was also synthesized by the same procedure of BiOBr/UiO-66-3, excluding the addition of UiO-66.

6.3 Results and discussion

6.3.1 Material characterization

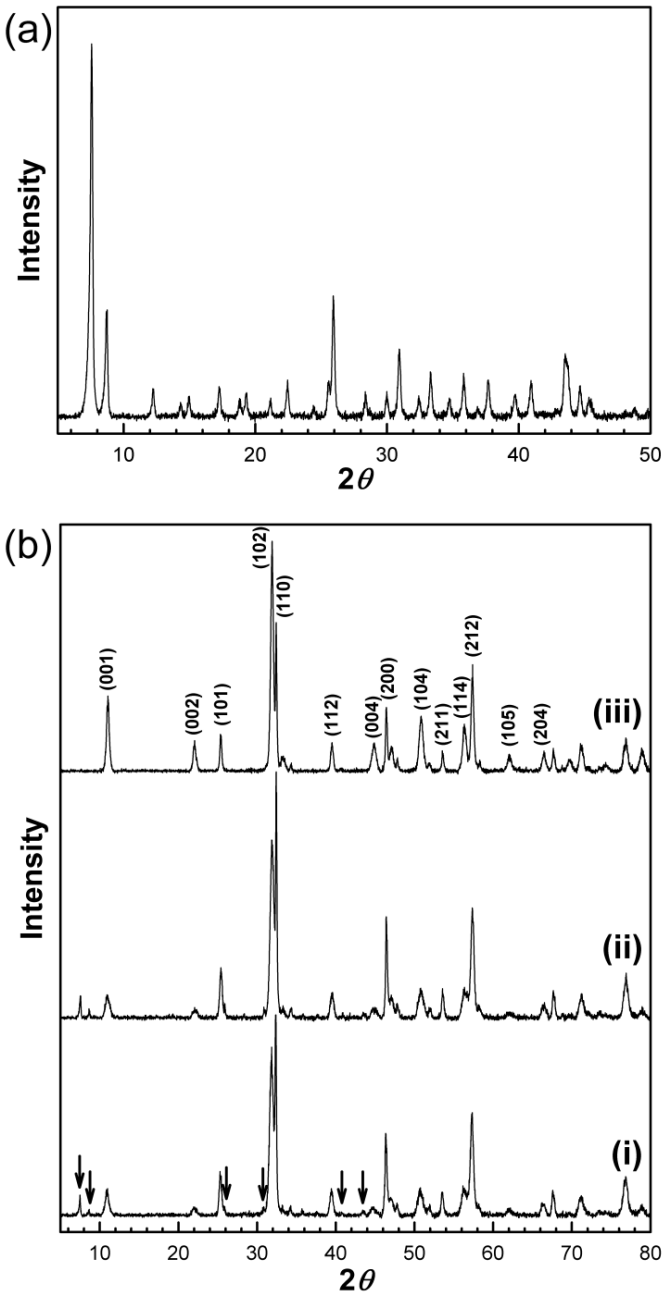

Fig. 6-1 XRD patterns of (a) pristine UiO-66; (b) BiOBr/UiO-66-3 (i), BiOBr/UiO-66-3 after RhB degradation experiment (ii), and pristine BiOBr (iii).

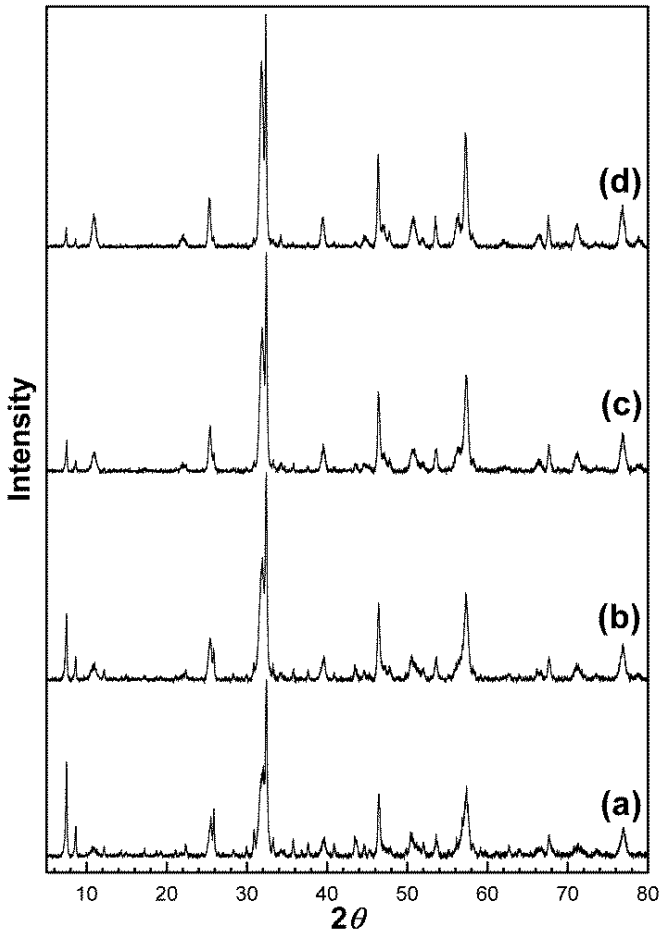

Fig. 6-2 XRD patterns of (a) BiOBr/UiO-66-0.5, (b) BiOBr/UiO-66-1, (c) BiOBr/UiO-66-2, and (d) BiOBr/UiO-66-4.

The composition of different samples was characterized by XRD. As shown in Fig. 6-1a, the XRD diffraction pattern of pristine UiO-66 is in line with the pattern described in literature, indicating the successful synthesis of UiO-66 in this study.[58] All the diffraction peaks of pristine BiOBr shown in Fig. 6-1b can be assigned to the tetragonal BiOBr phase (JCPDS: 73-2061), and these peaks can also be observed in the XRD diffraction patterns of BiOBr/UiO-66-3 (Fig. 6-1b) and other BiOBr/UiO-66 composites (Fig. 6-2). Several strong diffraction peaks from UiO-66 are discernable in BiOBr/UiO-66-3 (indicated by arrows in Fig. 6-1b), suggesting that the structure of UiO-66 remains undamaged under the conditions of BiOBr synthesis. Although the strength of

the diffraction peaks of UiO-66 gets weaker with the decrease in the content of UiO-66 in the BiOBr/UiO-66 composites, the two peaks between 6 ° and 10 ° can be observed readily even in the pattern of BiOBr/UiO-66-4, which possesses the highest BiOBr and lowest UiO-66 content in this study (Fig. 6-2). Interestingly, compared to the XRD pattern of pristine BiOBr (Fig. 6-1b), there is an intensity change in the peaks belonging to different facets of BiOBr that is as a component of the composite, especially in terms of the (001), (102) and (110) facets. Thus, it is expected that UiO-66 may affect the growth process of BiOBr crystals, leading to different growing preference of the crystal facets.

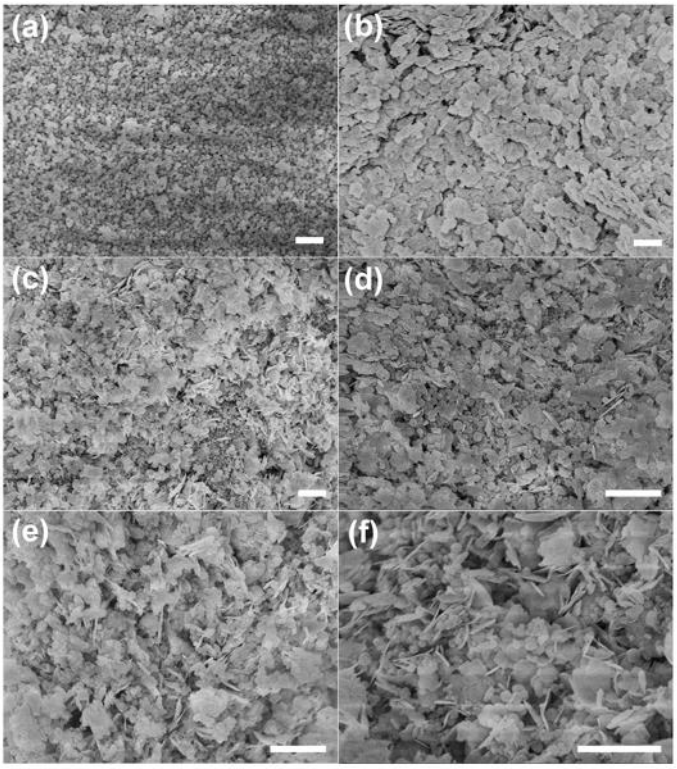

Fig. 6-3 SEM images of (a) pristine UiO-66, (b) pristine BiOBr, (c, d) BiOBr/UiO-66-3, and (e, f) BiOBr/UiO-66-3 after RhB degradation experiment (all scale bars are 1 μm).

Fig. 6-3a shows the SEM images of pristine UiO-66. The pristine UiO-66 appears as relatively uniform particles, and the size of these particles are less than 200 nm. As shown in Fig. 6-3c and 6-3d, after the incorporation of BiOBr,

the BiOBr/UiO-66-3 sample reveals some feature of a hybrid composite that particles and flakes are combined together evenly. The particles should be UiO-66, which also supports the XRD result that UiO-66 is stable during the synthesis of BiOBr. The flakes inserted among the UiO-66 particles are believed to be BiOBr, and BiOBr with similar morphology has also been described in previous studies.[237, 238] The dimension of the BiOBr flakes in BiOBr/UiO-66-3 is around a few hundred nanometers and their thickness is less than 50 nm. It is also discernable that these BiOBr flakes arrange randomly, and their interspace is visibly increased due to the presence of UiO-66 particles. In addition, from the EDS mapping images of BiOBr/UiO-66-3, Zr, Bi and Br elements are found evenly distributing in the composite (Fig. 6-4), further confirming the uniform combination of UiO-66 and BiOBr to form the composite. Although pristine BiOBr also presents similar morphology, their arrangement is in a more orderly pattern. As shown in Fig. 6-3b, the flakes in pristine BiOBr pack together in a more compact manner than that in the BiOBr/UiO-66 composite, thus pristine BiOBr is expected to possess smaller accessible interspace.

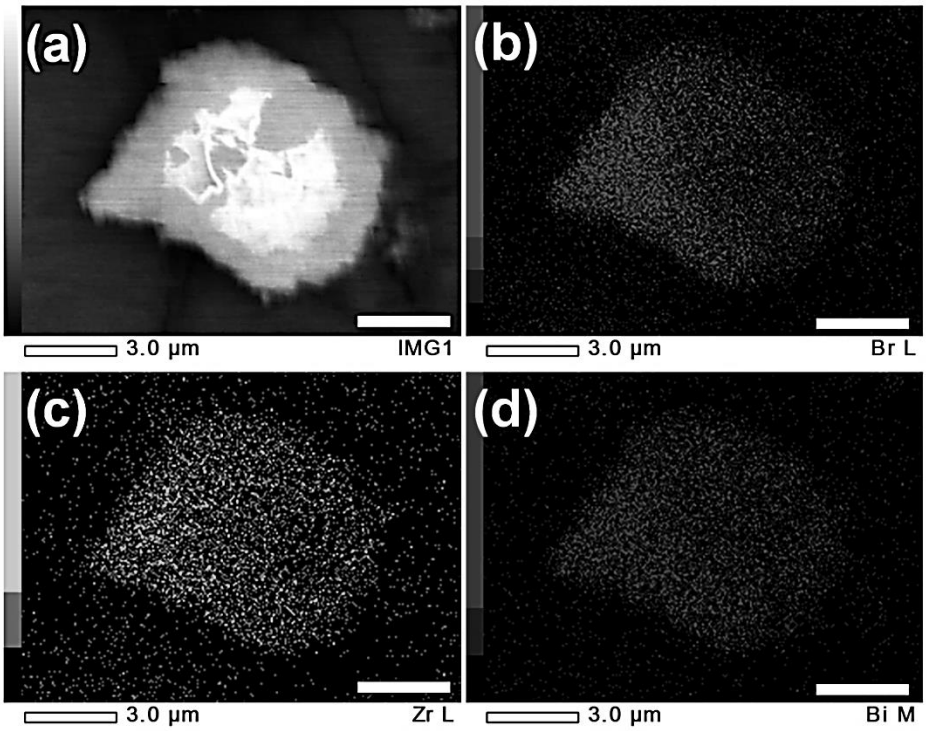

Fig. 6-4 (a) SEM image of BiOBr/UiO-66-3, and corresponding EDS elemental mapping images of (b) Br and (c) Zr, and (d) Bi (scale bars are 3 µm).

The morphology of these samples was also characterized by TEM. It can be seen from Fig. 6-5a that most of the UiO-66 particles are around 100 nm in size. For BiOBr/UiO-66-3, the UiO-66 particles are still clearly identifiable, in agreement with the results of XRD and SEM (Fig. 6-3c, 6-3d). Among the UiO-66 particles, the BiOBr flakes can also be observed. Although the exact size of the BiOBr flakes is difficult to estimate from the TEM images, the thickness of the flakes is within the range of 10 to 20 nm. Besides, pristine BiOBr flakes are about 200–400 nm in size with a rounded edge, and they also exhibit a compact pattern, as shown in the TEM image (Fig. 6-5b).

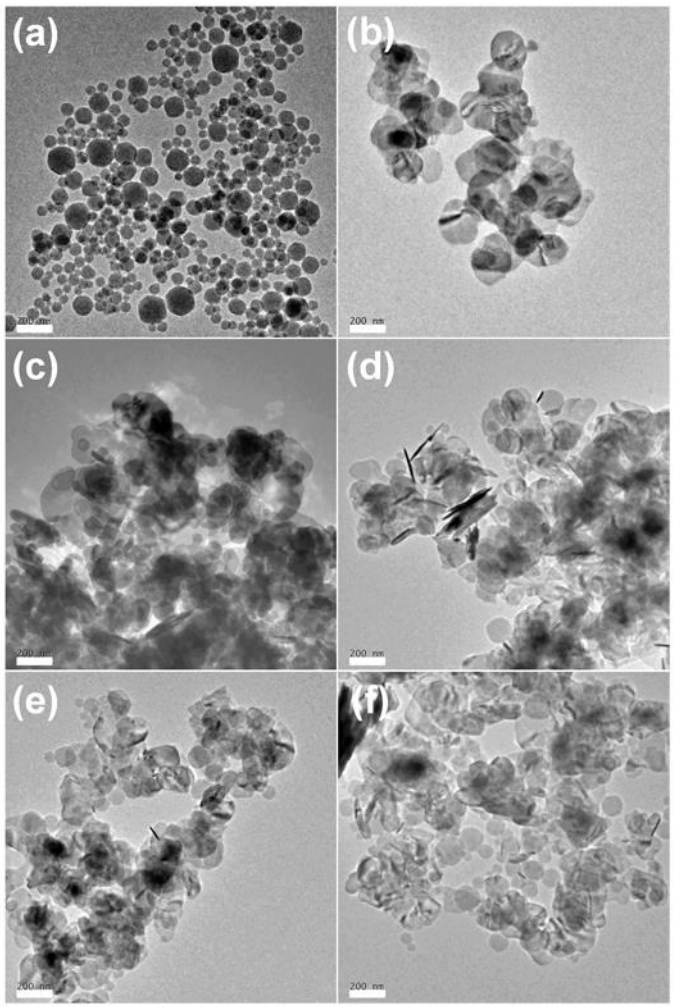

Fig. 6-5 TEM images of (a) pristine UiO-66, (b) pristine BiOBr, (c, d) BiOBr/UiO-66-3, and (e, f) BiOBr/UiO-66-3 after RhB degradation experiment (all scale bars are 200 nm).

Table 6-1 Comparison of the properties (*i.e.*, Bi : Zr ratio, specific surface area and total pore volume) and photocatalytic activity (reaction rate constant) of different catalyst samples.

Sample	Bi : Zr ratio[a]	Specific surface area[b] / $m^2\ g^{-1}$	Total pore volume[c] / $cm^3\ g^{-1}$	Reaction rate constant (k)[d] / min^{-1}
BiOBr/UiO-66-0.5	0.5 : 1	486	0.75	0.1815
BiOBr/UiO-66-1	1 : 1	382	0.61	0.2261
BiOBr/UiO-66-2	2 : 1	278	0.55	0.2508
BiOBr/UiO-66-3	3 : 1	204	0.36	0.2554
BiOBr/UiO-66-4	4 : 1	149	0.29	0.2179
Pristine UiO-66	–	869	1.19	0.0044[e]
Pristine BiOBr	–	14.8	0.12	0.1206[f]
Control (UiO-66&BiOBr mixture)	3 : 1	–	–	0.1333[g]

[a] The Bi : Zr ratios were molar ratios, and were determined based on the reaction precursor. [b] The specific surface areas were evaluated by the BET method. [c] The total pore volumes were obtained at $P/P_0 = 0.99$. [d] The reaction rate constants (k) were calculated based on a pseudo-first-order kinetic model. [e] The reaction rate constant was obtained from the control experiment in which only pristine UiO-66 was used, and the amount of UiO-66 was equal to the actual amount of that contained in BiOBr/UiO-66-3. [f] The reaction rate constant was obtained from the control experiment in which only pristine BiOBr was used, and the amount of BiOBr was equal to the actual amount of that contained in BiOBr/UiO-66-3. [g] The reaction rate constant was obtained from the control experiment in which the mixture of pristine UiO-66 and BiOBr was used, and the amount of UiO-66 or BiOBr was equal to the actual amount of that contained in BiOBr/UiO-66-3.

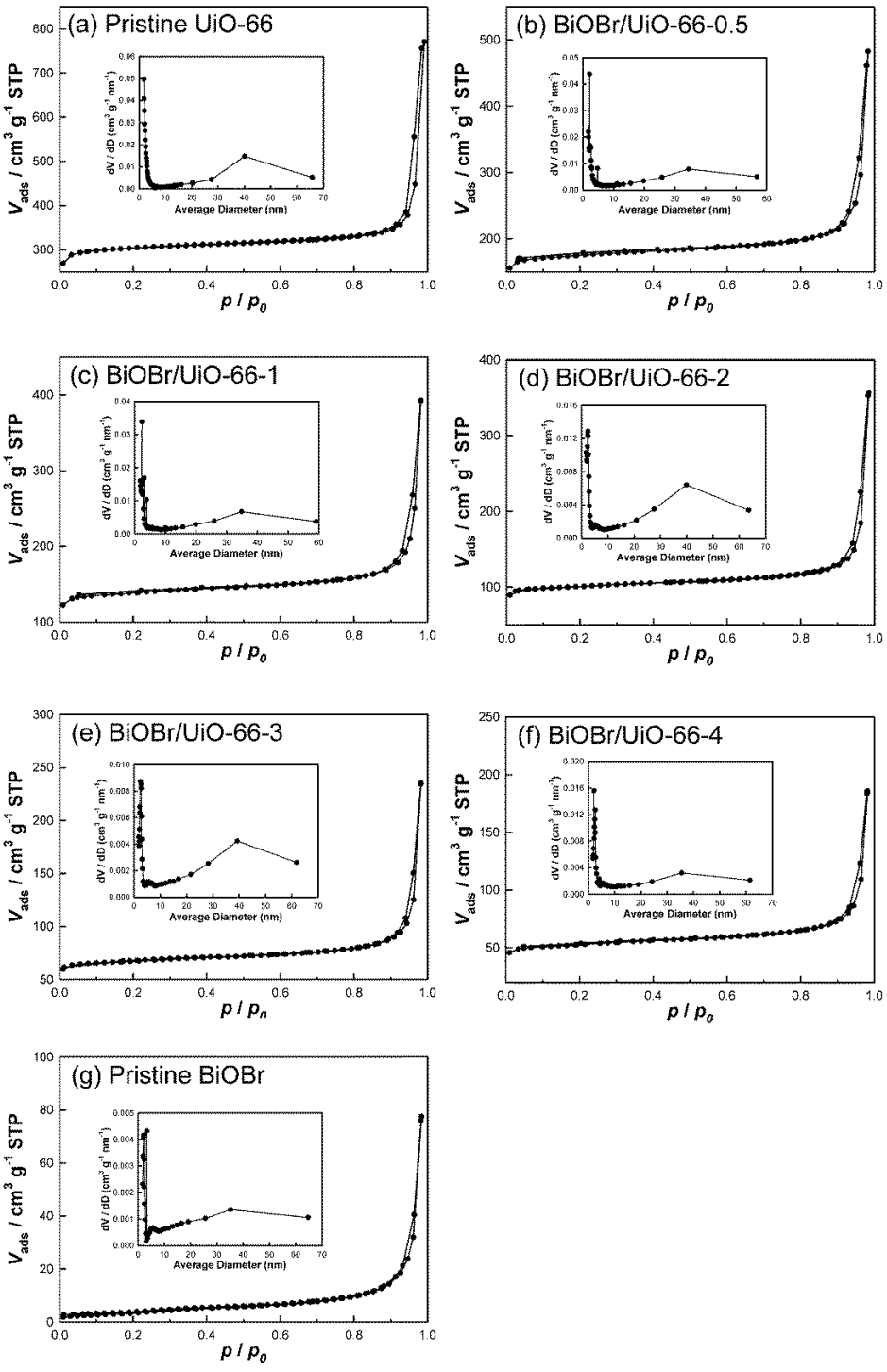

Fig. 6-6 Nitrogen adsorption-desorption isotherms and pore size distributions (inset) of (a) pristine UiO-66, (b) BiOBr/UiO-66-0.5, (c) BiOBr/UiO-66-1, (d) BiOBr/UiO-66-2, (e) BiOBr/UiO-66-3, (f) BiOBr/UiO-66-4, and (g) pristine BiOBr.

The specific surface areas of the BiOBr/UiO-66 composites, pristine UiO-66 and pristine BiOBr were evaluated by N_2 adsorption (Table 6-1). And the plots

of adsorption-desorption isotherms and pore size distributions are shown in Fig. 6-6. As shown in Table 6-1, the specific surface area of pristine UiO-66 is 869 m^2 g^{-1}. Because the synthesis conditions were not optimized, this value is slightly lower than that of some model examples, such as 1069 m^2 g^{-1} and 1110 m^2 g^{-1},[176, 192] but it is comparable to the value reported by other studies, *e.g.*, 850 m^2 g^{-1} or 931 m^2 g^{-1}.[193, 239] After the incorporation of BiOBr, the specific surface areas of the BiOBr/UiO-66 composites remarkably decrease with the enhancement of BiOBr contents. This is not an unexpected result, since the specific surface area of pristine BiOBr is only 14.8 m^2 g^{-1}, about 58-fold smaller compared to that of pristine UiO-66. Similarly, because of the smaller total pore volume of pristine BiOBr than that of pristine UiO-66, the same trend of the total pore volumes of BiOBr/UiO-66 composites decreasing with the increase in BiOBr content is also observed.

The optical absorption abilities of the samples at different wavelengths were investigated by UV-Vis diffuse reflectance measurement. As illustrated in Fig. 6-7a, pristine UiO-66 is transparent in the range of 340 to 800 nm, inferring that UiO-66 can only absorb UV-light. A similar absorption edge at about 440 nm is observed in pristine BiOBr and all the BiOBr/UiO-66 composites, demonstrating that their optical absorption extends to the visible-light range. In addition, the band gap energies (E_g) of these samples can be extrapolated from the spectra. According to Fig. 6-7b and 6-7c, the E_g of pristine UiO-66 and BiOBr are about 4.0 eV and 2.8 eV, in line with the reported results.[155, 240] Furthermore, the E_g of all the BiOBr/UiO-66 composites closely distribute in the range between 2.8 eV and 2.9 eV, implying their potential ability to utilize the visible-light energy.

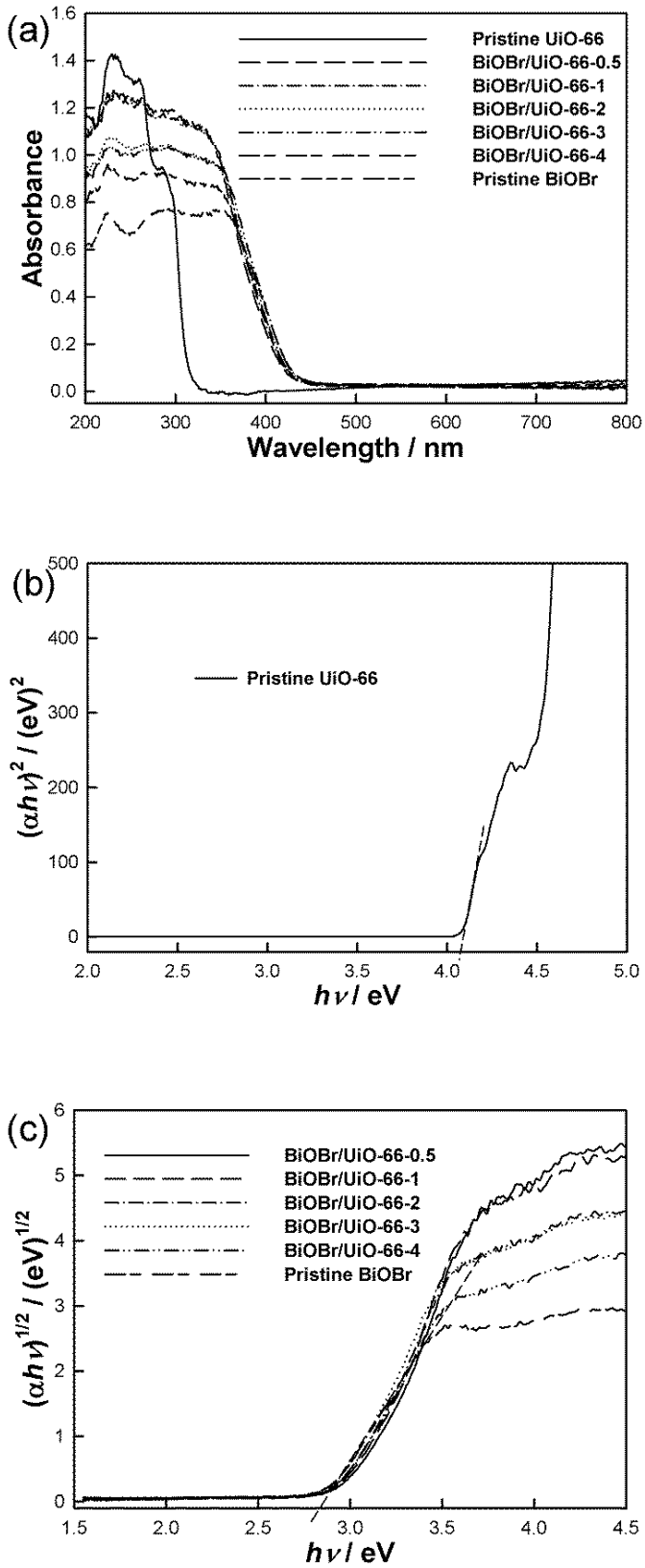

Fig. 6-7 (a) UV-Vis diffuse reflectance spectra, (b) plots of $(\alpha h\nu)^2$ versus energy ($h\nu$) to obtain the band gap energy of pristine UiO-66, and (c) plots of $(\alpha h\nu)^{1/2}$ versus energy ($h\nu$) to obtain the band gap energy of the samples.

6.3.2 Photocatalytic activity

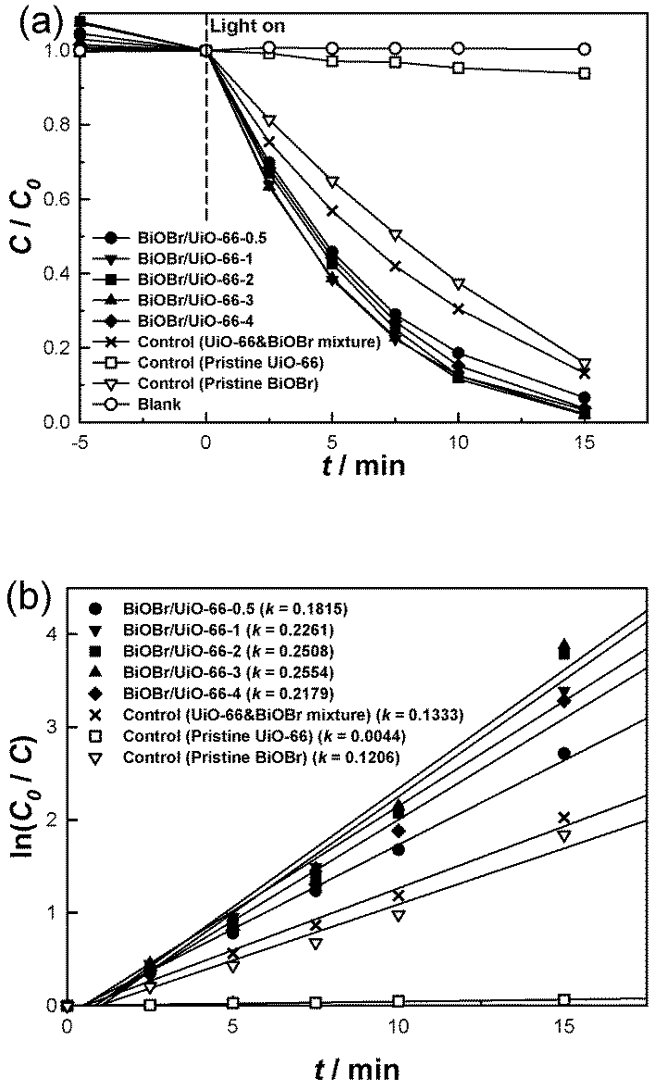

Fig. 6-8 (a) Photocatalytic degradation of RhB in the presence and absence (blank) of different catalysts (BiOBr/UiO-66-0.5, BiOBr/UiO-66-1, BiOBr/UiO-66-2, BiOBr/UiO-66-3, BiOBr/UiO-66-4) under visible-light irradiation. For the three control experiments, the amount of pristine UiO-66 or BiOBr was equal to the actual amount of that contained in BiOBr/UiO-66-3. (b) Comparison of the reaction rate constant (*k*) in the presence of different catalysts (assuming that the reactions follow the pseudo-first-order kinetic model).

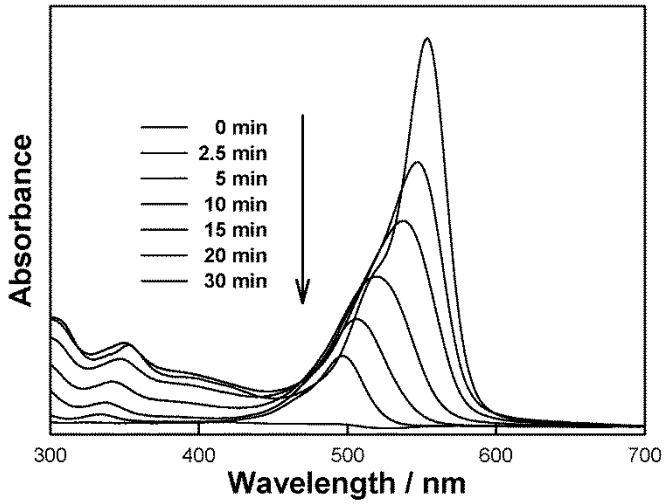

Fig. 6-9 UV-Vis spectral changes of RhB solutions as a function of irradiation time in the presence of BiOBr/UiO-66-3.

To evaluate the photocatalytic activity of different samples, the degradation of RhB by these samples in aqueous solution under visible-light irradiation was examined. As illustrated in Fig. 6-8a, all the BiOBr/UiO-66 composites show remarkably high activity, as nearly all RhB molecules could be completely degraded in merely 15 min. However, it is not easy to distinguish the activity order of different BiOBr/UiO-66 composites. Thus, by assuming that the reactions follow a pseudo-first-order kinetic model, the reaction rate constants (*k*) were calculated to quantify the degradation rates of different experiments (Fig. 6-8b and Table 6-1).[194] Based on the comparison of reaction rate constants, it is not difficult to find that BiOBr/UiO-66-3 exhibits the fastest degradation rate and as such, the highest photocatalytic activity. Furthermore, when the degradation experiment of BiOBr/UiO-66-3 is extended to 30 min, the intermediate degradation products of RhB can be further degraded, and no distinguishable absorption peak in the range of 300–700 nm can be observed (Fig. 6-9). For the control experiment with the mechanical mixture of pristine

UiO-66 and BiOBr, although the components are the same as those in the BiOBr/UiO-66-3 sample, its photocatalytic activity is much lower than that of any BiOBr/UiO-66 composite. The similar result can also be observed from the control experiment in which pristine BiOBr is used. Besides, if pristine UiO-66 is introduced in the degradation experiment, only slight decrease in RhB concentration can be observed. As described earlier, pristine UiO-66 does not possess visible-light activity, it is inferred that this tiny concentration drop is attributed to the weak physical adsorption after the equilibrium. Besides, the result of the blank experiment reveals that the photolysis of RhB without the addition of any catalyst is trifling (Fig. 6-8a, blank).

Since the photocatalytic activity of BiOBr/UiO-66-3 is much higher than that of the mechanical mixture with the same components, a potential interaction is anticipated to form between UiO-66 and BiOBr in the BiOBr/UiO-66 composite. As described previously, the morphology of pristine BiOBr shows a compact pattern and the BiOBr flakes pack together so that the accessible interspace between the flakes is very limited. In contrast, in the presence of UiO-66, the synthesized BiOBr flakes expose in a more random manner, which may be resulted from two reasons. First, the UiO-66 particles uniformly distribute and insert between the BiOBr flakes, preventing the overlap of these flakes. Another possible reason is the potential interaction between UiO-66 and BiOBr, through which the growth of BiOBr can be affected by UiO-66. Due to the random distribution of the UiO-66 particles, the growth of BiOBr crystals also exhibits such random behavior. As a result, both effects give rise to the random arrangement of BiOBr flakes in the BiOBr/UiO-66 composite, increasing the accessible interspace in the composite. Therefore, compared to pristine BiOBr,

the BiOBr/UiO-66 composites have more accessible BiOBr surface to contact with RhB molecules, leading to the enhancement of RhB degradation rate. In addition, the content of BiOBr in the BiOBr/UiO-66 composite is another factor to be considered. From the reaction rate constants summarized in Table 6-1, the photocatalytic activity of the BiOBr/UiO-66 composite rises with the Bi : Zr ratio increasing from (0.5 : 1) to (3 : 1). It is obvious that the increased BiOBr content results in the increased active sites of BiOBr in the BiOBr/UiO-66 composite, so that the RhB degradation rate is enhanced. However, when the Bi : Zr ratio is further increased to (4 : 1), the photocatalytic activity of the composite apparently drops to the level even lower than that of the composite with (1 : 1) Bi : Zr ratio. A possible explanation is that when excessive BiOBr is incorporated to the BiOBr/UiO-66 composite, the amount of UiO-66 may not be enough to separate most of the BiOBr flakes, and therefore the growth of the excessive BiOBr could not be affected. As a result, the behavior of the exceeding BiOBr should be more similar to that of pristine BiOBr, tending to aggregate on the composite surface. This may reduce the accessible surface area of BiOBr and also block the potential channels formed in the final BiOBr/UiO-66 composite, through which RhB molecules can contact with more exposing surface of BiOBr. Consequently, exceeding BiOBr content may reduce the accessible surface area of BiOBr, and have negative effect on the photocatalytic activity of the BiOBr/UiO-66 composite. Therefore, to obtain the highest photocatalytic activity in this study, the optimum BiOBr content in the BiOBr/UiO-66 composite is obtained when Bi : Zr ratio equals (3 : 1).

6.3.3 Photocatalyst stability

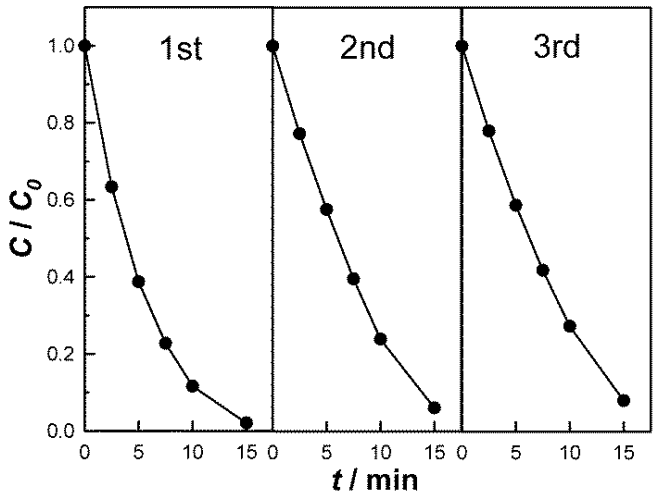

Fig. 6-10 Three cycles of the RhB degradation in the presence of BiOBr/UiO-66-3 under visible-light irradiation.

The structural stability of the BiOBr/UiO-66 composite was evaluated by comparing the change in XRD diffraction patterns and morphology before and after the dye degradation experiment. As shown in Fig. 6-1b, no apparent difference can be found in the XRD patterns of BiOBr/UiO-66-3 used for dye degradation compared to the freshly prepared composite. In addition, from the SEM images, the morphology of BiOBr/UiO-66-3 used for RhB degradation (Fig. 6-3e, 6-3f) almost remains the same as that before the degradation (Fig. 6-3c, 6-3d). The same conclusion can also be drawn based on the TEM results (Fig. 6-5e, 6-5f). The stability and reusability of BiOBr/UiO-66-3 were further examined by reusing the catalyst for two more degradation cycles. As illustrated in Fig. 6-10, although the degradation rate drops slightly in the second cycle, most of the dye can still be degraded in 15 min. With regard to the decrease of photocatalytic activity for the recycled catalyst, one possible explanation is that part of the degradation products generated in the first degradation cycle might be adsorbed on the surface or trapped in the porous structure of the composite, causing the reduction in the surface area of BiOBr accessible to the dye

molecules in the second cycle.[195] However, no further decay in the degradation rate is observed in the third cycle, which proves that BiOBr/UiO-66 composite is a stable photocatalyst for long term degradation process.

Apparently, the superior stability of UiO-66 should be an important factor contributing to the remarkable stability of the BiOBr/UiO-66 composite. And the good interaction between UiO-66 and BiOBr may also be beneficial to the stability of the final composite. As interpreted earlier, this interaction may affect the growth process of the BiOBr crystals. In fact, this interaction might also be essential to establish a good combination between UiO-66 particles and the synthesized BiOBr flakes. To achieve this effect, during the preparation process of BiOBr/UiO-66 composites, bromide salt was first introduced in the UiO-66 aqueous suspension. Because the $Zr_6O_4(OH)_4$ octahedra in the UiO-66 structure (dark grey clusters shown in Fig. 3-12) are positively charged, there should be electrostatic interactions occurring between the octahedra and the negatively charged bromide ions.[176] As a result, these bromide ions might accumulate around the UiO-66 frameworks and react with the subsequently added $Bi_2O_2^{2+}$ cations. Finally, the BiOBr crystal seeds generated initially could attach to the UiO-66 particles, and the BiOBr flakes grown around should form good interaction with UiO-66.

6.3.4 Photocatalytic mechanism

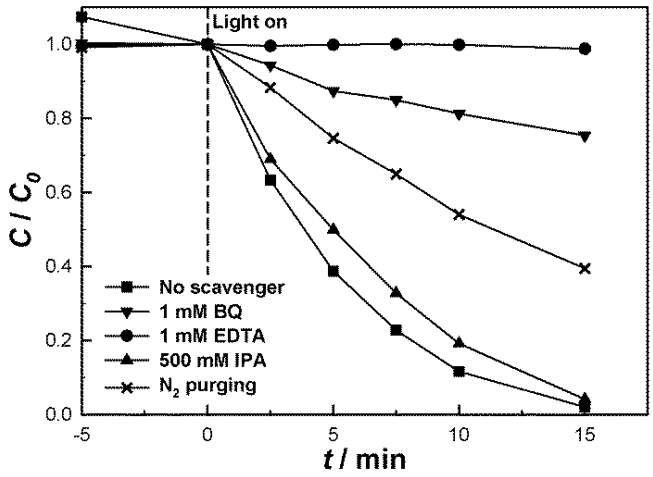

Fig. 6-11 Effects of different scavengers on the degradation of RhB in the presence of BiOBr/UiO-66-3 under visible-light irradiation.

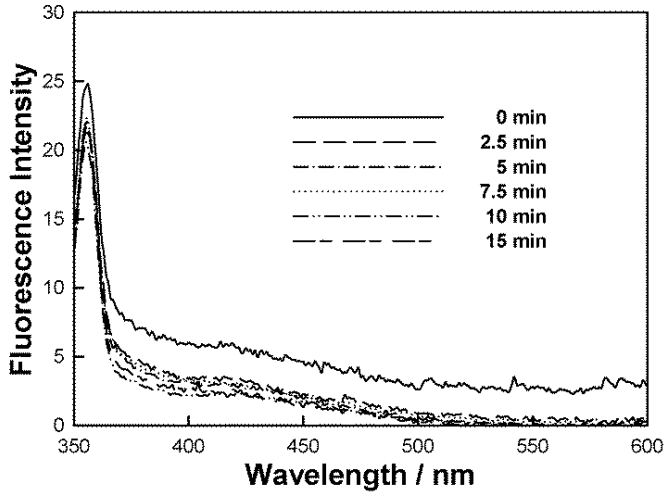

Fig. 6-12 Photoluminescence spectral changes with visible-light irradiation time in the presence of BiOBr/UiO-66-3 in a 5×10^{-4} M basic solution of terephthalic acid.

To study the photocatalytic mechanism of the BiOBr/UiO-66 composite for the degradation of RhB, the potential roles of HO•, O_2^-•, and h^+ (the three main active species involved in the photocatalytic oxidation process) during the degradation process were investigated.[5, 19, 196, 197] IPA, BQ, and EDTA were separately introduced in the degradation process to attempt to trap HO•, O_2^-•, and h^+.[179-181] As shown in Fig. 6-11, the degradation rate is significantly restrained in the presence of BQ, which is able to quench O_2^-•,

inferring that O_2^{-}• should be a major contributor to the decomposition of RhB. Considering that the dissolved O_2 is the crucial reagent to form O_2^{-}•, instead of air N_2 was purged in the degradation system to study its effect on the degradation rate. Similarly, N_2 purging also has a negative effect on the degradation rate, further confirming the important role of O_2^{-}•. However, either the addition of BQ or the N_2 purging only partially suppresses the degradation reaction, implying that RhB was also degraded by other routes. Afterwards, IPA was added as a scavenger of HO•. However, the degradation rate almost does not affected, suggesting that HO• is not a dominant active species involved in the degradation process. To further confirm the role of HO•, a photoluminescence technique was applied, in which terephthalic acid was used as a probe molecule to monitor the HO• generated on the surface of the photocatalyst.[182] As shown in Fig. 6-12, no obvious enhancement in the fluorescence intensity is observable during the test period, further verifying that HO• is an unimportant active species for degradation system. To have a further understanding of the photocatalytic mechanism, EDTA was introduced to the system to suppress the photogenerated h^{+}. As illustrated in Fig. 6-11, the degradation of RhB is almost totally restrained. It is known that EDTA can suppress the activity of h^{+} and may also accelerate the recombination of e^{-} and h^{+}, hence the formation of O_2^{-}• was also suppressed in the presence of EDTA. As a result, the degradation of RhB was almost inhibited by EDTA due to the suppressed generation of h^{+} and O_2^{-}•. Therefore, the photogenerated h^{+} is also involved in the RhB degradation process. The conclusion that O_2^{-}• and h^{+} are the two main active species for the BiOBr based photocatalyst system was also confirmed by other research groups.[231, 241, 242]

6.4 Conclusion

In summary, a novel BiOBr/UiO-66 composite was prepared through a convenient solution method for the degradation of RhB under visible-light irradiation. All the BiOBr/UiO-66 composites with different BiOBr contents exhibited excellent photocatalytic activity for the degradation of RhB. Specifically, the composite with Bi : Zr molar ratio equaling (3 : 1) could decompose all RhB molecules in 15 min, and also was able to further degrade the intermediate degradation products in another 15 min. Compared to the control experiments in which pristine UiO-66 and/or BiOBr was used, the enhanced photocatalytic activity provided by the BiOBr/UiO-66 composite should be ascribed to the enlarged accessible surface area of BiOBr in the composite, which was achieved with the assistance of UiO-66 and the good interaction between BiOBr and the UiO-66 frameworks. In addition, such good interaction as well as the outstanding stability of UiO-66 is believed to be beneficial to establish the good stability and reusability of the BiOBr/UiO-66 composite in the RhB degradation. The study on the photocatalytic mechanism of the BiOBr/UiO-66 composite implies that O_2^{-}• and h^{+} should be the main active species involved in the RhB degradation process.

Chapter 7 Conclusions and Recommendations

In this study, a series of MOF based photocatalysts, such as Bi_2WO_6/UiO-66, AgI/UiO-66, Ag_2CO_3/UiO-66, and BiOBr/UiO-66 were prepared and used for the degradation of organic dye in water treatment. The compositions of components in these photocatalysts were optimized, and their degradation mechanisms were also investigated in depth.

All these MOF based photocatalysts exhibited enhanced dye degradation activity compared to the pristine active materials, such as Bi_2WO_6, AgI, Ag_2CO_3, and BiOBr. The improved activity could be attributed to different reasons. For the Bi_2WO_6/UiO-66 composite, through coupling with the UiO-66 substrate, Bi_2WO_6 was able to form strong interaction with the MOF substrate. Hence, by meticulously designed band gap matching, the active materials and MOF substrate could form a heterogeneous junction, which should facilitate the photogenerated electron-hole separation, *i.e.*, increase the lifetime of the electron-hole pairs. With longer lifetime, the photogenerated electrons or holes would have more opportunities to contact with the dye molecules in the solution, leading to the decomposition of more dye molecules. Therefore, the overall photocatalytic activity of the composite was enhanced. For the AgI/UiO-66 and Ag_2CO_3/UiO-66 composites, without the specially designed synthesis strategies, the specific surface areas of the active materials (*i.e.*, AgI and Ag_2CO_3) are usually very low, leading to the restricted contact areas between the materials and the dye molecules so that the photocatalytic activity of the materials was greatly limited. In contrast, by coupling with the UiO-66 substrate, the specific surface areas of AgI and Ag_2CO_3 could be increased through the involvement of UiO-66, thus the photocatalytic activity of the active materials could be

further enhanced with the support of MOF. In the case of the BiOBr/UiO-66 composite, compared to the control experiments in which pristine UiO-66 and/or BiOBr was used, the enhanced photocatalytic activity provided by the composite should be ascribed to the enlarged accessible surface area of BiOBr in the composite, which was achieved with the assist of UiO-66 and the good interaction between BiOBr and the UiO-66 framework. In details, the presence of UiO-66 not only prevented the overlap of the BiOBr flakes, but also induced random arrangement effect of these flakes during the growing of BiOBr. As a result, compared to pristine BiOBr, the BiOBr/UiO-66 composites had more accessible BiOBr surface to contact with the dye molecules, therefore enhancing the dye degradation rate.

Another advantage of these MOF based photocatalysts is their good stability for long term dye degradation. This is partially due to the superior chemical and structural stability of the selected MOF material (*i.e.*, UiO-66). In addition, the active materials incorporated with MOF were stable enough during the degradation process (except the partial photocorrosion of Ag_2CO_3). Moreover, by elaborately designed synthesis procedures, a good interaction could be formed between the MOF substrate and the active materials, which is another important factor to improve the stability of the composites and also contribute to the reusability of the catalysts.

The study on the degradation mechanisms of diverse MOF based photocatalysts shows that superoxide radicals and holes were the two main active species involved in the degradation process. Although another important active species, hydroxyl radicals, were not found in the current study, the other

active species were powerful enough to degrade organic contaminants at a considerably high rate.

For comparison, the key features, advantages and disadvantages of the UiO-66 based photocatalysts are summarized and listed in Table 7-1.

Although MOFs have been studied for several decades, MOF based visible-light prompted photocatalysis for water treatment is still a highly challenging research area. Thus, this study is one of the limited yet significantly important of its kind in this promising direction. Additionally, the methods of preparing the MOF based photocatalysts are relatively simple and convenient. Besides, MOFs are comparatively inexpensive and easy to be mass-produced. Therefore, this study also has considerable potential for practical application, which may be utilized in the current water treatment system. This study also opens up numerous opportunities to the development of various MOF based functional materials for water treatment and other related fields in the future.

It is acknowledged that there are a few limitations in this study. First, the synthesis of UiO-66 involved a considerable amount of DMF as solvent, which may cause cost issue for synthesis in large scale, especially for the potential practical production of catalyst. Nevertheless, different strategies should be available to optimize the synthesis procedure to reduce the cost to acceptable level, such as increase the amount of starting materials, recycle DMF to enhance its efficiency, search for other synthesis method wherein cheaper solvent is used, *etc*. Second, the current study used only one organic dye (*i.e.*, RhB) as the model dye contaminant. The reason is that the composition of dyes in real wastewater is usually very complicated, making the results unreliable and difficult to reproduce. Third, instead of total degradation, this study focused on partial

degradation of the organic dye, which is still considered practically beneficial. Finally, due to the current limited experimental conditions, the photocatalysis mechanism was studied based on qualitative analysis.

Based on the experimental results and discussions of the current study, future research is particularly required in the following directions:

- In future studies, a more complicated dye system which contains two or more than two types of dyes may be used to mimic the real dye contaminated wastewater. The potential interaction between different types of dyes should also be studied during the degradation process.
- The future research should attempt to improve these MOF based photocatalysts to approach the total degradation of the organic dyes.
- Quantitative analysis is desired in future work since the degradation mechanism can be better understood, and the results may further guide the design of the photocatalyst. It is expected that more accurate quantitative analysis may be achieved through advanced analytical instruments and elaborately designed method.
- Another possible avenue of the future work is to search for more types of MOFs with outstanding properties and high stability, based on which more MOF based high performance photocatalysts can be developed for the application in wastewater treatment.

Table 7-1 Comparison of the UiO-66 based photocatalysts.

	Preparation method	**Optimal composition**	**Proposed reason for enhanced photocatalytic activity**	**Photocatalyst stability**	**Photocatalytic mechanism**	**Advantages**	**Disadvantages**
Bi_2WO_6/ UiO-66	Hydrothermal method	Bi : Zr = 1 : 1	Formation of heterogeneous junction between Bi_2WO_6 and UiO-66	Good	Superoxide radicals and holes	UiO-66 is involved in photocatalysis process	Relatively complicated preparation procedure
BiOBr/ UiO-66	Solution method	Bi : Zr = 3 : 1	Enlarged accessible surface area of BiOBr with the assistance of UiO-66	Good	Superoxide radicals and holes	Superior photocatalytic activity; simple preparation procedure	UiO-66 is not involved in photocatalysis process
AgI/UiO -66	Solution method	Ag : Zr = 1 : 1	Increased specific surface area of AgI with the support of UiO-66	Good	Superoxide radicals and holes	High photocatalytic activity; simple preparation procedure	UiO-66 is not involved in photocatalysis process
Ag_2CO_3/ UiO-66	Solution method	Ag : Zr = 0.5 : 1	Increased specific surface area of Ag_2CO_3 with the support of UiO-66	Partial photocorrosion of Ag_2CO_3	Superoxide radicals and holes	Simple preparation procedure	Photocorrosion of Ag_2CO_3 may affect long term performance of photocatalyst

References

[1] F. Han, V.S.R. Kambala, M. Srinivasan, D. Rajarathnam, R. Naidu, *Appl. Catal., A*, 359 (2009) 25-40.

[2] P.R. Gogate, A.B. Pandit, *Adv. Environ. Res.*, 8 (2004) 501-551.

[3] M.A. Brown, S.C. De Vito, *Crit. Rev. Environ. Sci. Technol.*, 23 (1993) 249-324.

[4] H. Zhang, G. Chen, D.W. Bahnemann, *J. Mater. Chem.*, 19 (2009) 5089-5121.

[5] M.R. Hoffmann, S.T. Martin, W. Choi, D.W. Bahnemann, *Chem. Rev.*, 95 (1995) 69-96.

[6] R. Asahi, T. Morikawa, T. Ohwaki, K. Aoki, Y. Taga, *Science*, 293 (2001) 269-271.

[7] M. Alvaro, E. Carbonell, B. Ferrer, F.X. Llabrés i Xamena, H. Garcia, *Chem. Eur. J.*, 13 (2007) 5106-5112.

[8] F.R. Spellman, Handbook of Water and Wastewater Treatment Plant Operations, 2nd ed., CRC Press, Boca Raton, FL, 2009.

[9] http://www.unwater.org/water-cooperation-2013/water-cooperation/facts-and-figures/en/, Facts and Figures from International Year of Water Cooperation, in: 2013.

[10] B. Bradley, G. Daigger, R. Rubin, G. Tchobanoglous, *Clean Techn. Environ. Policy*, 4 (2002) 87-99.

[11] L. Lapeña, M. Cerezo, P. Garcá-Augustín, *Bull. Environ. Contam. Toxicol.*, 55 (1995) 697-703.

[12] P.V.A. Padmanabhan, K.P. Sreekumar, T.K. Thiyagarajan, R.U. Satpute, K. Bhanumurthy, P. Sengupta, G.K. Dey, K.G.K. Warrier, *Vacuum*, 80 (2006) 1252-1255.

[13] U.I. Gaya, A.H. Abdullah, *J. Photochem. Photobiol., C*, 9 (2008) 1-12.

[14] S. Malato, P. Fernández-Ibáñez, M.I. Maldonado, J. Blanco, W. Gernjak, *Catal. Today*, 147 (2009) 1-59 – Reprinted with permission from Elsevier.

[15] Y. Wei, R.T. Van Houten, A.R. Borger, D.H. Eikelboom, Y. Fan, *Water Res.*, 37 (2003) 4453-4467.

[16] I. Oller, S. Malato, J.A. Sánchez-Pérez, *Sci. Total Environ.*, 409 (2011) 4141-4166.

[17] W.H. Glaze, J.-W. Kang, D.H. Chapin, *Ozone: Sci. Eng.*, 9 (1987) 335-352.

[18] S. Esplugas, J. Giménez, S. Contreras, E. Pascual, M. Rodríguez, *Water Res.*, 36 (2002) 1034-1042.

[19] M. Pera-Titus, V. García-Molina, M.A. Baños, J. Giménez, S. Esplugas, *Appl. Catal., B*, 47 (2004) 219-256.

[20] D.G. Rao, R. Senthilkumar, J.A. Byrne, S. Feroz, Wastewater Treatment: Advanced Processes and Technologies, CRC Press: Boca Raton, 2013.

[21] A. Kubacka, M. Fernández-García, G. Colón, *Chem. Rev.*, 112 (2011) 1555-1614.

[22] H. Gerischer, *Electrochim. Acta*, 35 (1990) 1677-1699.

[23] C. Renz, *Helv. Chimi. Acta*, 4 (1921) 961-968.

[24] C.F. Goodeve, J.A. Kitchener, *Trans. Faraday Soc.*, 34 (1938) 570-579.

[25] S. Kato, F. Mashiro, Autooxidation by TiO_2 as a photocatalyst, in: Abtr BookAnnu Meet Chemical Society of Japan, 1956, pp. 223.

[26] A.L. Linsebigler, G. Lu, J.T. Yates, *Chem. Rev.*, 95 (1995) 735-758.

[27] T.L. Thompson, J.T. Yates, *Chem. Rev.*, 106 (2006) 4428-4453.

[28] D.O. Scanlon, C.W. Dunnill, J. Buckeridge, S.A. Shevlin, A.J. Logsdail, S.M. Woodley, C.R.A. Catlow, M.J. Powell, R.G. Palgrave, I.P. Parkin, G.W. Watson, T.W. Keal, P. Sherwood, A. Walsh, A.A. Sokol, *Nat. Mater.*, 12 (2013) 798-801.

[29] http://news.panasonic.net/stories/2014/1223_30520.html, Panasonic Develops 'Photocatalytic Water Purification Technology' - Creating Drinkable Water with Sunlight and Photocatalysts, in: 2014.

[30] S. Malato, J. Blanco, A. Vidal, C. Richter, *Appl. Catal., B*, 37 (2002) 1-15.

[31] S. Rehman, R. Ullah, A.M. Butt, N.D. Gohar, *J. Hazard. Mater.*, 170 (2009) 560-569.

[32] S.G. Kumar, L.G. Devi, *J. Phys. Chem. A*, 115 (2011) 13211-13241.

[33] Z. Zhang, M.F. Hossain, T. Takahashi, *Appl. Catal., B*, 95 (2010) 423-429.

[34] S.-W. Cao, Y.-J. Zhu, G.-F. Cheng, Y.-H. Huang, *J. Hazard. Mater.*, 171 (2009) 431-435.

[35] D. Chen, J. Ye, *Adv. Funct. Mater.*, 18 (2008) 1922-1928.

[36] Y. Hu, X. Gao, L. Yu, Y. Wang, J. Ning, S. Xu, X.W. Lou, *Angew. Chem. Int. Ed.*, 52 (2013) 5636-5639.

[37] L. Zhou, W. Wang, H. Xu, S. Sun, M. Shang, *Chem. Eur. J.*, 15 (2009) 1776-1782.

[38] D. Farrusseng, Metal-Organic Frameworks: Applications from Catalysis to Gas Storage, Wiley-VCH Verlag & Co. KGaA: Weinheim, Germany, 2011.

[39] K. Sumida, D.L. Rogow, J.A. Mason, T.M. McDonald, E.D. Bloch, Z.R. Herm, T.-H. Bae, J.R. Long, *Chem. Rev.*, 112 (2011) 724-781.

[40] H. Furukawa, N. Ko, Y.B. Go, N. Aratani, S.B. Choi, E. Choi, A.Ö. Yazaydin, R.Q. Snurr, M. O'Keeffe, J. Kim, O.M. Yaghi, *Science*, 329 (2010) 424-428.

[41] J.L.C. Rowsell, O.M. Yaghi, *J. Am. Chem. Soc.*, 128 (2006) 1304-1315.

[42] H. Furukawa, J. Kim, N.W. Ockwig, M. O'Keeffe, O.M. Yaghi, *J. Am. Chem. Soc.*, 130 (2008) 11650-11661.

[43] Z. Wang, S.M. Cohen, *Chem. Soc. Rev.*, 38 (2009) 1315-1329.

[44] K.K. Tanabe, S.M. Cohen, *Chem. Soc. Rev.*, 40 (2011) 498-519.

[45] A.U. Czaja, N. Trukhan, U. Muller, *Chem. Soc. Rev.*, 38 (2009) 1284-1293.

[46] J. Klinowski, F.A. Almeida Paz, P. Silva, J. Rocha, *Dalton Trans.*, 40 (2011) 321-330.

[47] D.-W. Jung, D.-A. Yang, J. Kim, J. Kim, W.-S. Ahn, *Dalton Trans.*, 39 (2010) 2883-2887.

[48] C.G. Carson, A.J. Brown, D.S. Sholl, S. Nair, *Cryst. Growth Des.*, 11 (2011) 4505-4510.

[49] A. Pichon, S.L. James, *CrystEngComm*, 10 (2008) 1839-1847.

[50] M. Klimakow, P. Klobes, A.F. Thünemann, K. Rademann, F. Emmerling, *Chem. Mater.*, 22 (2010) 5216-5221.

[51] M. Li, M. Dincă, *J. Am. Chem. Soc.*, 133 (2011) 12926-12929.

[52] H. Li, M. Eddaoudi, M. O'Keeffe, O.M. Yaghi, *Nature*, 402 (1999) 276-279.

[53] H. Furukawa, O.M. Yaghi, *J. Am. Chem. Soc.*, 131 (2009) 8875-8883.

[54] H.K. Chae, D.Y. Siberio-Perez, J. Kim, Y. Go, M. Eddaoudi, A.J. Matzger, M. O'Keeffe, O.M. Yaghi, *Nature*, 427 (2004) 523-527.

[55] O.K. Farha, I. Eryazici, N.C. Jeong, B.G. Hauser, C.E. Wilmer, A.A. Sarjeant, R.Q. Snurr, S.T. Nguyen, A.Ö. Yazaydın, J.T. Hupp, *J. Am. Chem. Soc.*, 134 (2012) 15016-15021.

[56] M. Eddaoudi, J. Kim, N. Rosi, D. Vodak, J. Wachter, M. O'Keeffe, O.M. Yaghi, *Science*, 295 (2002) 469-472.

[57] T. Loiseau, C. Serre, C. Huguenard, G. Fink, F. Taulelle, M. Henry, T. Bataille, G. Férey, *Chem. Eur. J.*, 10 (2004) 1373-1382.

[58] J.H. Cavka, S. Jakobsen, U. Olsbye, N. Guillou, C. Lamberti, S. Bordiga, K.P. Lillerud, *J. Am. Chem. Soc.*, 130 (2008) 13850-13851 – Reprinted with permission from The American Chemical Society.

[59] M. Kandiah, M.H. Nilsen, S. Usseglio, S. Jakobsen, U. Olsbye, M. Tilset, C. Larabi, E.A. Quadrelli, F. Bonino, K.P. Lillerud, *Chem. Mater.*, 22 (2010) 6632-6640.

[60] K.S. Park, Z. Ni, A.P. Côté, J.Y. Choi, R. Huang, F.J. Uribe-Romo, H.K. Chae, M. O'Keeffe, O.M. Yaghi, *Proc. Natl. Acad. Sci.*, 103 (2006) 10186-10191.

[61] W. Morris, B. Volosskiy, S. Demir, F. Gándara, P.L. McGrier, H. Furukawa, D. Cascio, J.F. Stoddart, O.M. Yaghi, *Inorg. Chem.*, 51 (2012) 6443-6445.

[62] V. Colombo, S. Galli, H.J. Choi, G.D. Han, A. Maspero, G. Palmisano, N. Masciocchi, J.R. Long, *Chem. Sci.*, 2 (2011) 1311-1319.

[63] Y. He, W. Zhou, G. Qian, B. Chen, *Chem. Soc. Rev.*, 43 (2014) 5657-5678.

[64] N.L. Rosi, J. Eckert, M. Eddaoudi, D.T. Vodak, J. Kim, M. O'Keeffe, O.M. Yaghi, *Science*, 300 (2003) 1127-1129.

[65] M.P. Suh, H.J. Park, T.K. Prasad, D.-W. Lim, *Chem. Rev.*, 112 (2011) 782-835.

[66] O.K. Farha, A. Özgür Yazaydın, I. Eryazici, C.D. Malliakas, B.G. Hauser, M.G. Kanatzidis, S.T. Nguyen, R.Q. Snurr, J.T. Hupp, *Nat. Chem.*, 2 (2010) 944-948.

[67] J.B. DeCoste, M.H. Weston, P.E. Fuller, T.M. Tovar, G.W. Peterson, M.D. LeVan, O.K. Farha, *Angew. Chem. Int. Ed.*, 53 (2014) 14092-14095.

[68] Q. Min Wang, D. Shen, M. Bülow, M. Ling Lau, S. Deng, F.R. Fitch, N.O. Lemcoff, J. Semanscin, *Microporous Mesoporous Mater.*, 55 (2002) 217-230.

[69] S. Bourrelly, P.L. Llewellyn, C. Serre, F. Millange, T. Loiseau, G. Férey, *J. Am. Chem. Soc.*, 127 (2005) 13519-13521.

[70] R. Banerjee, H. Furukawa, D. Britt, C. Knobler, M. O'Keeffe, O.M. Yaghi, *J. Am. Chem. Soc.*, 131 (2009) 3875-3877.

[71] Z.R. Herm, J.A. Swisher, B. Smit, R. Krishna, J.R. Long, *J. Am. Chem. Soc.*, 133 (2011) 5664-5667.

[72] R. Banerjee, A. Phan, B. Wang, C. Knobler, H. Furukawa, M. O'Keeffe, O.M. Yaghi, *Science*, 319 (2008) 939-943.

[73] J.W. Yoon, S.H. Jhung, Y.K. Hwang, S.M. Humphrey, P.T. Wood, J.S. Chang, *Adv. Mater.*, 19 (2007) 1830-1834.

[74] L.J. Murray, M. Dinca, J. Yano, S. Chavan, S. Bordiga, C.M. Brown, J.R. Long, *J. Am. Chem. Soc.*, 132 (2010) 7856-7857.

[75] S. Shimomura, M. Higuchi, R. Matsuda, K. Yoneda, Y. Hijikata, Y. Kubota, Y. Mita, J. Kim, M. Takata, S. Kitagawa, *Nat. Chem.*, 2 (2010) 633-637.

[76] S. Shimomura, R. Matsuda, S. Kitagawa, *Chem. Mater.*, 22 (2010) 4129-4131.

[77] J.-R. Li, R.J. Kuppler, H.-C. Zhou, *Chem. Soc. Rev.*, 38 (2009) 1477-1504.

[78] S.-C. Xiang, Z. Zhang, C.-G. Zhao, K. Hong, X. Zhao, D.-R. Ding, M.-H. Xie, C.-D. Wu, M.C. Das, R. Gill, K.M. Thomas, B. Chen, *Nat. Commun.*, 2 (2011) 204.

[79] D. Britt, D. Tranchemontagne, O.M. Yaghi, *Proc. Natl. Acad. Sci.*, 105 (2008) 11623-11627.

[80] U. Mueller, M. Schubert, F. Teich, H. Puetter, K. Schierle-Arndt, J. Pastre, *J. Mater. Chem.*, 16 (2006) 626-636.

[81] O.M. Yaghi, G. Li, H. Li, *Nature*, 378 (1995) 703-706.

[82] O.M. Yaghi, C.E. Davis, G. Li, H. Li, *J. Am. Chem. Soc.*, 119 (1997) 2861-2868.

[83] K.A. Cychosz, A.G. Wong-Foy, A.J. Matzger, *J. Am. Chem. Soc.*, 130 (2008) 6938-6939.

[84] J.M. Castillo, T.J.H. Vlugt, S. Calero, *J. Phys. Chem. C*, 113 (2009) 20869-20874.

[85] J.S. Seo, D. Whang, H. Lee, S.I. Jun, J. Oh, Y.J. Jeon, K. Kim, *Nature*, 404 (2000) 982-986.

[86] M. Plabst, L.B. McCusker, T. Bein, *J. Am. Chem. Soc.*, 131 (2009) 18112-18118.

[87] B. Chen, L. Wang, F. Zapata, G. Qian, E.B. Lobkovsky, *J. Am. Chem. Soc.*, 130 (2008) 6718-6719.

[88] M.G. Goesten, F. Kapteijn, J. Gascon, *CrystEngComm*, 15 (2013) 9249-9257.

[89] S. Hasegawa, S. Horike, R. Matsuda, S. Furukawa, K. Mochizuki, Y. Kinoshita, S. Kitagawa, *J. Am. Chem. Soc.*, 129 (2007) 2607-2614.

[90] P. Valvekens, F. Vermoortele, D. De Vos, *Catal. Sci. Technol.*, 3 (2013) 1435-1445.

[91] M. Fujita, Y.J. Kwon, S. Washizu, K. Ogura, *J. Am. Chem. Soc.*, 116 (1994) 1151-1152.

[92] F.X. Llabrés i Xamena, A. Abad, A. Corma, H. Garcia, *J. Catal.*, 250 (2007) 294-298.

[93] C. Di Nicola, Y.Y. Karabach, A.M. Kirillov, M. Monari, L. Pandolfo, C. Pettinari, A.J.L. Pombeiro, *Inorg. Chem.*, 46 (2006) 221-230.

[94] Y. Lu, M. Tonigold, B. Bredenkötter, D. Volkmer, J. Hitzbleck, G. Langstein, *Z. anorg. allg. Chem.*, 634 (2008) 2411-2417.

[95] R.-Q. Zou, H. Sakurai, Q. Xu, *Angew. Chem. Int. Ed.*, 45 (2006) 2542-2546.

[96] J. Lee, O.K. Farha, J. Roberts, K.A. Scheidt, S.T. Nguyen, J.T. Hupp, *Chem. Soc. Rev.*, 38 (2009) 1450-1459.

[97] S. Hermes, M.-K. Schröter, R. Schmid, L. Khodeir, M. Muhler, A. Tissler, R.W. Fischer, R.A. Fischer, *Angew. Chem. Int. Ed.*, 44 (2005) 6237-6241.

[98] T. Ishida, M. Nagaoka, T. Akita, M. Haruta, *Chem. Eur. J.*, 14 (2008) 8456-8460.

[99] M. Müller, S. Hermes, K. Kähler, M.W.E. van den Berg, M. Muhler, R.A. Fischer, *Chem. Mater.*, 20 (2008) 4576-4587.

[100] F.L.i. Xamena, J. Gascon, Metal Organic Frameworks as Heterogeneous Catalysts, The Royal Society of Chemistry: Cambridge, UK, 2013 – Reproduced by permission of The Royal Society of Chemistry, http://dx.doi.org/10.1039/9781849737586-00365.

[101] M. Fuentes-Cabrera, D.M. Nicholson, B.G. Sumpter, M. Widom, *J. Chem. Phys.*, 123 (2005) 124713.

[102] B. Civalleri, F. Napoli, Y. Noel, C. Roetti, R. Dovesi, *CrystEngComm*, 8 (2006) 364-371.

[103] A. Kuc, A. Enyashin, G. Seifert, *J. Phys. Chem. B*, 111 (2007) 8179-8186.

[104] C.G. Silva, A. Corma, H. Garcia, *J. Mater. Chem.*, 20 (2010) 3141-3156.

[105] R. Li, J. Hu, M. Deng, H. Wang, X. Wang, Y. Hu, H.-L. Jiang, J. Jiang, Q. Zhang, Y. Xie, Y. Xiong, *Adv. Mater.*, 26 (2014) 4783-4788.

[106] M.C. Das, H. Xu, Z. Wang, G. Srinivas, W. Zhou, Y.-F. Yue, V.N. Nesterov, G. Qian, B. Chen, *Chem. Commun.*, 47 (2011) 11715-11717.

[107] M.E. Foster, J.D. Azoulay, B.M. Wong, M.D. Allendorf, *Chem. Sci.*, 5 (2014) 2081-2090.

[108] C.A. Kent, D. Liu, L. Ma, J.M. Papanikolas, T.J. Meyer, W. Lin, *J. Am. Chem. Soc.*, 133 (2011) 12940-12943.

[109] H.-J. Son, S. Jin, S. Patwardhan, S.J. Wezenberg, N.C. Jeong, M. So, C.E. Wilmer, A.A. Sarjeant, G.C. Schatz, R.Q. Snurr, O.K. Farha, G.P. Wiederrecht, J.T. Hupp, *J. Am. Chem. Soc.*, 135 (2012) 862-869.

[110] C.A. Kent, B.P. Mehl, L. Ma, J.M. Papanikolas, T.J. Meyer, W. Lin, *J. Am. Chem. Soc.*, 132 (2010) 12767-12769.

[111] Y. Fu, D. Sun, Y. Chen, R. Huang, Z. Ding, X. Fu, Z. Li, *Angew. Chem. Int. Ed.*, 51 (2012) 3364-3367.

[112] A.G. Condie, J.C. González-Gómez, C.R.J. Stephenson, *J. Am. Chem. Soc.*, 132 (2010) 1464-1465.

[113] P. Wu, C. He, J. Wang, X. Peng, X. Li, Y. An, C. Duan, *J. Am. Chem. Soc.*, 134 (2012) 14991-14999.

[114] M.-H. Xie, X.-L. Yang, C. Zou, C.-D. Wu, *Inorg. Chem.*, 50 (2011) 5318-5320.

[115] C. Gomes Silva, I. Luz, F.X. Llabrés i Xamena, A. Corma, H. García, *Chem. Eur. J.*, 16 (2010) 11133-11138.

[116] M.A. Nasalevich, M.G. Goesten, T.J. Savenije, F. Kapteijn, J. Gascon, *Chem. Commun.*, 49 (2013) 10575-10577.

[117] T. Zhou, Y. Du, A. Borgna, J. Hong, Y. Wang, J. Han, W. Zhang, R. Xu, *Energy Environ. Sci.*, 6 (2013) 3229-3234.

[118] J. He, Z. Yan, J. Wang, J. Xie, L. Jiang, Y. Shi, F. Yuan, F. Yu, Y. Sun, *Chem. Commun.*, 49 (2013) 6761-6763.

[119] S. Abedi, A. Morsali, *ACS Catal.*, 4 (2014) 1398-1403.

[120] C. Wang, Z. Xie, K.E. deKrafft, W. Lin, *J. Am. Chem. Soc.*, 133 (2011) 13445-13454.

[121] C. Wang, J.-L. Wang, W. Lin, *J. Am. Chem. Soc.*, 134 (2012) 19895-19908.

[122] K. Sasan, Q. Lin, C. Mao, P. Feng, *Chem. Commun.*, 50 (2014) 10390-10393.

[123] M.A. Nasalevich, M. van der Veen, F. Kapteijn, J. Gascon, *CrystEngComm*, 16 (2014) 4919-4926.

[124] C. Wang, K.E. deKrafft, W. Lin, *J. Am. Chem. Soc.*, 134 (2012) 7211-7214.

[125] J. He, J. Wang, Y. Chen, J. Zhang, D. Duan, Y. Wang, Z. Yan, *Chem. Commun.*, 50 (2014) 7063-7066.

[126] L. Shen, W. Wu, R. Liang, R. Lin, L. Wu, *Nanoscale*, 5 (2013) 9374-9382.

[127] D. Sun, W. Liu, Y. Fu, Z. Fang, F. Sun, X. Fu, Y. Zhang, Z. Li, *Chem. Eur. J.*, 20 (2014) 4780-4788.

[128] L.E. Kreno, K. Leong, O.K. Farha, M. Allendorf, R.P. Van Duyne, J.T. Hupp, *Chem. Rev.*, 112 (2011) 1105-1125.

[129] Z. Hu, B.J. Deibert, J. Li, *Chem. Soc. Rev.*, 43 (2014) 5815-5840.

[130] P. Horcajada, C. Serre, M. Vallet-Reg í, M. Sebban, F. Taulelle, G. F érey, *Angew. Chem.*, 118 (2006) 6120-6124.

[131] P. Horcajada, T. Chalati, C. Serre, B. Gillet, C. Sebrie, T. Baati, J.F. Eubank, D. Heurtaux, P. Clayette, C. Kreuz, J.-S. Chang, Y.K. Hwang, V. Marsaud, P.-N. Bories, L. Cynober, S. Gil, G. Ferey, P. Couvreur, R. Gref, *Nat. Mater.*, 9 (2010) 172-178.

[132] P. Horcajada, R. Gref, T. Baati, P.K. Allan, G. Maurin, P. Couvreur, G. F érey, R.E. Morris, C. Serre, *Chem. Rev.*, 112 (2011) 1232-1268.

[133] Y. Cui, Y. Yue, G. Qian, B. Chen, *Chem. Rev.*, 112 (2011) 1126-1162.

[134] H. Furukawa, K.E. Cordova, M. O'Keeffe, O.M. Yaghi, *Science*, 341 (2013) 1230444.

[135] Q.-L. Zhu, Q. Xu, *Chem. Soc. Rev.*, 43 (2014) 5468-5512.

[136] E. Haque, J.W. Jun, S.H. Jhung, *J. Hazard. Mater.*, 185 (2011) 507-511.

[137] E.-Y. Choi, K. Park, C.-M. Yang, H. Kim, J.-H. Son, S.W. Lee, Y.H. Lee, D. Min, Y.-U. Kwon, *Chem. Eur. J.*, 10 (2004) 5535-5540.

[138] Z. Hasan, J. Jeon, S.H. Jhung, *J. Hazard. Mater.*, 209–210 (2012) 151-157.

[139] F. Zou, R. Yu, R. Li, W. Li, *ChemPhysChem*, 14 (2013) 2825-2832.

[140] F. Ke, L.-G. Qiu, Y.-P. Yuan, F.-M. Peng, X. Jiang, A.-J. Xie, Y.-H. Shen, J.-F. Zhu, *J. Hazard. Mater.*, 196 (2011) 36-43.

[141] Z.-Q. Bai, L.-Y. Yuan, L. Zhu, Z.-R. Liu, S.-Q. Chu, L.-R. Zheng, J. Zhang, Z.-F. Chai, W.-Q. Shi, *J. Mater. Chem. A*, 3 (2015) 525-534.

[142] E. Haque, J.E. Lee, I.T. Jang, Y.K. Hwang, J.-S. Chang, J. Jegal, S.H. Jhung, *J. Hazard. Mater.*, 181 (2010) 535-542.

[143] B. Liu, F. Yang, Y. Zou, Y. Peng, *J. Chem. Eng. Data*, 59 (2014) 1476-1482.

[144] Z. Hasan, E.-J. Choi, S.H. Jhung, *Chem. Eng. J.*, 219 (2013) 537-544.

[145] E.Y. Park, Z. Hasan, N.A. Khan, S.H. Jhung, *J. Nanosci. Nanotechnol.*, 13 (2013) 2789-2794.

[146] K.-Y.A. Lin, H. Yang, C. Petit, F.-K. Hsu, *Chem. Eng. J.*, 249 (2014) 293-301.

[147] Z.-Q. Li, M. Zhang, B. Liu, C.-Y. Guo, M. Zhou, *Inorg. Chem. Commun.*, 36 (2013) 241-244.

[148] W.-T. Xu, L. Ma, F. Ke, F.-M. Peng, G.-S. Xu, Y.-H. Shen, J.-F. Zhu, L.-G. Qiu, Y.-P. Yuan, *Dalton Trans.*, 43 (2014) 3792-3798.

[149] J. Gao, J. Miao, P.-Z. Li, W.Y. Teng, L. Yang, Y. Zhao, B. Liu, Q. Zhang, *Chem. Commun.*, 50 (2014) 3786-3788.

[150] J.-J. Du, Y.-P. Yuan, J.-X. Sun, F.-M. Peng, X. Jiang, L.-G. Qiu, A.-J. Xie, Y.-H. Shen, J.-F. Zhu, *J. Hazard. Mater.*, 190 (2011) 945-951.

[154] L. Ai, C. Zhang, L. Li, J. Jiang, *Appl. Catal., B*, 148–149 (2014) 191-200.

[152] J. Gascon, A. Corma, F. Kapteijn, F.X. Llabrés i Xamena, *ACS Catal.*, 4 (2013) 361-378.

[153] C.-F. Zhang, L.-G. Qiu, F. Ke, Y.-J. Zhu, Y.-P. Yuan, G.-S. Xu, X. Jiang, *J. Mater. Chem. A*, 1 (2013) 14329-14334.

[154] S.-T. Gao, W.-H. Liu, N.-Z. Shang, C. Feng, Q.-H. Wu, Z. Wang, C. Wang, *RSC Adv.*, 4 (2014) 61736-61742.

[155] E. Flage−Larsen, A. Røyset, J.H. Cavka, K. Thorshaug, *J. Phys. Chem. C*, 117 (2013) 20610-20616.

[156] W. Zhang, G. Lu, C. Cui, Y. Liu, S. Li, W. Yan, C. Xing, Y.R. Chi, Y. Yang, F. Huo, *Adv. Mater.*, 26 (2014) 4056-4060.

[157] K. Na, K.M. Choi, O.M. Yaghi, G.A. Somorjai, *Nano Lett*, 14 (2014) 5979-5983.

[158] J. Ren, H.W. Langmi, B.C. North, M. Mathe, D. Bessarabov, *Int. J. Hydrogen Energy*, 39 (2014) 890-895.

[159] X. Zhu, J. Gu, Y. Wang, B. Li, Y. Li, W. Zhao, J. Shi, *Chem. Commun.*, 50 (2014) 8779-8782.

[160] J.B. DeCoste, G.W. Peterson, H. Jasuja, T.G. Glover, Y.-g. Huang, K.S. Walton, *J. Mater. Chem. A*, 1 (2013) 5642-5650.

[161] H. Furukawa, F. Gándara, Y.-B. Zhang, J. Jiang, W.L. Queen, M.R. Hudson, O.M. Yaghi, *J. Am. Chem. Soc.*, 136 (2014) 4369-4381.

[162] H. Wu, Y.S. Chua, V. Krungleviciute, M. Tyagi, P. Chen, T. Yildirim, W. Zhou, *J. Am. Chem. Soc.*, 135 (2013) 10525-10532.

[163] K.-K. Yee, N. Reimer, J. Liu, S.-Y. Cheng, S.-M. Yiu, J. Weber, N. Stock, Z. Xu, *J. Am. Chem. Soc.*, 135 (2013) 7795-7798.

[164] X. Zhao, D. Liu, H. Huang, W. Zhang, Q. Yang, C. Zhong, *Microporous Mesoporous Mater.*, 185 (2014) 72-78.

[165] Y. Li, Y. Liu, W. Gao, L. Zhang, W. Liu, J. Lu, Z. Wang, Y.-J. Deng, *CrystEngComm*, 16 (2014) 7037-7042.

[166] A. Shahat, H.M.A. Hassan, H.M.E. Azzazy, *Anal. Chim. Acta*, 793 (2013) 90-98.

[167] Z. Hasan, M. Tong, B.K. Jung, I. Ahmed, C. Zhong, S.H. Jhung, *J. Phys. Chem. C*, 118 (2014) 21049-21056.

[168] J. Long, S. Wang, Z. Ding, S. Wang, Y. Zhou, L. Huang, X. Wang, *Chem. Commun.*, 48 (2012) 11656-11658.

[169] R. Lin, L. Shen, Z. Ren, W. Wu, Y. Tan, H. Fu, J. Zhang, L. Wu, *Chem. Commun.*, 50 (2014) 8533-8535.

[170] L. Shen, S. Liang, W. Wu, R. Liang, L. Wu, *Dalton Trans.*, 42 (2013) 13649-13657.

[171] L. Shen, L. Huang, S. Liang, R. Liang, N. Qin, L. Wu, *RSC Adv.*, 4 (2014) 2546-2549.

[172] L. Shen, R. Liang, M. Luo, F. Jing, L. Wu, *Phys. Chem. Chem. Phys.*, 17 (2015) 117-121.

[173] S. Pu, L. Xu, L. Sun, H. Du, *Inorg. Chem. Commun.*, 52 (2015) 50-52.

[174] A. Schaate, P. Roy, A. Godt, J. Lippke, F. Waltz, M. Wiebcke, P. Behrens, *Chem. Eur. J.*, 17 (2011) 6643-6651.

[175] M.A. Butler, *J. Appl. Phys.*, 48 (1977) 1914-1920.

[176] L. Valenzano, B. Civalleri, S. Chavan, S. Bordiga, M.H. Nilsen, S. Jakobsen, K.P. Lillerud, C. Lamberti, *Chem. Mater.*, 23 (2011) 1700-1718.

[177] R.H. Victora, *Phys. Rev. B*, 56 (1997) 4417-4421.

[178] W.L. Huang, Q. Zhu, *J. Comput. Chem.*, 30 (2009) 183-190.

[179] C. Shifu, J. Lei, T. Wenming, F. Xianliang, *Dalton Trans.*, 42 (2013) 10759-10768.

[180] T.B. Li, G. Chen, C. Zhou, Z.Y. Shen, R.C. Jin, J.X. Sun, *Dalton Trans.*, 40 (2011) 6751-6758.

[181] S. Shenawi-Khalil, V. Uvarov, S. Fronton, I. Popov, Y. Sasson, *Appl. Catal., B*, 117–118 (2012) 148-155.

[182] K.-i. Ishibashi, A. Fujishima, T. Watanabe, K. Hashimoto, *Electrochem. Commun.*, 2 (2000) 207-210.

[183] J. Tang, Z. Zou, J. Ye, *Catal. Lett.*, 92 (2004) 53-56.

[184] H. Fu, C. Pan, W. Yao, Y. Zhu, *J. Phys. Chem. B*, 109 (2005) 22432-22439.

[185] L. Zhang, W. Wang, L. Zhou, H. Xu, *Small*, 3 (2007) 1618-1625.

[186] J. Wu, F. Duan, Y. Zheng, Y. Xie, *J. Phys. Chem. C*, 111 (2007) 12866-12871.

[187] M. Shang, W. Wang, L. Zhang, S. Sun, L. Wang, L. Zhou, *J. Phys. Chem. C*, 113 (2009) 14727-14731.

[188] Q. Xiao, J. Zhang, C. Xiao, X. Tan, *Catal. Commun.*, 9 (2008) 1247-1253.

[189] C. Zhang, Y. Zhu, *Chem. Mater.*, 17 (2005) 3537-3545.

[190] H. Xie, D. Shen, X. Wang, G. Shen, *Mater. Chem. Phys.*, 103 (2007) 334-339.

[191] S. Zhang, J. Shen, H. Fu, W. Dong, Z. Zheng, L. Shi, *J. Solid State Chem.*, 180 (2007) 1456-1463.

[192] S.J. Garibay, S.M. Cohen, *Chem. Commun.*, 46 (2010) 7700-7702.

[193] S. Chavan, J.G. Vitillo, D. Gianolio, O. Zavorotynska, B. Civalleri, S. Jakobsen, M.H. Nilsen, L. Valenzano, C. Lamberti, K.P. Lillerud, S. Bordiga, *Phys. Chem. Chem. Phys.*, 14 (2012) 1614-1626.

[194] I.K. Konstantinou, T.A. Albanis, *Appl. Catal., B*, 49 (2004) 1-14.

[195] S. Song, F. Hong, Z. He, Q. Cai, J. Chen, *J. Colloid Interface Sci.*, 378 (2012) 159-166.

[196] M.D. Hernandez-Alonso, F. Fresno, S. Suarez, J.M. Coronado, *Energy Environ. Sci.*, 2 (2009) 1231-1257.

[197] K. Rajeshwar, M.E. Osugi, W. Chanmanee, C.R. Chenthamarakshan, M.V.B. Zanoni, P. Kajitvichyanukul, R. Krishnan-Ayer, *J. Photochem. Photobiol., C*, 9 (2008) 171-192.

[198] C. Wang, H. Zhang, F. Li, L. Zhu, *Environ. Sci. Technol.*, 44 (2010) 6843-6848.

[199] Y. Zhang, N. Zhang, Z.-R. Tang, Y.-J. Xu, *Chem. Sci.*, 4 (2013) 1820-1824.

[200] Y. Bi, S. Ouyang, J. Cao, J. Ye, *Phys. Chem. Chem. Phys.*, 13 (2011) 10071-10075.

[201] M. Zhu, P. Chen, M. Liu, *ACS Nano*, 5 (2011) 4529-4536.

[202] H. Shi, J. Chen, G. Li, X. Nie, H. Zhao, P.-K. Wong, T. An, *ACS Appl. Mater. Interfaces*, 5 (2013) 6959-6967.

[203] H. Xu, J. Yan, Y. Xu, Y. Song, H. Li, J. Xia, C. Huang, H. Wan, *Appl. Catal., B*, 129 (2013) 182-193.

[204] C. Hu, X. Hu, L. Wang, J. Qu, A. Wang, *Environ. Sci. Technol.*, 40 (2006) 7903-7907.

[205] Y. Li, H. Zhang, Z. Guo, J. Han, X. Zhao, Q. Zhao, S.-J. Kim, *Langmuir*, 24 (2008) 8351-8357.

[206] H. Cheng, B. Huang, Y. Dai, X. Qin, X. Zhang, *Langmuir*, 26 (2010) 6618-6624.

[207] Z. Chen, W. Wang, Z. Zhang, X. Fang, *J. Phys. Chem. C*, 117 (2013) 19346-19352.

[208] S. Feng, H. Xu, L. Liu, Y. Song, H. Li, Y. Xu, J. Xia, S. Yin, J. Yan, *Colloids Surf., A*, 410 (2012) 23-30.

[209] Q. Kuang , X. Zheng, S. Yang, *Chem. Eur. J.*, 20 (2014) 2637-2645.

[210] J. Cao, B. Xu, B. Luo, H. Lin, S. Chen, *Appl. Surf. Sci.*, 257 (2011) 7083-7089.

[211] W. Jiang, C. An, J. Liu, S. Wang, L. Zhao, W. Guo, J. Liu, *Dalton Trans.*, 43 (2014) 300-305.

[212] C. Xu, Y. Liu, B. Huang, H. Li, X. Qin, X. Zhang, Y. Dai, *Appl. Surf. Sci.*, 257 (2011) 8732-8736.

[213] G. Dai, J. Yu, G. Liu, *J. Phys. Chem. C*, 116 (2012) 15519-15524.

[214] H. Dong, G. Chen, J. Sun, C. Li, Y. Yu, D. Chen, *Appl. Catal., B*, 134–135 (2013) 46-54.

[215] C. Yu, L. Wei, J. Chen, Y. Xie, W. Zhou, Q. Fan, *Ind. Eng. Chem. Res.*, 53 (2014) 5759-5766.

[216] Y. Song, J. Zhu, H. Xu, C. Wang, Y. Xu, H. Ji, K. Wang, Q. Zhang, H. Li, *J. Alloys Compd*, 592 (2014) 258-265.

[217] S. Park, J.M. Lee, Y.K. Jo, I.Y. Kim, S.-J. Hwang, *Dalton Trans.*, 43 (2014) 10566-10573.

[218] H. Xu, Y. Song, Y. Song, J. Zhu, T. Zhu, C. Liu, D. Zhao, Q. Zhang, H. Li, *RSC Adv.*, 4 (2014) 34539-34547.

[219] G. Dai, S. Liu, Y. Liang, K. Liu, *RSC Adv.*, 4 (2014) 34226-34231.

[220] C. Dong, K.-L. Wu, X.-W. Wei, X.-Z. Li, L. Liu, T.-H. Ding, J. Wang, Y. Ye, *CrystEngComm*, 16 (2014) 730-736.

[221] C. Feng, G. Li, P. Ren, Y. Wang, X. Huang, D. Li, *Appl. Catal., B*, 158–159 (2014) 224-232.

[222] W. Wang, B. Cheng, J. Yu, G. Liu, W. Fan, *Chem. Asian J.*, 7 (2012) 1902-1908.

[223] Q. Liang, Y. Shi, W. Ma, Z. Li, X. Yang, *Phys. Chem. Chem. Phys.*, 14 (2012) 15657-15665.

[224] H. Xu, J. Zhu, Y. Song, T. Zhu, W. Zhao, Y. Song, Z. Da, C. Liu, H. Li, *J. Alloys Compd.*, 622 (2015) 347-357.

[225] Y. Wang, P. Ren, C. Feng, X. Zheng, Z. Wang, D. Li, *Mater. Lett.*, 115 (2014) 85-88.

[226] X. Yao, X. Liu, *J. Hazard. Mater.*, 280 (2014) 260-268.

[227] X. Zhang, Z. Ai, F. Jia, L. Zhang, *J. Phys. Chem. C*, 112 (2008) 747-753.

[228] X. Chang, J. Huang, C. Cheng, Q. Sui, W. Sha, G. Ji, S. Deng, G. Yu, *Catal. Commun.*, 11 (2010) 460-464.

[229] L. Chen, R. Huang, M. Xiong, Q. Yuan, J. He, J. Jia, M.-Y. Yao, S.-L. Luo, C.-T. Au, S.-F. Yin, *Inorg. Chem.*, 52 (2013) 11118-11125.

[230] H. Cheng, B. Huang, Y. Dai, *Nanoscale*, 6 (2014) 2009-2026.

[231] X. Tu, S. Luo, G. Chen, J. Li, *Chem. Eur. J.*, 18 (2012) 14359-14366.

[232] X.-X. Wei, C.-M. Chen, S.-Q. Guo, F. Guo, X.-M. Li, X.-X. Wang, H.-T. Cui, L.-F. Zhao, W. Li, *J. Mater. Chem. A*, 2 (2014) 4667-4675.

[233] H. Li, J. Liu, X. Liang, W. Hou, X. Tao, *J. Mater. Chem. A*, 2 (2014) 8926-8932.

[234] J. Zhang, F. Shi, J. Lin, D. Chen, J. Gao, Z. Huang, X. Ding, C. Tang, *Chem. Mater.*, 20 (2008) 2937-2941.

[235] H. Cheng, B. Huang, Z. Wang, X. Qin, X. Zhang, Y. Dai, *Chem. Eur. J.*, 17 (2011) 8039-8043.

[236] Y. Huo, J. Zhang, M. Miao, Y. Jin, *Appl. Catal., B*, 111–112 (2012) 334-341.

[237] D. Zhang, J. Li, Q. Wang, Q. Wu, *J. Mater. Chem. A*, 1 (2013) 8622-8629.

[238] H. Zhang, Y. Yang, Z. Zhou, Y. Zhao, L. Liu, *J. Phys. Chem. C*, 118 (2014) 14662-14669.

[239] X. Zhang, Q. Han, M. Ding, *RSC Adv.*, 5 (2015) 1043-1050.

[240] M. Shang, W. Wang, L. Zhang, *J. Hazard. Mater.*, 167 (2009) 803-809.

[241] J. Cao, B. Xu, B. Luo, H. Lin, S. Chen, *Catal. Commun.*, 13 (2011) 63-68.

[242] X.-X. Wei, H. Cui, S. Guo, L. Zhao, W. Li, *J. Hazard. Mater.*, 263, Part 2 (2013) 650-658.